P. Hemberger, A. Bodi, T. Bierkandt, M. Köhler, D. Kaczmarek, T. Kasper, Photoelectron Photoion Coincidence Spectroscopy Provides Mechanistic Insights in Fuel Synthesis and Conversion, Energy Fuels 35 (2021) 16265-16302.

https://doi.org/10.1021/acs.energyfuels.1c01712

Photoelectron Photoion Coincidence Spectroscopy Provides Mechanistic Insights in Fuel Synthesis and Conversion

Patrick Hemberger,[a*] Andras Bodi,[a] Thomas Bierkandt,[b] Markus Köhler,[b] Dennis Kaczmarek[c] and Tina Kasper[c]

[a]Laboratory for Synchrotron Radiation and Femtochemistry – Paul Scherrer Institute, Villigen 5232, Switzerland, patrick.hemberger@psi.ch

[b]Institute of Combustion Technology, German Aerospace Center (DLR), Pfaffenwaldring 38-40, D-70569 Stuttgart, Germany

[c]Mass Spectrometry in Reactive Flows – Institute for Combustion and Gas Dynamics (IVG), University Duisburg-Essen, Duisburg 47057, Germany

ABSTRACT: Clean combustion, *i.e.,* the reduction of NOx and soot emissions, and carbon neutrality, achieved in part by biofuel synthesis, are major milestones in the transition to a sustainable future. To overcome empiric and time-consuming process optimization steps, we need detailed reaction mechanistic and chemical insights of these processes. Be it in combustion or in catalysis, highly reactive intermediates, such as radicals, carbenes, and ketenes drive chemical reactions. Knowing the fate of these species helps develop strategies to optimize chemical energy conversion processes. This calls for advanced mass spectrometric tools, which enable the detection of transient species. In this review, we report on the application of state-of-the-art photoelectron photoion coincidence (PEPICO) spectroscopy with vacuum ultraviolet (VUV) synchrotron radiation as advanced diagnostic tool in catalysis and combustion research. We discuss reaction mechanisms in biomass conversion to sustainable fuels, where we report on the pyrolysis of wood samples probed using VUV photoionization mass spectrometry (PIMS), and obtain deep mechanistic insights in the (non-)catalytic pyrolysis of lignin model compounds with PEPICO detection. PEPICO is also shown to contribute to the mechanistic understanding of catalysis by unveiling catalytic alkane valorization mechanisms. We discuss how PEPICO detection advances combustion diagnostics, thanks to the application of photoelectron spectroscopy and velocity map imaging. We report on mechanistic aspects of ignition, such as fuel radical formation and oxidation to peroxy species, and discuss reaction pathways of pollutant formation. In addition, we zoom into the elementary reactions of combustion and discuss isomer-selective kinetics experiments on radical oxidation. Newly revealed reaction pathways to polycyclic aromatic hydrocarbon (PAH) formation are also detailed. Finally, we describe current instrumental developments to improve PEPICO detection and report on innovative sources, reactors, and reaction sampling approaches to be combined with this technique.

1. Introduction

The expectations towards clean combustion processes have changed dramatically in perspective and meaning over the past years. For example, NOx and particulate emissions from cars have been more and more stringently regulated by the European emission standards since the 1990's, but the full impact of CO_2 emissions on global warming has only been recognized in the last decades. In the wake of a global sense of ecological responsibility, accelerating climate change, increased public awareness, and protests, we have never valued our resources more than today. Working towards a sustainable future became a common global goal. To achieve the ambitious climate goals set by policy makers around the globe,[1-3] CO_2 emissions must be reduced in all parts of modern life, i.e., in industry, transport, residential and energy sectors. In addition, carbon sequestration and storage or utilization will have to be employed to achieve the two-degree limit on temperature increase set by the Paris agreement on climate change.[4-6] While there is a broad public agreement on the goals, the methods how to decarbonize the energy supply and industrial processes are much less well-defined. Rapid development of various new technologies is required, e.g., from carbon fixation to utilization in thermal and chemical conversion processes, and electrification of industrial processes and the mobility sector. In the case of industrial processes, such as glass or concrete production, combustion is commonly used to generate heat. In some of these cases, electrification is possible. The situation is more complex when the fuel is not only used as source of thermal energy, but simultaneously as reactant, for example, as a reducing agent in metal reforming. Another example is the transport sector with a wide array of requirements and constraints. While urban mobility is predestined to be electrified, the same path appears to be impassable in aviation in the near future. Marine applications and freight transport will also rely on combustion processes for at least 20 years to come.[7-8]

Combustion for energy and heat conversion is an advanced and reliable technology, which can help mitigate the risks posed to the stability of the electrical grid by the transition to electricity production by renewable sources, such as solar and wind.

Combustion sources with carbon-neutral fuels are reliable and sustainable baseload suppliers.[9] A first aspect and, at the same time, short to mid-term solution, is to make combustion processes more carbon-neutral by the use of biofuels and synthetic fuels. The benefits are striking: the possible use of existing infrastructure and fleets, known safety and handling procedures, as well as demonstrated production chains. Moreover, biofuels offer the chance to not only mimic existing fossil-based gasolines but make them better in terms of efficiency and pollutant formation. While power-to-liquid technologies from renewable sources to synthetic fuels are already commercially available (Fuel Readiness Level (FRL) 9 for bio-based routes and FRL 7-8 for Fischer–Tropsch derived routes), they are fragmented and linking individual steps is a contemporary challenge.[10] Especially catalytic fuel synthesis and conversion are far from being optimized with regard to the product spectrum: conventional (e.g. Fischer–Tropsch synthesis) to non-conventional (e.g. biomass valorization, CO_2 to methanol, methanol to olefines, hydrocarbons, benzene or kerosine) to blue sky (e.g. fermentation) routes show much untapped potential.[11] A clear path has not yet emerged but multiple technologies will be needed to achieve the ambitious climate goals and (electro)catalysis will play a major role here.

The second aspect is to make existing combustion processes more efficient by gaining better control over them and choosing process conditions that avoid unwanted emissions, such as soot and NOx. A clear understanding of the combustion properties of the fuels can help to move to carbon-neutral or -free fuels. Even simple and comparatively clean fuels, such as H_2 and natural gas can provide challenges but also offer technological options when used in mixtures. For example, it is possible to match the flame speed of H_2/NH_3 mixtures to the flame speed of CH_4 which can potentially facilitate the use of renewable, carbon-free fuels in existing infrastructure, such as turbines.[12] Yet, challenges are to be expected when uncommon reaction conditions are applied, e.g., even methane exhibits negative temperature-coefficients at fuel-rich conditions and intermediate pressures.[13]

In the transition from a fossil fuel-based economy to an economy based on renewable resources, the process development itself needs to be optimized to reach advanced solutions to reduce CO_2 emissions sufficiently and to achieve the climate goals as soon as possible. How can this be achieved?

Predictive process simulation of catalytic fuel synthesis and thermal fuel conversion can overcome empiric and time-consuming process optimization. Be it combustion or the synthesis of sustainable fuels, all these processes are controlled by the kinetics of the reacting system. Accurate simulations require at least a basic understanding of the underlying reactions[14] and a detailed description of the kinetics. These reaction mechanisms include thermodynamic data and rate coefficients from theoretical and experimental studies and must be validated experimentally. Consequently, simple and reproducible kinetic experiments are needed to provide the concentration dependence of the important reactive intermediates, such as radicals and carbenes, as function of process parameters (pressure, temperature, and reaction time). These experiments must be coupled to diagnostic techniques that identify the important reacting species at all stages of the reaction and, ideally, also determine their concentration. In recent years, different diagnostic methods were designed and constructed to gain the necessary mechanistic insights by, e.g., the detection of highly reactive and elusive intermediates.

In this review, we focus on state-of-the-art photoelectron photoion coincidence (PEPICO) techniques with vacuum ultraviolet (VUV) synchrotron radiation. PEPICO picked up speed as a versatile reaction microscope for reactive environments during the last decade. In this review, we summarize most recent advances in unveiling reaction mechanisms in catalytic fuel synthesis and combustion, and refer the reader to further reviews covering photoionization mass spectrometry combined with reactors and flame sampling,[15-18] the photoionization of reactive intermediates,[19] and the unimolecular decomposition dynamics of cations.[20]

First, we discuss the need for a universal, multiplexed, and sensitive detection tool to investigate energy conversion processes, such as catalysis and combustion.

During the first aspect of a clean combustion approach, we detail how PEPICO helped shine new light on biomass conversion mechanisms to produce sustainable fuels. We discuss photoionization approaches to probe wood pyrolysis directly in a top-down approach, as well as studies to investigate the elementary reactions of (catalytic) pyrolysis of lignin model compounds in a bottom-up approach. This chapter is complemented by unveiling rate-limiting reactions in catalytic alkane oxyhalogenation, a natural gas valorization approach, as well as its side reactions, such as coking and decomposition.

The second aspect of clean combustion involves the combustion the process itself. Here, we dig deeper into how PEPICO detection has enhanced combustion diagnostics by introducing photoelectron spectroscopy and ion velocity map imaging as second and third analytical dimensions to conventional photoionization mass spectrometry. We focus on understanding the initial fuel decomposition steps, such as radical formation, oxidation to peroxy and ketohydroperoxy species, and decomposition. Pollutant formation processes such as soot, polycyclic aromatic hydrocarbons (PAHs), and NOx formation are inspected by taking advantage of the novel analytical dimensions associated with PEPICO.

As far as combustion chemistry is concerned, a combustion model can only be as good as the individual reactions are understood. Thus, we review most recent advances in measuring isomer-selective rate constants of radical + oxygen reactions, we probe new PAH formation channels as well as how organophosphorus species inhibit or control combustion processes.

This review concludes by a discussion of new instrumental developments to improve PEPICO detection and a summary of new sources, reactors, and sampling reactions to be combined with this technique.

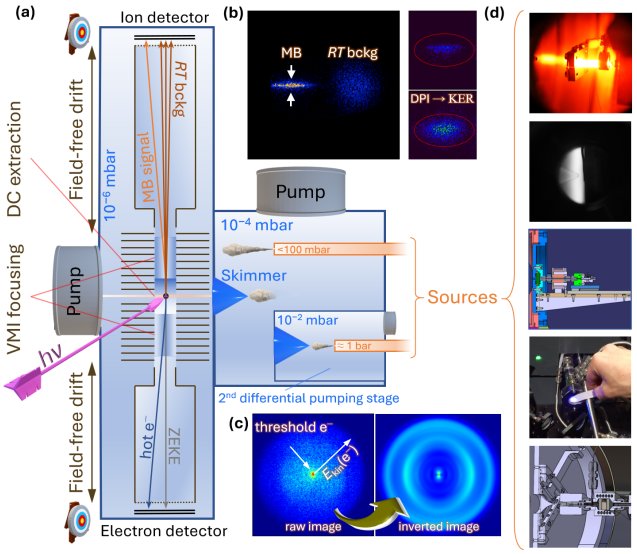

Figure 1. (a) Double imaging photoelectron photoion coincidence spectroscopy. Velocity map imaging (VMI) allows us (b, left) to separate the molecular beam (MB) ion signal spatially from that of the scattered and thermalized background. Furthermore, (b, right) the lateral broadening of the MB signal indicates kinetic energy released (KER) in dissociative photoionization. Thus, fragmentation free ionization and dissociative photoionization can also be distinguished. (c, left) Photoelectron VMI is used to discriminate for threshold ionization to plot photoion mass selected threshold photoelectron spectra (ms-TPES). (c, right) Alternatively, the photoelectron spectrum can be reconstructed by inverting the VMI image. A wide spectrum of sources can be used, including (d, top to bottom) pyrolysis microreactors, flames, temporal analysis of products (TAP-type) reactors, photolysis, and catalysis reactors. Some figures were reprinted (adapted) with permission from Refs. [21] and [22]. Copyright 2017 American Chemical Society. Reproduced with permission from [23-24].

Elusive and reactive intermediates are key to understanding chemical processes, be it fuel synthesis, conversion, or combustion. They are, by definition, short-lived, and only present in trace amounts in the reaction mixture. Detection methods to reveal reaction mechanisms must be fast and sensitive. Furthermore, versatile and universal tools are called for to deliver a complete picture of the reactive environment and to transcend mechanistic preconceptions. Measurements at high pressures and temperatures are often confounded by peak broadening or by fast isomerization processes in the condensed phase. This can in part be counteracted by freezing out reactive intermediates and unstable species in cold noble gas matrices and applying UV and IR spectroscopy at temperatures of a few Kelvin.[25] Although matrix isolation spectroscopy can be used to trap elusive species,[26] its low sensitivity means that its application in combustion chemistry is limited to the simplest systems.[27]

Alternatively, laser-induced fluorescence (LIF) is a fast and selective method to detect, *e.g.,* ·OH radicals, and it is applied in atmospheric and combustion chemistry[28-29] and in the study of the photodissociation of acetylacetone.[30] The striking advantage of LIF is the non-intrusive application resolving processes with up to femtosecond time resolution. However, it is very specific and far from being universal. This explains how LIF missed 15 unique acetylacetone photoproducts later detected by mass spectrometry.[28-29, 31]

On the one hand, methods tailored to the fast and selective detection of a specific species or species class may be advantageous to follow these accurately. On the other, such methods may miss the rich chemistry in even the simplest systems. The chemical understanding is only complete if the detection is selective, *i.e.,* it allows for an unambiguous and isomer-specific assignment, fast, sensitive, universal, and multiplexed, *i.e.,* it delivers a full picture of the sample simultaneously. Multiwell potential energy surfaces play a prominent role in combustion and atmospheric chemistry, and direct sampling from collisional environments is required to reveal the driving forces behind macroscopic reaction mechanisms.[32] Photoionization mass spectrometry (PIMS), pioneered by Bayes and Gutman and colleagues,[33-34] probes the mixture in the isolated gas phase, and is, as all mass spectrometric techniques, a fast, universal, and sensitive detection technique. With respect to hard electron ionization sources, soft single-photon ionization allows for the suppression of fragmentation processes by tuning the photon energy, *hν*. This makes laborious signal apportioning approaches[35] superfluous and photoionization mass spectra comparatively sparse.[36-37]

In multiplexed photoionization mass spectrometry (MPIMS), quickly tunable synchrotron radiation is used as ionization source, which allows one to "image" a chemical reaction by measuring a 3D dataset resolved by the mass-to-charge (*m/z*) ratio, the kinetic time, and the ionizing photon energy.[25] By way of ionization energy differences or based on reference photoionization spectra, (M)PIMS is often capable of isomer-specific identification of fleeting reaction intermediates,[38] even in complex environments, such as catalysis.[39-40] Thus, MPIMS relies on valence photoionization by tunable monochromatic synchrotron radiation and is a fast, universal, sensitive, and quite selective technique to detect and assign reactive intermediates after sampling from a collisional environment, such as a flow tube, a high-pressure photolysis reactor,[41] or a miniature, high repetition rate, diaphragmless shock tube.[42]

The selectivity of PIMS is limited if species of the same mass have a similar ionization energy (IE). Also, the detection limit for the higher ionization energy species in a pair depends strongly on the abundance of the low-IE constituent. A suitably high mass resolution can help distinguish species of different sum formulae at the same integer mass, such as ketene at *m/z* 42.01 and propene at *m/z* 42.05,[25] but cannot tell isomers of the same mass apart.

Photoelectron photoion coincidence (PEPICO) spectroscopy,[20] in particular when combined with velocity map imaging of electrons and ions,[43] improves on the capabilities of MPIMS in terms of selectivity, sampling effects, and, more generally, renders it a more complete experiment to study photoionization.[44] In PEPICO (**Figure 1**a), a gas phase sample is ionized by tunable monochromatic vacuum ultraviolet (VUV) radiation, corresponding to the energy range of valence photoionization. Synchrotrons represent the most intense and easily tunable VUV light sources, which is why, similar to PIMS and MPIMS experiments, contemporary PEPICO setups are mostly found at VUV beamlines.[45-48] Continuous extraction of photoelectrons and photoions yields better signal levels and allows for more versatile applications than high-resolution pulsed field approaches,[49] while still being capable of sub-meV (better than 0.1 kJ mol^{-1}) overall energy resolution in favorable cases.[50-51] By photoelectron kinetic energy analysis, the analytical dimension, thus, the selectivity, of MPIMS is expanded by a further

dimension, *i.e.,* the photoelectron spectrum, which often offers an isomer-specific fingerprint.

The photoelectron and photoion kinetic energy distributions are measured by velocity map imaging (**Figure 1** (b and c)) or, for photoions, by 3-D momentum imaging, as well. In multiple-start/multiple-stop data acquisition,[52] all events are recorded, and electrons with a negligible time of flight (TOF) serve as the start signal to measure the TOF distribution of the photoions. False coincidences, *i.e.,* electron and ion detections belonging to different ionization events, result in a constant background signal. This can be subtracted from the experimental data to obtain the true coincidence signal: photoelectron and mass spectra as well as cation velocity map images. In the end, the true coincidence signal allows us to approach a complete experiment, in which all observables are recorded after photoionization.

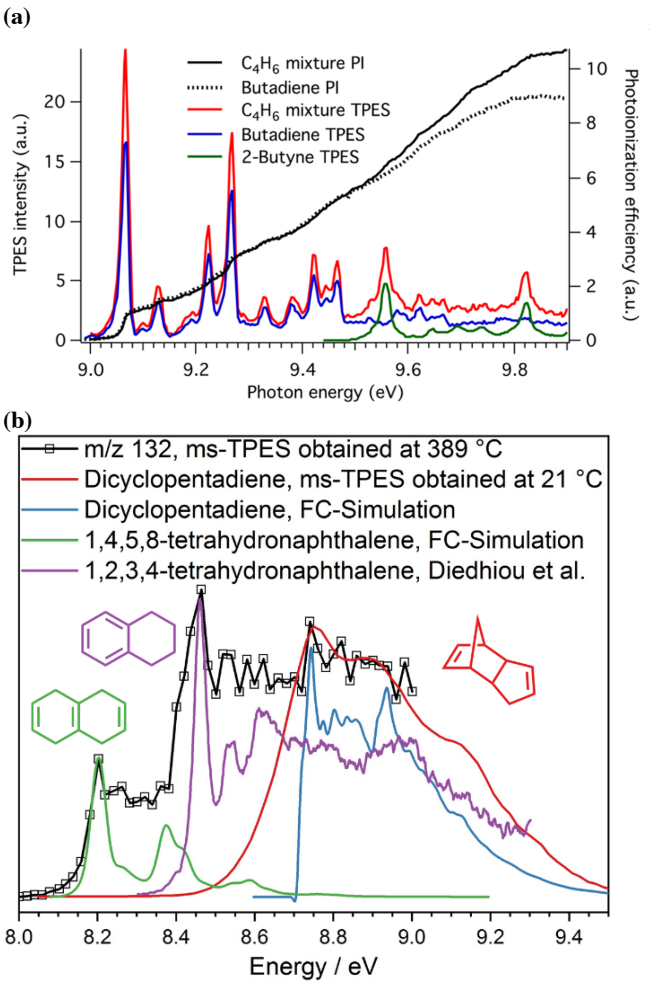

Figure 2. (a) Comparison of the photoionization spectrum and the threshold photoelectron spectrum for the assignment of a C_4H_6 mixture to 1,3-butadiene and 2-butyne. The 2-butyne resonance at 9.56 eV is much more evident in the TPES than in the photoionization spectrum. Reprinted with permission from [44]. Copyright 2013 American Chemical Society. (b) Assignment of the *m*/*z* 132 ms-TPES to isomeric $C_{10}H_{12}$ species with the help of measured reference and Franck–Condon simulated spectra. Taken from [24], Published by The Royal Society of Chemistry.

The combination of electron kinetic energy analysis and ion TOF mass analysis enables internal energy selection. If threshold, *i.e.,* close to zero kinetic energy electrons are discriminated for, the excess photon energy above the ionization energy is deposited in the parent ion and is available for fragmentation. By scanning the photon energy, recording, and modeling the dissociative photoionization (DPI) processes in the breakdown diagram, crucial insights can be obtained regarding ionic fragmentation mechanisms and thresholds,[53] which can in turn be used in the interpretation of pyrolysis data.[54]

Slow photoelectron imaging was originally developed to analyze photodetachment spectra of anions by velocity map imaging conditions and zooming in on low kinetic energy electrons. It only focuses them onto the detector for better energy resolution.[55] The best absolute kinetic energy resolution is achieved at near-zero kinetic energies, and particles with negligible initial kinetic energy are imaged onto a single spot in the center of the detector. Thus, discriminating for threshold electrons after subtracting the hot electron contamination of the center signal[56-57] yields superior signal-to-noise ratios at high energy resolution to plot the photoion mass-selected threshold photoelectron spectrum (ms-TPES), *i.e.,* the TPES belonging to a single cation *m*/*z* channel. ***Figure 2***(a) shows the photoionization spectrum of 1,3-butadiene and a C_4H_6 mixture of 1,3-butadiene and 2-butyne together with the corresponding threshold photoelectron spectra. Clearly, the latter offer more specificity, as also illustrated by an *m*/*z* 132 ms-TPES in ***Figure 2***(b), which could be used to identify three isomeric $C_{10}H_{12}$ spectral carriers.

Pyrolysis experiments have been carried out to prepare and record reference photoelectron spectra of free radicals,[19] including the nitrogen organic picolyl isomers.[58] The latter work also shows the TPES to be a sensitive isomer-specific identification tool. Furthermore, while isomerization energy differences and significantly different ground-state band structures are often evident in photoionization spectra, too,[59] even species with a broad and featureless ground-state peak may exhibit well-defined characteristic resonances in excited states, which are clearly seen in the TPES.[60-61] TPES bands correspond to cation electronic states, and their fine structure is governed by the Franck–Condon (FC) principle. This states that the nuclear wave function overlap integral between the neutral (normally ground) and the cation vibronic state will determine the observed vibrational progressions.[62-63] Franck–Condon analysis of numerous TPES has shown that vibrational fingerprints are predicted reliably by density functional theory calculations in the double harmonic approximation, and FC simulations are now routinely used to assign ms-TPES when reference spectra are unavailable.

Slow photoelectron spectroscopy (SPES) is a complementary approach offering higher signal levels at somewhat worse resolution. In SPES, the photoelectron spectrum is obtained at each photon energy based on inverting the (photoion mass-filtered) electron velocity map image,[64] and integrating the signal at constant ($h\nu$ – EKE) but only up to a third of the energy range of the detector.[65]

Isomer-specific assignment based on ms-TPES and reference or FC-simulated spectra was relied on in the study of the unimolecular thermal decomposition of cyclopentanone[66] and the surprisingly rich pyrolysis chemistry of phthalide,[67] as well as the almost clean bimolecular allyl + *o*-benzyne reaction yielding indene.[68] Such achievements have fueled the use of PEPICO detection, the focus of this review, to understand more complex

reactive environments from catalysis to combustion, *e.g.,* in flames.[69-70]

Before reviewing the contributions of PEPICO detection to fuel production and combustion mechanisms, we briefly point out the benefits of cation velocity map imaging in molecular beam sampling, long established to probe the fundamental chemistry of flames.[16, 71] To form a molecular beam, the sample expands from a pressure of typically 100 mbar to 10 bar into vacuum. Up to nine orders of pressure difference are bridged by skimming the beam in one or two differential pumping stages. Thanks to collisional cooling by the inert backing gas and the quickly decaying rate of reactive collisions in the expansion, the reactive mixture is frozen out, and the chemical identity of intermediates and radicals is conserved during sampling.

In the photoion VM images, species emanating directly from the reactor are spatially separated from the backscattered background signal (**Figure *1*** (b)) because of their increased velocity along the sampling axis. This was shown to be particularly useful when quantifying the concentration of hydroxyl radicals (see chapter 4).[72] While stable molecules are detected efficiently after scattering in the ionization chamber, OH does not survive wall collisions. Thus, the OH signal is suppressed in the thermalized background and only the direct molecular beam signal is indicative of its true abundance.

Furthermore, although the photon energy can often be tuned to a value at which only direct ionization takes place, ion imaging also presents an alternative approach to distinguish direct ionization of neutrals from dissociative photoionization of heavier species contributing to the same *m*/*z* channel. As seen in **Figure *1*** (b), the sample velocity lateral to the expansion axis is negligible. The measurement is therefore quite sensitive to kinetic energy release in DPI, which may be readily observable to identify dissociative ionization processes **Figure *1*** (b, right).[54]

These benefits make double imaging PEPICO an attractive analytical tool to interface to a wide variety of sources (**Figure *1*** (d)) from a supersonic expansion source to study cold and weakly bound systems,[73] through pyrolysis microreactors to reveal unimolecular thermal decomposition processes.[74] as well as bimolecular chemistry,[68] microwave discharge flow tube reactors,[75] flames,[69-70] shock tubes,[76] to pressurized flow reactors.[77]

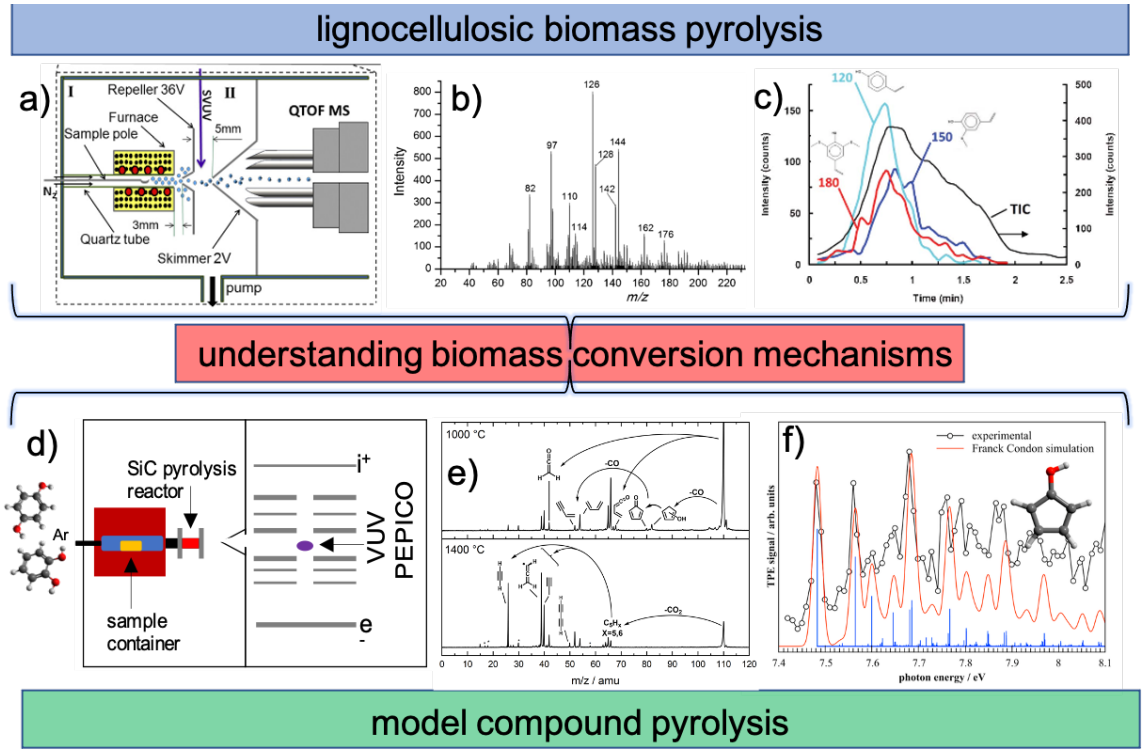

Figure 3. Photoionization methods to study biomass (lignin, left) conversion. (a) VUV-PIMS endstation at the National Synchrotron Radiation Lab (Hefei, China) to investigate the mechanistic aspects of lignocellulosic biomass conversion. (b and c) Lignin, xylan, and cellulose markers are identified in the mass spectrum as a function of the process conditions. Reproduced from Ref. [78] with permission from the Royal Society of Chemistry. (d) PEPICO endstation with a pyrolysis microreactor unveils (e) temperature-dependent decomposition processes at the Swiss Light Source (f). A photoion mass-selected threshold photoelectron spectrum of hydroxy cyclopentadienyl radicals during guaiacol decomposition provide insights into elementary reactions. Reproduced from Ref. [79] with permission from the PCCP Owner Societies. Reprinted (adapted) with permission from Ref. [80]. Copyright 2014 American Chemical Society.

3. Mechanistic Insights Into Sustainable Fuel Production

The idea of sustainable combustion started with biofuels such as methanol and ethanol, produced via fermentation of sugars and starch, found in corn, sugarcane, and sugar beet. Biodiesels, on the other hand, are synthesized via transesterification of fatty acids, mainly from colza and soybean oil. These fuel resources are often criticized, because they are in direct competition with food production.[81] Thus, alternative strategies, such as lignocellulosic biomass valorization, are required to manufacture sustainable and CO_2-neutral fuels. Besides wet chemical valorization routes, namely hydrothermal liquefaction and carbonization,[82] thermal conversion at anaerobic conditions, e.g., pyrolysis is an alternative way to treat the feedstock and obtain renewable fuels (benzene, toluene, and xylenes) and fine chemicals (phenols). Due to the large variety of biomass resources, their valorization is far from being trivial or uniform. Biomass source-specific mechanistic insights are required to optimize the valorization processes. Yet, standard analytical approaches such as thermogravimetry and gas chromatography/mass spectrometry only detect final products, which is often insufficient. This gave rise to novel in-situ, operando, and online mass spectrometric analysis tools, described in the previous chapter. Mechanistic insights can be obtained from two directions: First, by pyrolyzing biomass in form of lignocellulosic feedstock, such as wood, which is referred to as top-down approach (Figure 3 upper trace). Second, the complex chemistry of lignin model compounds, such as guaiacol or syringol, must also be studied to gain mechanistic insights into the elementary reactions in a bottom-up-approach (Figure 3, lower trace). In the following, we discuss both approaches and show how they are connected.

3.1. Biomass Pyrolysis

Dufour et al. constructed a synchrotron VUV photoionization mass spectrometer, which combines a quadrupole-time-of-flight MS with a high-vacuum interface to sample directly from a solid-state biomass pyrolysis apparatus (Figure a) operated at a few millibars.[78] They have investigated numerous biomass samples, including microcrystalline cellulose (see mass spectra in Figure 3b), miscanthus, and oak wood, at a range of photon energies and pyrolysis temperatures. In their mechanistic top-down approach, they studied the evolution of, e.g., 4-vinylphenol, 5-hydroxymethyl-furfural, and lactone species as function of time and reactor temperature (see Figure 3c), which are markers for the lignin, cellulose, and xylane content in biomass, respectively.[83-84] They found new pyrolysis intermediates of cellulose and tentatively assigned the observed signals in the mass spectrum to 5-methyl-4-oxotetrahydrofuran-2-carbaldehyde or to a similar isomer.

Weng et al.[85] extended this study by pyrolyzing 20 mg bar-shaped poplar lignin samples at 26 mbar and temperatures from 300 to 700 °C and VUV-PIMS sampling of the gaseous products. Thanks to the tunability of the light source, they could suppress fragmentation during ionization, which helped spectral assignment. Their measurements show that coniferyl and sinapyl alcohol, subunits of lignin, exhibit different temperature-dependent gas-phase decomposition reactions. Time-resolved

studies of the pyrolysis process revealed interesting correlations: *m*/*z* 114 (4-hydroxy-5,6-dihydro-2H-pyran-2-one), is produced first from hemicellulose, while coniferyl alcohol appears at longer reaction times. Lighter lignin products, such as guaiacols and benzenediols, are produced at later stages of the pyrolysis process. This sequence of products is probably caused by insufficient hydrogen supply. Hydrogen is needed to hydrogenate and volatilize intermediates, as also pointed out by Evans et al.[86] The authors concluded that, compared to hemicellulose, lignin particles require an increased reaction time for complete pyrolysis in industrial processes. In their follow-up studies with similar instrumentation, deoxygenation reactions yielding polycyclic aromatic hydrocarbons (PAHs) were also identified and [87-88] the authors review different ionization light sources utilizing REMPI laser schemes, VUV lamps, synchrotron radiation, and higher harmonic generation.

These studies utilized advanced sampling techniques and mass spectrometric approaches to contribute to the global mechanistic picture of direct lignocellulosic feedstock conversion. The top-down approach reveals macroscopic trends, such as marker signatures as function of the temperature and reaction time. These are in turn important to solve chemical engineering challenges of biomass conversion. To gain a solid fundamental understanding of these large reaction networks, we must reveal the elementary reactions driving biomass conversion.

3.2. Pyrolysis of Lignin Model Compounds

The overall kinetics of lignin conversion are determined by a multitude of complex reactions, initiated by direct bond cleavage of the lignin macromolecule, and primarily yielding highly reactive radicals. These intermediates are quenched to stable lignin subunits (guaiacol or syringol) or undergo further decomposition reactions, depending on the process conditions. By studying lignin model compound pyrolysis, we can simplify the secondary reactions and eliminate the effect of the irregular and complex lignin structure on the process. This bottom-up approach reveals deep mechanistic and kinetic insights, which aid our understanding of lignin pyrolysis.[89]

What are the experimental requirements to unveil the basic unimolecular reactions of model compounds? The density of the model compound in the reactor must be low and the residence time must be short to avoid bimolecular chemistry. These experimental conditions allow us to focus on the initial unimolecular reactions, which yield elusive radicals, and study these primary intermediates and their fate. In 1992, Chen et al. introduced a silicon carbide (SiC) microreactor, as depicted in Figures 1(d, top) and 3(d) for *in-situ* synthesis of reactive intermediates for spectroscopic studies.[90] Numerous variants of this device have been constructed up to now and some have been coupled with PIMS and PEPICO endstations at synchrotrons to investigate the unimolecular decomposition of lignin model compounds or as high temperature chemical reactor.[91-94] The version at the Swiss Light Source is comprised of a sample container in which involatile model compounds are heated, vaporized, and mixed with an inert carrier gas (argon or helium). The mixture is expanded through a 100–500 μm nozzle into the hot SiC reactor, where reactions take place at a residence time of only 10–100 μs.[95] Extensive modeling of this reactor by Guan et al. revealed that the flow conditions are laminar, with large pressure and temperature changes along the heating zone.[95] Due to these conditions the reactions happen in a shorter time scale as compared to the residence time. The authors further stated that this type of reactor may allow for extracting kinetic information. Similar findings were also reported by other groups and a strategy to obtain kinetic information was proposed.[96-97] The gaseous sample leaving the hot reactor expands into high vacuum to ca. 10^{-4} mbar, forms a molecular beam, and is skimmed. The collision frequency in the molecular beam is small enough so that the initial composition of the mixture is preserved until the gas sample reaches the PEPICO spectrometer. Among the simplest lignin model compounds, the unimolecular decomposition of benzenediol isomers was investigated by PEPICO detection. The mass spectra show only a few peaks due to thermal decomposition (see **Figure** *3*e). There are common reaction channels in all three isomers. Catechol (ortho-), resorcinol (meta-), and hydroquinone (para-benzenediol) can decarbonylate by CO loss to produce isomeric hydroxycyclopentadienes (c-C_5H_5OH), according to R1:[79]

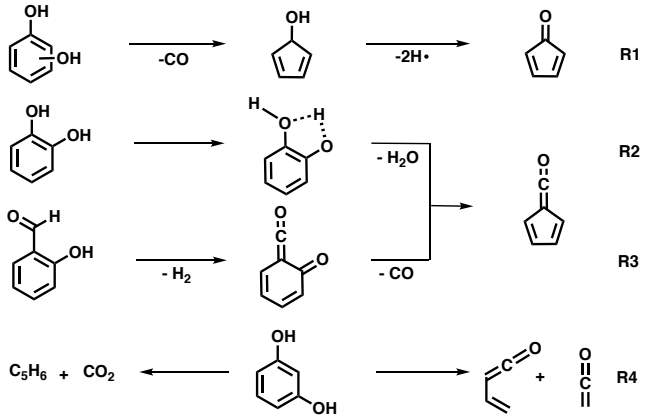

Hydroxycyclopentadienes are prone to dehydrogenation, and ultimately form cyclopentadienone (c-C_5H_4=O, R1), an

antiaromatic and, thus, quite unstable intermediate, as verified by measuring its ms-TPES (see **Figure 4**, upper trace).[79, 98]

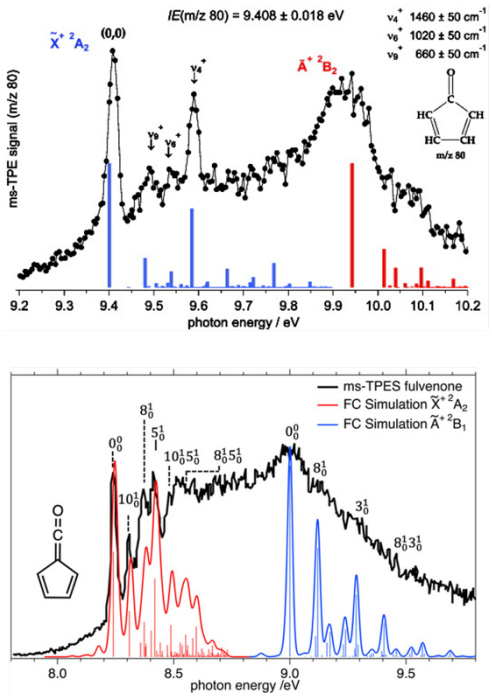

Figure 4 Photoion mass-selected threshold photoelectron spectra of two important lignin decomposition intermediates, cyclopentadienone (upper trace) and fulvenone ketene (lower trace). Both spectra show activity in C=C stretching modes located at the five-membered ring upon ionization. Ref [98] reprinted by permission of Taylor & Francis Ltd, http://www.tandfonline.com.Taken with permission from Ref. [99] copyright John Wiley and Sons.

Isomer-dependent reaction channels exclusive to resorcinol and catechol were also found. Thanks to the vicinity of the two OH groups in catechol, a dehydration reaction is observed (R2), which yields the fulvene ketene or fulvenone (c-C_5H_4=C=O) as corroborated by its unique TPES features (**Figure 4**, lower trace). The effect of the adjacent substitution pattern in benzenes could be confirmed by pyrolyzing salicylaldehyde (ortho-hydroxybenzaldehyde), which produces a ketene species at *m/z* 120 by H_2 loss, which further decarbonylates to fulvenone ketene (see R3) as found by Ormond et al.[100] Further CO loss intermediately yields the singlet cyclopentadienylidene carbene, which rearranges thermally to an acyclic alkyne species C_5H_4 at *m/z* 64.

The meta isomer, resorcinol, exhibits two unique reaction channels (see MS in **Figure 3e**) and yields C_5H_6 isomers in a decarboxylation reaction or produces two ketene species (ethenone and butadienone), as summarized in reaction R4 by Gerlach et al.[79]

By substituting hydrogen at the hydroxy functionality by methyl groups in benzenediols, the reactivity of lignin model compounds and the complexity of the mechanism can be increased by introducing predetermined breaking points. In guaiacol (2-methoxy phenol), the decomposition reaction is initiated by a methyl radical loss, producing the resonance-stabilized hydroxy-phenoxy radical (R5), which undergoes rapid CO loss to yield hydroxy cyclopentadienyl. The identity of these radicals was confirmed by measuring the ms-TPES at *m/z* 81, as depicted in **Figure 3e**. It shows a sharp resonance at 7.48 eV, corresponding to the adiabatic ionization energy, followed by vibrational transitions, which are very well reproduced by Franck–Condon spectral modeling confirming the isomer-selective assignment. This radical is prone to hydrogen loss and stabilizes to cyclopentadienone (c-C_5H_4=O, R6) at elevated temperatures. Further increasing the temperature favors the decarbonylation reaction to vinylacetylene (H_2C=CH-C≡CH, R6). These examples summarize the elementary reactions, including the primary radical intermediates, and lay the foundation of the reaction mechanism.

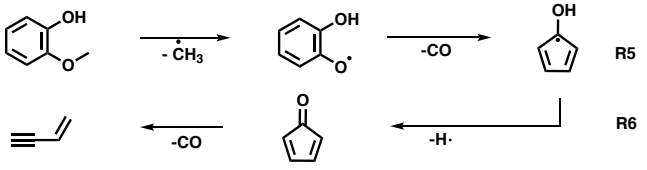

To connect the elementary reactions unveiled by the bottom-up approach with the lignin or wood pyrolysis experiments discussed in chapter 3.1, it is straightforward to increase the complexity of the lignin model compounds by adding a second benzene ring moiety. In the simplest case, this is achieved by connecting two benzene rings via an ether bond as typically present in unaltered protolignin. In unimolecular reaction conditions in the SiC microreactor, diphenylether decomposes to phenyl (C_6H_5) and phenoxy radicals (C_6H_5O) initially (see R7). The latter are thermally unstable and yield cyclopentadienyl radicals by CO loss:

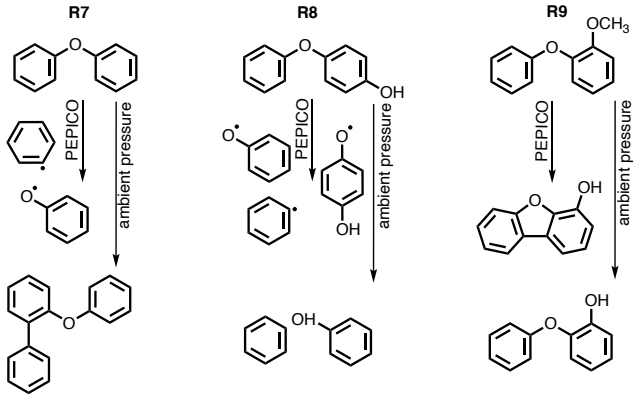

Phenyl radicals are highly reactive and stabilize either via hydrogen addition to yield benzene or produce benzyne (C_6H_4) upon hydrogen loss.[80] In pyrolysis at ambient pressure, studied by py-GC/MS, phenyl radicals are found to form larger molecules with up to four benzene ring moieties at lower temperatures or predominantly monomers, such as benzene, at higher ones (R7).[80]

The reactivity and the products change, and the reaction temperature can be reduced when diphenylether is further functionalized.[101] In 4-phenoxyphenol, mostly phenyl, phenoxy, and *p*-benzoquinone are formed via direct bond fission and subsequent dehydrogenation (R8). Alternatively, the decomposition of 2-methoxyphenoxybenzene is initiated by methyl radical loss, triggering more complex chemistry (R9). Custodis et al.[101] found multistep rearrangement reactions yielding dibenzofuranol (R9) and dibenzodioxin spectroscopically and verified them by quantum chemical reaction pathway calculations. This unimolecular reaction channel can be rationalized by the low energy of the O–CH_3 bond and the stability of the 4-*O*-5 ether

bond, which favors intramolecular C–C bond formation to dibenzofuranol and dibenzodioxin.[101] In contrast, in ambient pressure pyrolysis (R7-9), diphenylether (R7) produces recombination products, while 4-phenoxyphenol primarily yields benzene and phenol, similar to the initial unimolecular radical reaction identified by PEPICO. On the other hand, 2-methoxyphenoxybenzene (R9) yields 2-phenoxy-phenol and the ether bond remains intact.[101] These examples show microscopically how the aromatic ether bond influences the lignin depolymerization processes and identify the role this motif has in driving biomass pyrolysis.

3.3. Catalytic Pyrolysis of Model Compounds

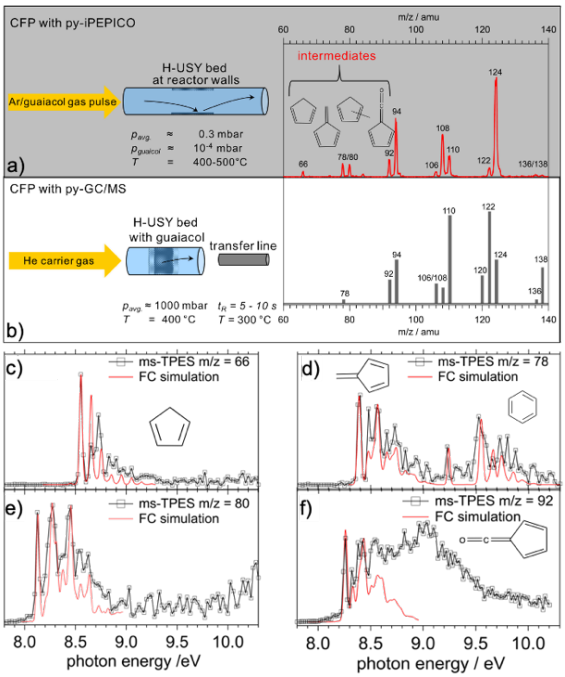

Figure 5 a) Schematic representation of the TAP-type catalytic fast pyrolysis reactor at the SLS along with a mass spectrum, showing both reaction products and reactive intermediates. The comparison with a batch-type reactor and GC/MS (b) detection shows similar final products. (c-f) ms-TPES confirm the identity of reactive intermediates in CFP of guaiacol. Reproduced from Ref.[23].

Top-down and bottom-up approaches to study depolymerization mechanisms of lignin of different origins help identify elementary reactions and structure–reactivity relationships to optimize the generation of pyrolysis gases. In a second stage, these gases are catalytically pyrolyzed utilizing zeolite catalysts in lignin valorization. Only a few large-scale pilot plants have been commissioned so far for this purpose,[102] and challenging technical difficulties are yet to be overcome. A more in-depth mechanistic understanding of catalytic processes may be key to solving some of the outstanding issues. For example, a detailed mechanistic picture of the reaction sequence involving the catalyst can help to avoid unwanted side reactions or reduce coking, fouling or any other deactivation channels of the catalyst surface.

In general, a catalyst speeds up the reaction, increases the conversion by lowering the activation energy, and controls the selectivity by affecting different pathways differently. For instance, when guaiacol, 2-methoxyphenol, is pyrolyzed at unimolecular conditions in the absence of a catalyst, it reacts in a straightforward manner, according to R5.[80, 103] The reaction is initiated by a methyl radical loss and proceeds by subsequent decarbonylation and dehydrogenation steps to yield cyclopentadienone.

In order to investigate the guaiacol catalytic fast pyrolysis, we developed a source at the SLS based on a temporal analysis of products (TAP) type reactor.[23] A diluted pulse of guaiacol in argon (1:2000) travels through a quartz glass reactor, coated with H-USY zeolite (see **Figure 5**a). The intermediates, products, and the remaining starting materials desorb from the catalyst surface and enter the PEPICO endstation directly. To bridge the pressure gap between the low average pressure in the reactor of 0.3 mbar and industrial CFP conditions, the results were compared with ambient pressure batch-type reactor pyrolysis analyzed by GC/MS (py-GC/MS, **Figure 5**b). The same high *m/z* products are observed in both setups, confirming that the sampling in the low-pressure py-iPEPICO experiment represents a snapshot of the same reactions taking place at ambient pressure. These products can be assigned to toluene (*m/z* 92), phenol (*m/z* 94), xylenes (*m/z* 106), cresols and anisole (*m/z* 108) based on their ms-TPE spectra in py-iPEPICO as well as retention time and fragmentation pattern in py-GC/MS. A marked difference in the low-mass-to-charge channel products (*m/z* 66–92) is found, which are prominent in the py-PEPICO spectra, owing to the short reaction time and low collision frequency, which extends the lifetime of highly reactive intermediates. For instance, the *m/z* 66 channel (**Figure 5**c) can be assigned to cyclopentadiene based on the adiabatic ionization energy (AIE = 8.64 eV) in combination with Franck–Condon spectral modeling of the ms-TPES vibrational envelope. This sensitivity towards reactive species becomes even more apparent when looking at the *m/z* 78 signal, which can mainly be ascribed to fulvene, a high-energy C_6H_6 isomer, thanks to its ground and excited state ms-TPES bands at 8.4 and 9.5 eV (**Figure 5**d), respectively. Benzene is only responsible for the minor peak at 9.2 eV. The signal at *m/z* 80 in the mass spectrum is assigned to the three methylcyclopentadiene isomers (**Figure 5**e). While *m/z* 92 was assigned to toluene in the GC/MS data, the ms-TPES shows a signal already at 8.24 eV photon energy, *i.e.,* much below the 8.8 eV AIE of toluene. With the help of ionization energy calculations and FC simulations, the *m/z* 92 ms-TPES (**Figure 5**f) was assigned to fulvenone, established as the central reactive intermediate in the guaiacol CFP. Recently, we have investigated the threshold photoelectron spectrum in more detail and found that the ground and excited cation states contribute to the first band of the spectrum (see **Figure 5**f). The latter state exhibits an ultrashort lifetime and is responsible for the lifetime broadening of the band above 8.5 eV (see **Figure *4***).[99]

The detection of numerous methylation products, such as methylcyclopentadiene and cresol isomers, led us to investigate the methylation chemistry in more detail by ^{13}C-labeling guaiacol. This revealed that the methoxy group is indeed the source of the methyl group in the methylation processes, the removal of which yields catechol, i.e., demethylated guaiacol, as the first reaction product. The liberated methyl group readily attaches to a wide variety of intermediates and products, in a Brønstedt acid-catalyzed reaction on the catalyst surface, shown by a unit mass shift upon $^{13}CH_3$ isotope labeling.[23] In addition, the

decomposition of the benzene ring moiety could be excluded, as the resulting methyl groups would yield a broad isotopic distribution in the product channels. Furthermore, control experiments with pure catechol yielded mainly cyclopentadiene, phenol, CO, CO_2, and fulvenone. Especially the detection of c-C_5H_4=C=O during the catechol CFP was crucial to deciphering the reaction mechanism, which is summarized as follows:

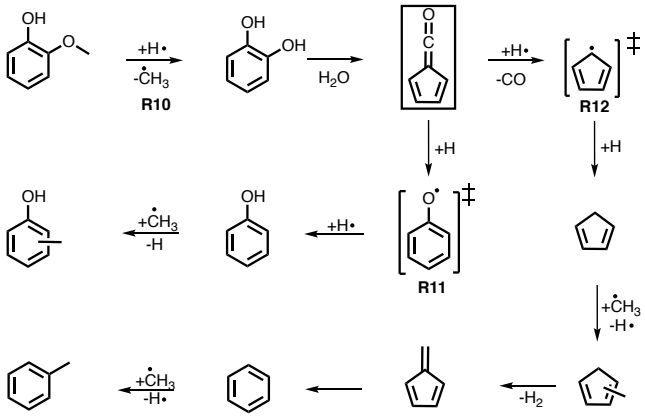

In a Brønsted acid-catalyzed demethylation reaction, guaiacol is converted to catechol, and subsequent dehydration yields the fulvenone ketene (c-C_5H_4=C=O). From the latter intermediate, a branching into phenoxy (R11) or cyclopentadienyl (R12) radicals takes place. The former is stabilized by hydrogenation to yield phenol, one of the major products particular in guaiacol, and in general lignin CFP, which may be readily methylated further forming cresols.[104]

Cyclopentadiene is produced after hydrogenation of the cyclopentadienyl radical (R12). It is subsequently methylated to yield methylcyclopentadiene isomers. Dehydrogenation produces fulvene (c-C_5H_4=CH_2), a reactive C_6H_6 intermediate and benzene precursor. Subsequent methylation reactions form toluene and xylenes. R10–R12 indeed describe the major reaction pathways to the main products of guaiacol CFP and how the fulvenone ketene is responsible for the formation of prototypical fuels (benzene) and fine chemicals (phenols). This is in line with recent findings on emphasizing the important role of ketenes in catalytic processes.[104]

Considering the formation and fate of the ketene intermediate fulvenone and its precursor, catechol, several questions arise: How do the reactivity, the product distribution, and the intermediates change as a function of the benzenediol isomer? Does the presence of a catalyst change the decomposition mechanism? To investigate this, Pan et al. studied catechol, resorcinol, and hydroquinone in a catalytic fast pyrolysis reactor coupled to the PEPICO endstation at the Swiss Light Source, as shown in **Figure 6**a. The reactor used in these experiments is operated at close to ambient pressure to mimic real-world CFP. [24]

By comparing catalytic and non-catalytic pyrolysis measurements, the addition of a zeolite significantly reduces the reaction temperature. In addition, the product distribution changes dramatically. While pyrolysis yields isomer-specific products as shown in R1-R4,[79, 100] catalytic pyrolysis generates virtually the same set of products, but at different conversion and selectivities. Fulvenone ketene is only a major product of catechol CFP, because vicinal OH groups favor dehydration (R2). Fulvenone can be seen as a shortcut in deoxygenation of benzenediols on H-ZSM-5 and explains the high reactivity of catechol, which proceeds similarly to the guaiacol experiments via R10-R12. Resorcinol and hydroquinone cannot form fulvenone and deoxygenate via dehydroxylation routes to yield phenol and benzene.

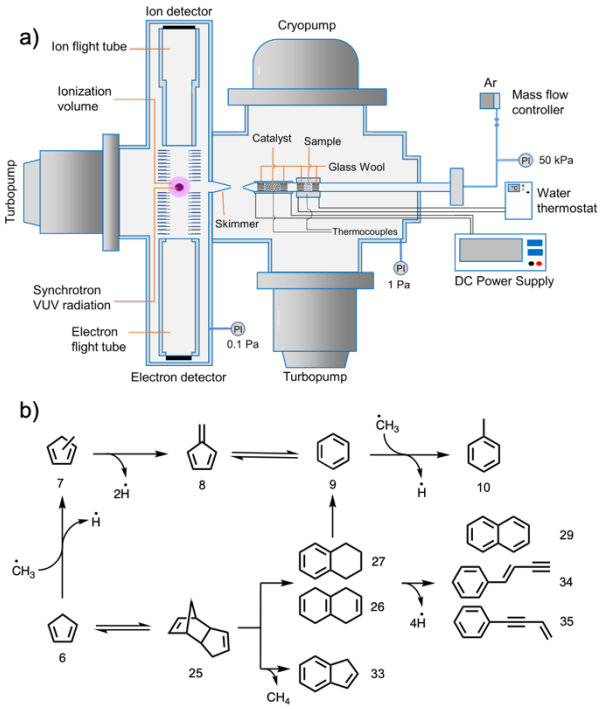

Figure 6 (a) Ambient pressure catalytic pyrolysis reactor at the VUV beamline of the SLS. Hot gases leave the reactor, form a molecular beam, which is skimmed and analyzed by imaging PEPICO techiques. (b) Initial PAH formation mechanism in catalytic pyrolyis of lignin model compounds. Reproduced from Ref [24] . Published by The Royal Society of Chemistry.

Pan et al. also pyrolyzed the primary decomposition products *p*-benzoquinone, cyclopentene-1-one, phenol, and cyclopentadiene over H-ZSM-5 to understand the decomposition chemistry of these specific intermediates.[24] It is known that naphthalene can be produced via dimerization and dehydrogenation of cyclopentadienyl radicals.[105] Intrigued by the large naphthalene abundance in phenol catalytic pyrolysis and guided by the insight that phenol may decarboxylate to cyclopentadiene, potential reaction pathways were investigated to yield polycyclic aromatic hydrocarbons (PAHs). Catalytic pyrolysis of freshly distilled cyclopentadiene is in part initiated by methylation and yields fulvene, benzene, toluene, and indene (see **Figure 6**b).[24] The large *m*/*z* 132, 130, and 128 signals point towards a second, probably more dominant reaction pathway. The *m*/*z* 132 ms-TPES (**Figure 2**b) revealed contributions of dicyclopentadiene formed in a Diels–Alder dimerization reaction as well as tetrahydronaphthalenes, similar to the product distribution of direct dicyclopentadiene pyrolysis. Besides naphthalene, the *m*/*z* 128 ms-TPES also showed contributions of butenylbenzenes pointing towards ring-opening in the *m*/*z* 132 isomers. In conclusion, cyclopentadiene does not only undergo stepwise methyl group additions in catalytic pyrolysis but also dimerizes to

naphthalene and other isomers after dehydrogenation (**Figure 6**b). This pathway is likely a major contributor to coke formation, which leads to prompt deactivation of the catalyst after only a few hours of operation.

The mechanistic pictures extracted from the py-PEPICO analysis of catalytic fast pyrolysis of lignin model compounds provide us with the missing puzzle pieces to complete our understanding of the pyrolysis mechanism. These insights can be relied on to take control of selectivity and increase the economic viability of CFP.

3.4. Alkane Functionalization

Natural gas is a key intermediate energy carrier during the transition from an oil-based economy to the renewables era thanks to its large availability and low environmental footprint in comparison to other fossil fuels if methane slip is avoided.[106] Its major components are methane, ethane, and propane, found in cavities in the Earth's crust either in gas reservoirs or together with crude oil. Currently, light alkane side products are mostly flared at oil wells, even though there are several ways to potentially valorize them. The most widespread method proceeds via steam reforming and syngas formation to yield olefins or liquid fuels, but this route is deemed neither economically nor environmentally viable.[25, 106] Alternatively, oxidative coupling of methane (OCM) over Li/MgO catalysts was found to be an efficient route to overcome the high stability of methane.[107] During methane activation, methyl radicals are produced[108-109] as also observed by Luo et al. using PIMS[107] by coupling a 4 torr catalysis reactor with a SVUV-PIMS system to measure mass and photoionization spectra. Using a novel, variable reactor interface,[107] they probed the evolution of reactive intermediates and stable products as a function of distance from the reactor surface. At low sampling distances close to the Li/MgO surface, they found only methyl radicals, ethylene, and ketene, which are formed catalytically. Upon increasing the distance from the catalyst, gas-phase reactions take over, and methylperoxy (CH_3OO), methyl hydroperoxide (CH_3OOH) as well as ethyl hydroperoxide (C_2H_5OOH) were detected.[107] They proposed a reaction network including the self-reaction of methyl and methylene on the catalyst surface to yield ethane and ethylene, respectively.[107]

Besides oxidative coupling, methane oxybromination into platform chemicals, such as methylbromide and dibromomethane are promising ways to upgrade methane. Paunovic et al. used PEPICO spectroscopy to show that the process is not surface-confined and gas-phase bromine and methyl radicals play a dominant role.[110] They used a mixture of CH_4, O_2, and HBr over EuOBr and $(VO)_2P_2O_7$ catalysts with a high-temperature reactor similar to the setup in **Figure 6**, and found a correlation between the appearance of methyl radicals and CH_3Br. Together with kinetic analysis and DFT calculations, a reaction mechanism was suggested, which is initiated by surface-catalyzed oxidation (see **Figure 7**) of HBr to atomic and molecular bromine. Gas-phase bromine radicals abstract hydrogen from methane to yield methyl radicals, which react with Br_2 to form CH_3Br.[110] PEPICO detection also contributed to assessing the structure–performance relationships of noble metal nanoparticles in methane oxyhalogenation.[111]

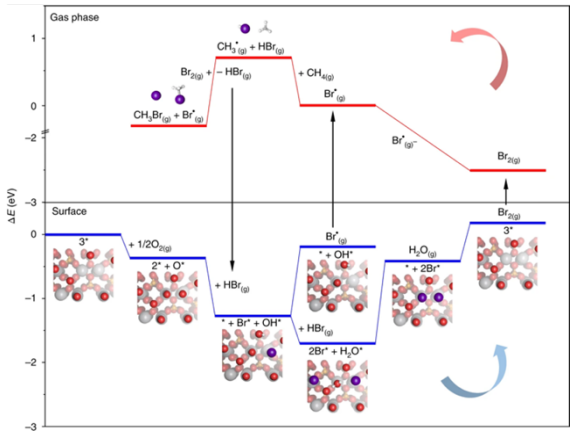

Figure 7 Summary of the reaction mechanism of the methane functionalization via oxybromination. Methyl and bromine radicals are the key players and were detected via PEPICO spectroscopy. Reproduced from Ref.[110].

The oxyhalogenation of ethane and propane is more challenging, as the reactivity increases, and more side reactions occur. Nevertheless, a clear halogen dependence (Cl vs. Br) was found for the $FePO_4$-catalyzed ethane activation mechanism. Oxychlorination follows a surfaced-confined reaction pathway, without liberation of chlorine radicals into the gas phase, with superior, catalyst-driven selectivity. This selectivity advantage is lost for X = Br, because gas-phase radical reactions take over, leading to decomposition and combustion reactions.[112] A similar trend was also observed for propane oxyhalogenation, at dramatically increased reaction complexity. Besides C–H activation, yielding bromopropanes and propene (green pathways in **Figure 8**a), dehydrohalogenation processes yielding bromopropenes (**Figure 8**a, light blue), combustion reactions (**Figure 8**a, red), coke pathways (**Figure 8**a, black), and decomposition reactions were also observed.[113] The operando PEPICO approach delivered detailed mechanistic insights into propane oxybromination chemistry. Photoion mass-selected threshold photoelectron spectra enable isomer-selective assignment of rate-

limiting reactive intermediates. For instance, 2-propyl radicals were found as major spectral contribution of the *m/z* 43 ms-TPES (**Figure 8**b) with the help of reference spectra by Holzmeier et al.[114] Although the ms-TPES is not structured, owing to the large geometry change upon ionization and the resulting unfavorable Franck–Condon factors for the origin transition, it still allowed for a robust assignment. This spectral evidence confirms that the thermodynamically more stable 2-propyl radical is clearly favored over 1-propyl, further corroborated by the detection of 2-propylbromide. Moreover, the ms-TPES of the *m/z* 41 decomposition product agrees well with the literature spectrum of the allyl radical, while the cyclopropyl contributions are negligible.[115-116] Ion velocity map imaging allows for the discrimination of the background gas from the molecular beam component (**Figure 8**b). The latter possesses an anisotropic and laterally narrow speed distribution, while the rethermalized, scattered gas in the vacuum chamber shows a broad and angularly isotropic spot, indicative of the room-temperature Boltzmann distribution (see chapter 2). The molecular beam signal intensity is a sensitive measure for the source alignment, which greatly helps radical detection in a collision-free environment (**Figure 8**c). Thanks to the advanced PEPICO detection method, reactive species and stable products could be detected sensitively upon propane oxybromination over $CrPO_4$, and the mechanism is summarized as follows: 2-propylbromide is formed via gas-phase reaction of bromine with propane and subsequent Br addition.[113] A dehydrobromination yields propene, but side reactions, such as additional hydrogen abstractions form allyl as well as propargyl radicals, which limit the selectivity of the oxybromination in comparison with oxychlorination. The stepwise hydrogen abstraction shows a clear shift to high temperatures favoring the resonance-stabilized propargyl radicals, which can dimerize to C_6H_6 isomer such as fulvene (c-C_5H_4=CH_2) and benzene, also observed during this reaction. Both five- and six-membered rings are coke precursor molecules par excellence and responsible for the deactivation of the catalyst.

Recent advances in applying PEPICO as an advanced analytical tool to detect reactive intermediates in the gas phase unveiled reaction mechanisms in biomass conversion and catalytic alkane valorization. These mechanistic insights can be relied on to develop viable strategies for producing sustainable fuels and fine chemicals not only from biomass but also from abundant natural gas, which may otherwise be flared. However, we not only have to make energy carriers, but also understand their application, i.e., the combustion mechanism. In the following, we will detail selected combustion chemistry aspects and the contributions of photoionization and PEPICO detection to our understanding of them.

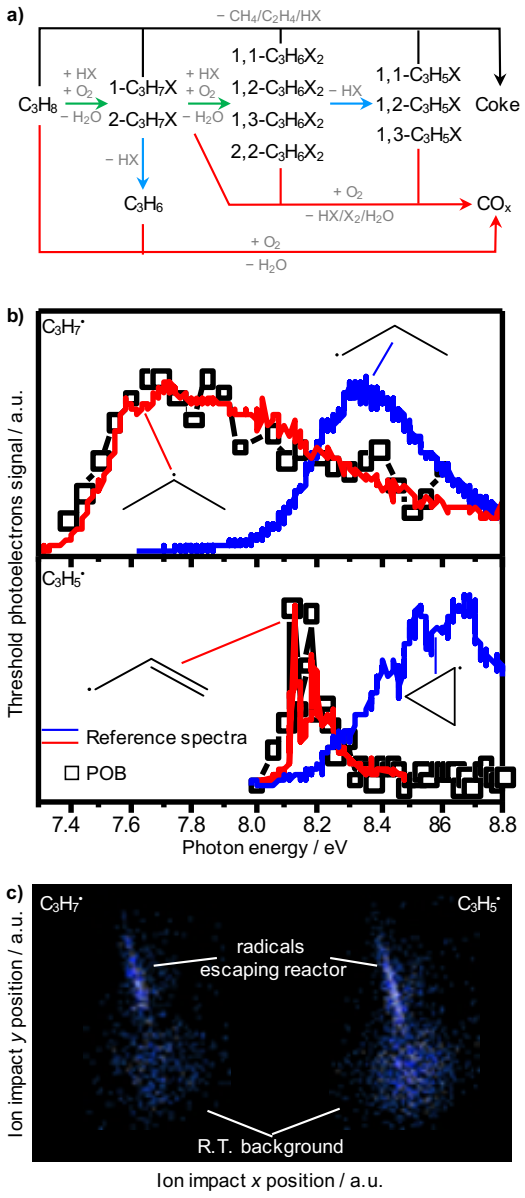

Figure 8 a) Oxyhalogenation of propane. Besides the desired product propene, C_3H_6, combustion, decomposition and coke formation reactions are observed. b) Experimental ms-TPES of C_3H_7 (*m/z* 43), exclusively assigned to 2-propyl radicals thanks to the reference data of Holzmeier et al.[114] The lower trace shows evidence for allyl radicals (C_3H_5, *m/z* 41) formed upon decomposition of propene via hydrogen abstraction of abundant bromine atoms. c) Velocity map images (VMI) of both allyl and propyl radicals. Two features are apparent. While the broad velocity distribution (bottom) results from rethermalized background gas in the vacuum chamber, the narrow part (upper) is indicative for radicals leaving the catalytic reactor, forming a molecular beam. Reprinted (adapted) with permission from Ref. [113]. Copyright 2020 American Chemical Society.

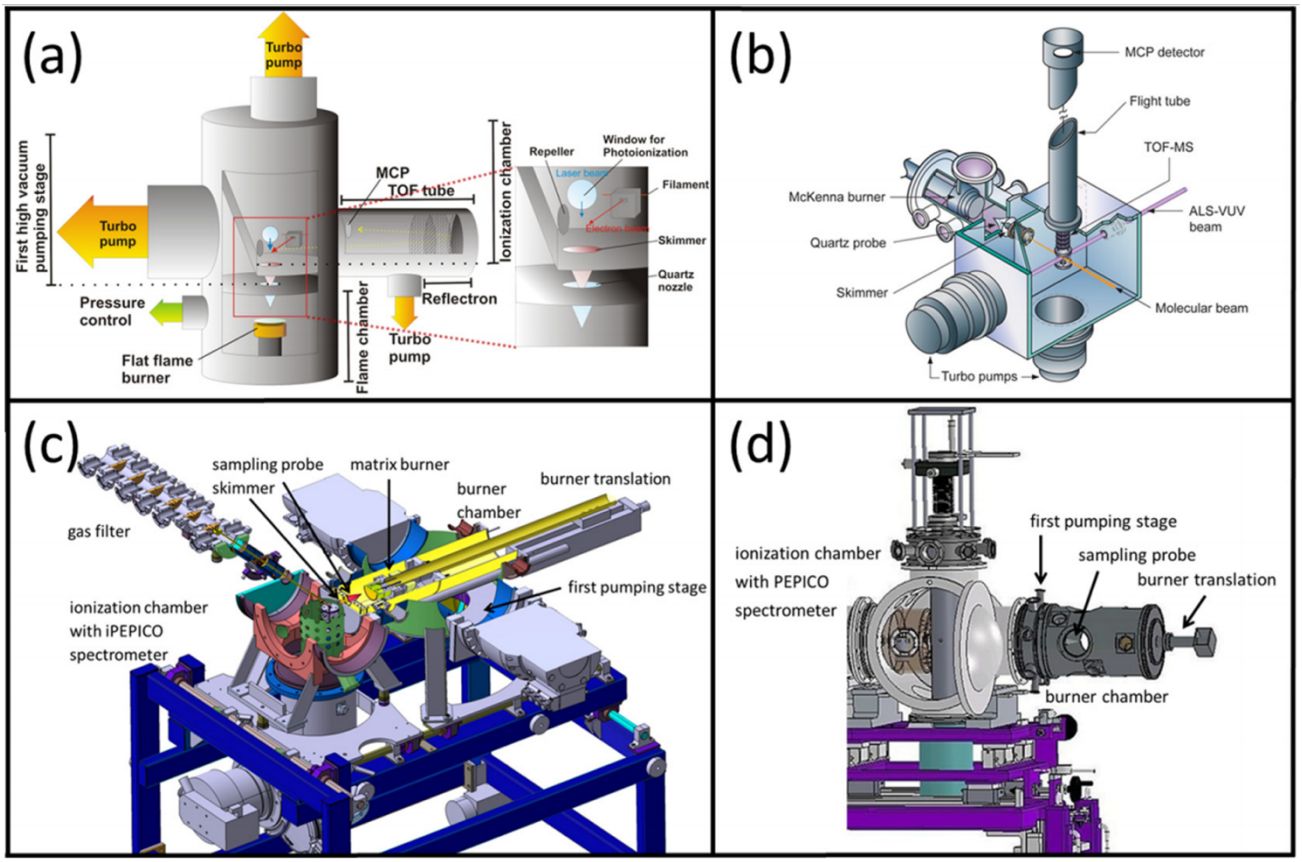

Figure 9 Comparison of combustion experiments for obtaining speciation data. a) EI-MBMS (Bielefeld University now at DLR Stuttgart), (b) PI-MBMS (ALS), and PEPICO-instruments at c) the SLS and d) SOLEIL synchrotron. Reprinted from Ref. [70], Copyright 2015, with permission from Elsevier.

4. Clean Combustion

The next step after biomass upgrading and fuel synthesis is recovering the stored chemical energy ecologically and economically. Thermal conversion processes will likely remain the main method to convert the chemical energy to heat and finally electricity, because they are proven to be robust and reliable.[117] The current research goals include controlling global combustion parameters and pollutant formation by understanding the underlying processes and enabling better numerical models with predictive value.[118]

For the development of such combustion models, experimental validation data are needed, especially quantitative species data as a function of process parameters, e.g., pressure, temperature, or reaction time. For example, detailed isomer-resolved speciation data from an anisole flame measured by PEPICO spectroscopy was used for validation of a new anisole kinetic reaction mechanism by Yuan et al.[119] Mass spectrometric combustion diagnostics are now standard techniques to provide quantitative speciation data in reactive environments. They give a broad overview of the species in the mixture without any prior knowledge about the complex chemistry. Typically, a gas sample is extracted from the combustion experiment and reactive species are preserved thanks to the rapid reduction in pressure and molecular beam formation. This technique is called molecular-beam mass spectrometry (MBMS) and has been coupled with electron ionization (EI) and photoionization (PI) methods. The latter is well established with numerous sophisticated experiments around the globe and particularly useful for screening purposes[120] The benefits of photoionization over electron ionization are isomer selectivity and suppression of dissociative ionization, as pointed out in chapter 2. Limitations are still present, especially in the sensitivity towards radical species and the ability for distinct isomer identification. The chemical model development by Kathrotia et al. for ethylene glycol, which serves as a pyrolysis oil surrogate for common bio-syncrude oil, is a typical example: The available experimental data did not distinguish ethenol (CH_2CHOH) from acetaldehyde (CH_3CHO). As a result, the major decomposition product by water elimination from ethylene glycol during the oxidation was elusive, which limited the capabilities of the model.[121] In the mid-2010s, experimental approaches at the synchrotrons SOLEIL[122] and SLS[123] were developed to apply iPEPICO spectroscopy in low-pressure flames. Thanks to superior isomer specificity and sensitivity towards radicals, distinguishing between ethenol and acetaldehyde became, for instance, readily possible.[120] The resulting data support initial mechanism development because unexpected intermediates can be detected and reaction pathways identified. In addition, the quantitative composition analysis with isomer-resolution as a function of process parameters is often a stringent test for model simulations.

4.1 Combustion Diagnostics With PEPICO Spectroscopy

Following these pioneering approaches, advancements followed shortly after as Felsmann et al. presented and discussed the use of double-imaging i^2PEPICO in flames.[70] Their

multiplexed approach was enhanced by (velocity map) imaging not only the electrons but also the ions in a double-imaging PEPICO scheme (i^{2}PEPICO). Felsmann et al. also compared state-of-the-art MBMS instruments using electron ionization, VUV photoionization experiments, and PEPICO diagnostics at the SLS and the SOLEIL synchrotron. Both EI-MBMS and PI-MBMS are based on the detection of ions only. The additional spectroscopic dimension of photoelectron detection to fingerprint the cation by photoelectron spectroscopy is, however, only possible through electron/ion coincidence techniques (**Figure 9**, Table 1).[70]

Table 1: Comparison of flame diagnostics experiments Felsmann et al.[70] Reprinted from Ref. [70], Copyright 2015, with permission from Elsevier.

	Bielefeld	ALS	SLS	SOLEIL
Burner				
Matrix material	Bronze	Stainless steel	Bronze	Bronze
Diameter	6.4 cm	6.0 cm	6.0 cm	6.5 cm
Flame sampling system				
Probe material	Quartz	Quartz	Quartz	Quartz
Probe angle	25°	Tapered 25–40°	40°	25°
Orifice diameter	500 µm	500 µm	500 µm	500 µm
Distance probe/skimmer	~1 cm	~1 cm	~3 cm	~1 cm
Distance probe/ionization	22 cm	40 cm	14 cm	57 cm
Detection	ToF-MS	ToF-MS	PEPICO	PEPICO
($m/\Delta m$)	4000	3500	300	300
Ionization method				
Source	Filament	Undulator	Bending magnet	Undulator
Ionizing particle	Electron	VUV photon	VUV photon	VUV photon
#electrons/pulse #photons/s	1.00E+09	1.00E+14	1.00E+12	1.00E+14
Energy range	5–70 eV	7.4–30 eV	5–30 eV	5–40 eV
Energy resolution ($E/\Delta E$)	1 eV (FWHM)	0.03 eV @10 eV	0.001 eV @10 eV	0.00008 eV @16 eV
Accessible data				
Burner profiles	Yes	Yes	Yes	Yes
PIE curves	No	Yes	Yes	Yes
Photoelectron spectra (PES)	No	No	Yes	Yes
Mass-resolved PES	No	No	Yes	Yes
Time/dataset	12 h	24 h	24 h	24 h

The imaging capabilities of i^{2}PEPICO detection were recently demonstrated by Krüger et al.[72] at the SLS by solving a long-standing challenge in MBMS quantification of OH radicals in flames. Because the observed OH ion signals are often an order of magnitude lower than expected and water can fragment to OH and may contribute to the radical signal in the same *m/z* channel, MBMS is considered less reliable than LIF for OH detection.[124] Using ion velocity map imaging, the signal from OH in the molecular beam and in the scattered background could be distinguished as shown in **Figure 10**. The relative abundance of OH in the molecular beam with respect to the total ion signal was found to be an order of magnitude larger than in the thermalized background. It can be concluded that OH radicals do not survive wall collisions with the vacuum chamber. Stable molecules do not suffer from the same loss mechanism. Although some of the investigated radicals, such as methyl and hydrogen atoms, appear in the thermalized background, quenching of reactive species cannot be fully ruled out, which may lead to discrepancies during quantification and model evaluation. The OH/H_2O ratio is truly affected and results in OH mole fractions that are an order of magnitude too low in the quantitative analysis. Using the imaging capabilities of i^{2}PEPICO spectroscopy this long-lasting challenge in OH quantification in MBMS could be resolved by only using the signals of the apparent molecular beam. Krüger et al. could clearly show that there is no species dependent discrimination for the scattering process by comparing stable combustion species like water, methane, and ethane. A beam factor was introduced as shown in **Figure 10** which is defined as the ratio between molecular beam fraction and total ion signal.

This beam factor is comparable for the all species except OH radicals. It follows from these observations, that the ratio of the total OH signal to the total ion signal can serve as a measure of the quality of the molecular beam alignment of any flame-sampling molecular-beam mass spectrometer.

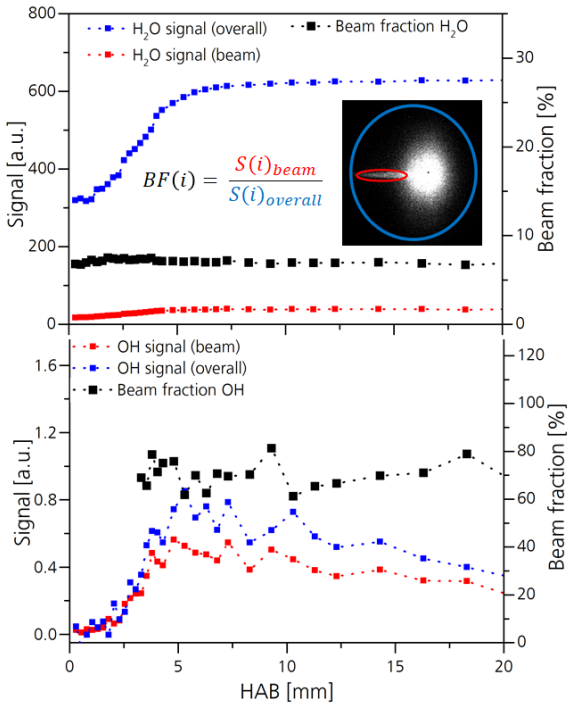

Figure 10 Advantage of the double imaging capabilities of i^{2}PEPICO: The H_2O photoion signal as function of height above the burner with the total ion signal (blue) vs the signal from the molecular beam (red) and the constant ratio (black). The bottom graph shows the signal of the OH radical, which has no prior wall collisions compared to the H_2O signal. Both beam fraction ratios are constant indicating signal loss due to wall collisions for stable species. Data taken from Ref [72].

Due to the chemical complexity in flames, numerous constitutional isomers must be taken into account. Such isomers have the same molecular formula but different structures. They can have very different chemical behavior and influence the further reaction steps in combustion. Unfortunately, the number of possible isomers increases exponentially with increasing molecular mass.[125] The number of possible isomers is typically manageable for C_3 or C_4 hydrocarbons. For example, there are four different isomers of butyl radicals. On the other hand, more than a hundred isomers are principally possible for C_7 hydrocarbons.[16] Of course, not all of them occur in flames and many can be excluded through analytic expertise. Measuring mass-selected threshold photoelectron spectra (ms-TPES) adds a second

analytical dimension to the established isomer specific detection strategy by photoionization spectra.

An example is given for the detection of C_9H_8 isomers in a *m*-xylene flame from the work of Bierkandt et al. shown in **Figure 11**.[126] Indene has the lowest ionization energy and can be identified with both methods clearly, but the assignment of thresholds at higher photon energies can be difficult because changes in the slopes of the photoionization efficiency curves do not necessarily correlate with ionization thresholds of other isomers.[127] In contrast, *m*-methylphenylacetylene and 3-phenylpropyne can clearly be identified as peaks in the ms-TPES (see also **Figure 11**). The cited flame experiment uses stationary flow conditions, and the steady operation allows for integration times long enough to obtain a good signal-to-noise ratios. However, beam time at synchrotrons is often limited so that detailed fingerprint spectra cannot be acquired for all species in a flame.

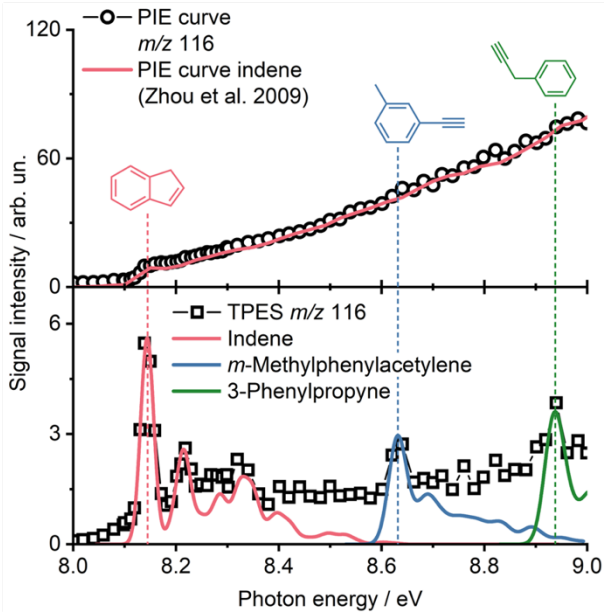

Figure 11 Identification of isomeric combustion species by photoelectron spectra and photoionization efficiency curves. Data taken from Ref.[126].

iPEPICO spectroscopy in combination with tunable synchrotron radiation for flame-sampling molecular-beam mass spectrometry experiments can provide detailed chemical speciation data and help to answer specific questions. Selected examples of how PEPICO experiments have advanced our understanding of crucial steps with the potential of controlling combustion reactions are presented below.

In the following, we discuss how advanced PEPICO detection contributes to our understanding of the underlying chemical reactions in flames. Specifically, we review examples at different stages of the combustion process, starting with early steps, such as ignition and formation of the first radical and oxygenated species. Then, mechanistic aspects of pollutant formation will be detailed.

4.2 Kinetic Tools

The results from different kinetic experiments often need to be combined to generate a consistent picture of the reaction pathways of the thermal decomposition of a fuel or the formation of pollutants. For example, it is useful to first identify unimolecular fuel destruction pathways in a pyrolysis reactor (as described in chapter 4.3.1) and then try to find the same reaction patterns within the complex reaction network in a flame from the appearance sequence and abundances of the expected intermediates. Flow reactors take an intermediate position between the pyrolysis experiments and the flame experiments with regard to the complexity of the observed chemistry and the interaction between fluid flow and the chemistry.[68] In the ideal pyrolysis experiment, the chemical interaction between different molecules is limited by dilution with an inert gas to such an extent that only unimolecular reactions occur. In a jet-stirred or well-stirred reactor, gases are mixed and heated very rapidly, so that the composition of the mixture depends only on the pressure, temperature, and residence time in the reactor (see chapter 4.3.2). Typically, two of these variables are fixed and the composition of the reacting mixture is measured as a function of the third variable. Jet-stirred reactors (see **Figure *12*a**), based on the design proposed by Matras and Villermaux[128] are often used to investigate controlled fuel conversion. They are pressurized fused-silica spheres with an inlet, an outlet, and an injection cross in the center. The injection cross typically has four small nozzles which are directed in the four cardinal directions. Using an appropriate volume flow rate this structure leads to turbulent mixing of the entering reactants and, isothermal conditions in the reactor. Consequently, jet-stirred reactors allow the investigation of the species pool formed during fuel conversion,

including radicals, under well-controlled boundary conditions and can provide high-accuracy data for model validation.

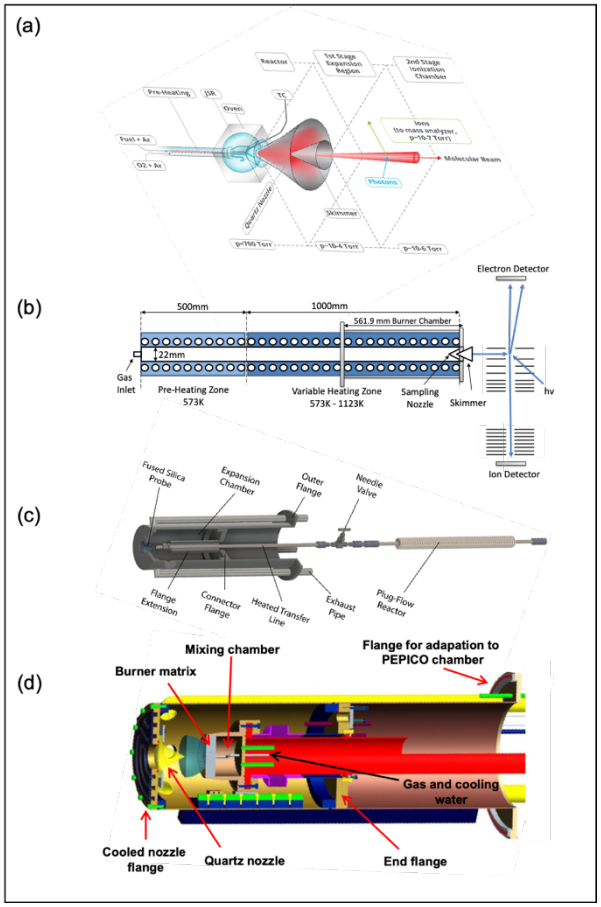

Figure 12 Overview of the kinetic tools for combustion studies with PEPICO. Reproduced from Refs. [129-130] Reprinted from Ref. [77] with permission of AIP Publishing.

The mixture composition at the outlet of a tubular flow reactor (see **Figure *12***b,c) also changes as a function of pressure, temperature, and residence time[18, 131-134]. A typical flow reactor consists of a long, heated tube made from an inert material. The residence time depends on the position in the tube, adding an extra experimental dimension to the simulations. Tubular flow reactors have the experimental benefit that less total gas flow is needed, which makes it easier to realize experiments at higher pressures compared to a JSR. In contrast to the pyrolysis microreactor (see section 5.2), intermolecular reactions are much more pronounced in both types of flow reactors.

In ideal premixed, laminar flames (see **Figure *12***d), the composition only changes as a function of distance from the burner surface (see HAB scans below) and the flame temperature. The flames are stabilized on a cooled burner by heat transfer to the burner. For a stable flame, the feed gas velocity has to match the flame speed and stable flames cannot be obtained for all equivalence ratios of interest. Speciation experiments in flames are typically performed at low pressures to reduce the flame speed and allow sampling from the flame with good spatial resolution.[125] Flame simulations also take, e.g., diffusion, convection, and heat transfer into account. The chemical complexity increases because flames reach much higher temperatures than can be achieved in reactor experiments. As a result, more radicals are formed and the experiments allow the investigation of the complex interplay between the fuel decomposition and the radical pool on the one hand and pollutant formation from combustion intermediates on the other.[77]

4.3 Ignition Chemistry

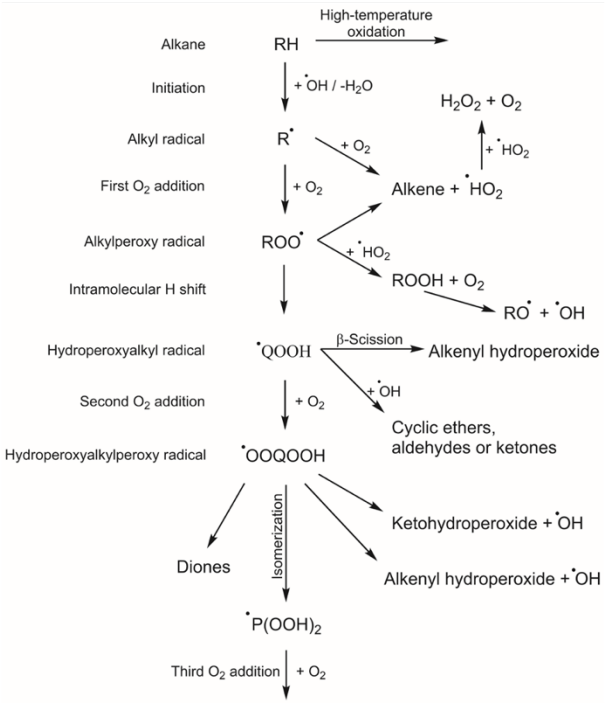

Figure 13 Low-temperature oxidation scheme of alkanes (adapted from [129] and taken from [135]).

To reduce NOx and soot formation in engines, advanced combustion strategies often involve relatively low temperatures, e.g., homogeneous (HCCI) or premixed charge compression ignition (PCCI). Both techniques rely on the autoignition of the fuel, which is mostly determined by chemical kinetics. Controlling autoignition timing and process operation is still a challenge.[136] For example, the timing of autoignition may be influenced by intermediate compression strokes and chemically or thermally, e.g., by additives or exhaust gas recirculation, respectively. These methods influence the reactivity of the mixture and require a profound understanding of the changes in ignition chemistry. Simulations, using detailed and accurate reaction mechanisms, can help gain predictive control of such processes. The first step of bimolecular decomposition and combustion processes is mostly the abstraction of atomic hydrogen by small radicals, such as O, OH, or H, forming a fuel radical. In some fuels, namely 1-hexene[137] or the acyclic monoterpene myrcene (7-methyl-3-methylideneocta-1,6-diene.),[138] the initial decomposition is initiated by a unimolecular dissociation of a C–C bond. While in a high-temperature environment, H-abstraction is followed by β-scission to form smaller species, e.g., alkenes and alkyl radicals in case of alkane fuels, O_2 is added to the fuel radical at low temperatures forming the alkylperoxy radical as shown in **Figure 13**. Hydroperoxyalkylperoxy radicals (OOQOOH) are finally formed by a reaction sequence consisting of an intramolecular H-shift intermediately yielding

hydroperoxyalkyl radicals, which add a second oxygen molecule.[129, 139] Typical branching agents of the OOQOOH radical are ketohydroperoxides, alkenyl hydroperoxides, and diones.

In complex fuels, the reaction sequence strongly depends on the isomeric forms of fuel radicals. Consequently, the detection of the different fuel radical isomers provides insights into the initial H-abstraction pathways. All subsequent reactions depend on this isomeric ratio and the predictive value of a reaction mechanism regarding pollutant formation can be compromised if the initial reactions are not captured correctly. In addition, an accurate prediction of the formation and consumption of low-temperature reaction products, such as hydroperoxides, is crucial to determine the moment of autoignition, which in turn plays a central role when developing new combustion strategies. In particular, OOQOOH and their derivatives are one of the key species for the low-temperature chain-branching mechanism.

In the following sections, we address the formation of fuel radicals and hydroperoxides in a flame and that of ketohydroperoxides in a jet-stirred reactor.

4.3.1 Fuel Radicals

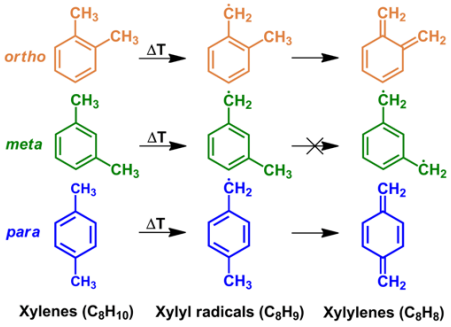

Figure 14 Decomposition pathways of xylenes (modified from Ref. [22]).

Xylenes are dimethyl-substituted aromatic hydrocarbons, which come in three isomers: *ortho*-, *meta*-, and *para*-xylene. They are naturally found in crude oil and are co-produced by catalytic reforming of naphtha. The monoaromatic xylene isomers as well as benzene, toluene, and ethylbenzene belong to the BTEX chemicals. The amount of BTEX in typical gasoline blends is up to 20%, of which *m*-xylene accounts for the highest fraction and improves the antiknock properties of the fuel.

In 2009, da Silva and coworkers have studied the decomposition of xylyl radicals theoretically in pyrolysis and oxidation of xylenes.[140] Their results suggested that the hydrogen-loss product, C_8H_8, the *m*-xylylene, is not the decomposition product of the *m*-xylyl radical (see

Figure 14).

The *m*-xylyl radical decomposes to *p*-xylylene and perhaps to the less stable *o*-xylylene over isomerization reactions. Hemberger et al. investigated the pyrolysis of the xylyl radicals experimentally using iPEPICO spectroscopy at the Swiss Light Source.[22, 141] Xylyl bromides were used as precursors to selectively generate the xylyl radical isomers in a pyrolysis reactor (see **Figure 3**d), mimicking the unimolecular decomposition conditions. Each xylyl radical isomer decomposes by hydrogen atom loss to yield *p*-xylylene, so the *m*-xylyl radical must undergo a rearrangement to *p*-xylyl as suggested previously by da Silva et al.[140] Bierkandt et al. investigated the isomerization of the *m*-xylyl radical in a rich *m*-xylene flame by iPEPICO spectroscopy.[126] The *m*-xylyl radical can be formed from the fuel by hydrogen abstraction on one of the two methyl groups. The threshold photoelectron spectrum of the *m*/*z* 105 in **Figure 15** identifies the *m*-xylyl radical as the dominant fuel radical, as corroborated by the Franck–Condon simulation. The peak at 7.05 eV was assigned to a hot band, which was also observed in the pyrolysis measurements by Hemberger et al. and is underestimated by the simulation. The adiabatic ionization energy of the *m*-xylyl radical is 7.11 eV. The other two characteristic peaks result from a bending vibration. A comparison of the photoionization spectra for all three xylyl radicals from the pyrolysis experiments shows that the best fit to match the measured curve from the flame is the ratio of *p*-xylyl to *m*-xylyl radicals of 15 to 85. This clearly shows that the *p*-xylyl radical is also formed in low concentrations besides the *m*-xylyl radical. The increase in the photoionization efficiency curve also clearly matches the adiabatic ionization energy of the p-xylyl radical at 6.94 eV. This observation can be explained if the isomerization from the *m*-xylyl to the *p*-xylyl radical takes place not only in the pyrolysis, but also in the flame.

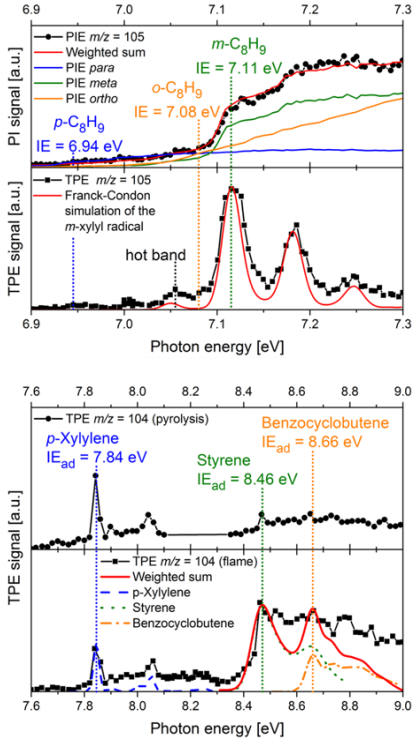

Figure 15 Threshold photoelectron spectrum and photoionization spectrum of *m*/*z* 105 in comparison with a Franck–Condon simulation of the *m*-xylyl radical and photoionization spectra from pyrolysis experiments (upper trace). Threshold photoelectron spectra of *m*/*z* 104 in pyrolysis and flame experiments (lower trace). Reprinted from [126] Copyright 2017, with permission from Elsevier.

The formation of the *ortho* isomer can only be proven by detection of the hydrogen loss to yield C_8H_8. Benzocyclobutene, styrene, and *p*-xylylene can be unequivocally identified in the flame and the observed C_8H_8 species pool agrees well with pyrolysis experiments (see **Figure 15**, lower trace). The *m*-xylyl radical was clearly identified as a fuel radical and it does not form

the corresponding *m*-xylylene, but rather undergoes a rearrangement to the other two xylyl isomers prior to hydrogen loss. *p*-Xylylene is then formed from the *p*-xylyl radical, while benzocyclobutene is formed from the *o*-xylyl radical via *o*-xylylene. Even if the *o*-xylyl and *o*-xylylene were not directly detected, the isomerization through the formation of benzocyclobutene could still be confirmed. Thus, the pyrolysis of the *m*-xylyl radical and the combustion of *m*-xylene in the flame confirm the statements made by da Silva et al. on the isomerization of the *m*-xylyl radical. This example demonstrates how theory and experiment go hand in hand to prove a proposed reaction pathway in a progressively more complex reactive environment. As shown by Bierkandt et al., the simulated mole fraction profiles of the *m*-xylyl radical from five current combustion models significantly overestimate the measured concentration. It was suggested that the isomerization reactions of the *meta*-xylyl radical to *ortho*- und *para*-xylyl radicals should be considered in future models to properly cover the formation of the observed C_8H_8 isomers *p*-xylyene and benzocyclobutene in the *m*-xylene flame. Thus, investigating elementary reactions via pyrolysis can support the interpretation of flame chemistry and help to generate predictive combustion models.

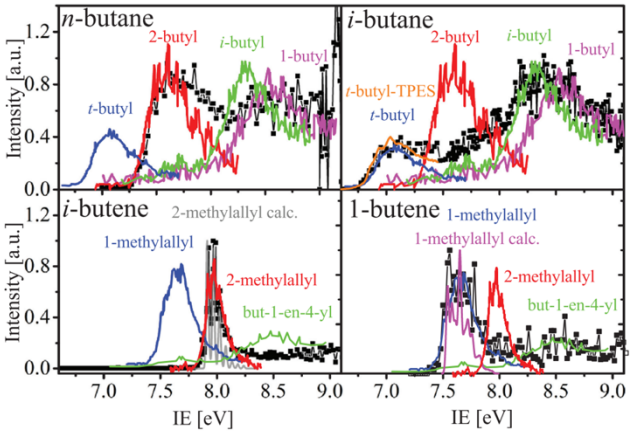

Figure 16 Top: ms-TPE spectra of *m*/*z* 57 (C_4H_9) from n-butane- (left, HAB = 0.5 mm) and *i*-butane-doped (right, HAB = 0.75 mm) flames together with reference PE spectra of 1-butyl, 2-butyl, *i*-butyl, and *t*-butyl as well as a measured TPE spectrum of t-butyl. Bottom: ms-TPE spectra of *m*/*z* 55 (C_4H_7) from the *i*-butene- (left, HAB = 0.75 mm) and 1-butene-doped (right, HAB = 0.5 mm) flames with reference spectra of 2-methylallyl, but-1-en-4-yl, and 1-methyllallyl and calculated TPE spectra of 1-methylallyl and 2-methylallyl. Reprinted from Ref. [142] Copyright 2018, with permission from Elsevier.

As shown above, PEPICO is well suited to gain in-depth knowledge of the initial fuel destruction chemistry. While theoretical studies and shock tube experiments are plentiful, experimental data on fuel radicals in flame environments are scarce. Schenk et al.,[143] Dias et al.,[144] and Oßwald et al.[145] reported molecular-beam mass spectrometric work on low-pressure, premixed flames of different butene and butane isomers. Despite the comprehensive composition analysis of the flames, these studies were not able to detect the initial fuel radicals. The H-abstraction channels of these fuels and their ratios in flames were finally reported by Krüger et al. using iPEPICO in a systematic approach to investigate C_4 fuels with different structures.[142] The measurements were performed with the iPEPICO setup at the SLS in a low-pressure hydrogen flame at 40 mbar doped with different alkanes (ethane, *n*-butane, *i*-butane) and alkenes (tetramethylethylene, 1-butene, *i*-butene). The flame conditions were chosen to keep the carbon flow constant and achieve comparable temperatures in all flames. The study reports abstraction reactions of primary, secondary, tertiary, and vinylic H atoms by a systematic, direct semiquantitative approach. **Figure 16** shows the measured ms-TPE spectra along with the reference photoelectron spectra of the expected fuel radicals. Based on these, up to seven dominant C_4 radicals could be identified in the flames.

The analysis of the complete dataset shows that the direct H-abstraction without rearrangement is the major reaction pathway for the formation of fuel radicals in these hydrogen-rich flames.

Figure 17 summarizes the identified pathways for the six investigated fuels. The relative H-abstraction ratios for *n*-butane, *i*-butane, and 1-butene were determined and give a clear tendency, in agreement with the expectations from theoretical studies: tertiary > primary; secondary > primary; allylic > non-resonance-stabilized form. Vinylic radicals were not observed.

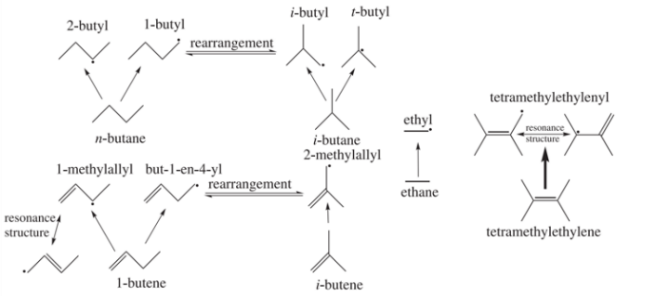

Figure 17 Observed reaction pathways of primary, secondary, and tertiary and vinylic H atom abstraction in flames. Reprinted from Ref. [142] Copyright 2018, with permission from Elsevier.

In addition to the identification, the peak positions of the HAB-profiles of radicals formed by hydrogen abstraction or addition to the fuel molecules show faster H-abstraction for unbranched alkanes and alkenes than for branched fuels and faster H-addition than H-abstraction, respectively.

The comparison of flame simulations using state-of-the-art reaction mechanisms and the experimentally observed branching ratios provides a stringent test of the accuracy of these rate constants. The PEPICO measurements must be complemented by advanced methods to determine rate constants of elementary combustion reactions based on rate constants measurements, e.g., in shock tubes, or calculations (see chapter 5.1), as these determine the branching ratios of the fuel radicals.

4.3.2 Peroxy and QOOH Radicals

In the last decade, advanced diagnostic tools such as PIMS have contributed significantly to the detection and quantification of the low-temperature species involved in the sequence shown in **Figure 13**. These oxygenated reactive species are thermally labile, which makes their detection in flames highly demanding.

Thus, it is not astonishing that these species were first detected in jet-stirred reactors. [128]

The first PIMS study of low-temperature speciation data was presented by Battin-Leclerc et al.[146] They identified methyl, ethyl, and butyl hydroperoxides, as well as C_4 ketohydroperoxides (KHP) during the low-temperature oxidation of *n*-butane using a jet-stirred reactor and SVUV-PIMS at the National Synchrotron Radiation Laboratory in Hefei. At the ALS, Moshammer et al. studied the low-temperature chemistry of dimethyl ether using a jet-stirred reactor coupled to an MBMS system.[147-148] They identified the ketohydroperoxide hydroperoxymethyl formate ($HOOCH_2OCHO$) and made the first step towards its quantification using computed photoionization cross sections. Further PIMS studies, focusing on the low-temperature chemistry of alkanes up to *n*-heptane were summarized by Herbinet et al.[149] and Wang et al.[129] Generally, the higher the molecular weight of the fuel, the more difficult it is to determine the isomeric distribution of low-temperature products using only photoionization spectra as they tend to exhibit similar features as the molecular size grows.

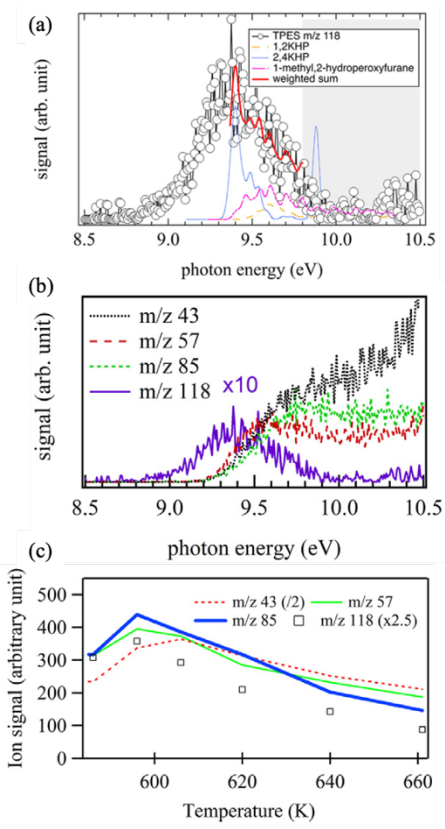

Figure 18 a) Comparison between the measured ms-TPE spectra for *m/z* 118 at 606 K and φ = 1/3, b) for *m/z* 118, 85, 57, and 43, c) ion signal at 10.5 eV as a function of temperature (numbers in the graphs indicate factors by which the signal is multiplied/divided). Reprinted from Ref. [150], Copyright 2020, with permission from Elsevier.

Bourgalais et al. studied the low-temperature oxidation of *n*-pentane in a jet-stirred reactor operated at atmospheric pressure using the i²PEPICO endstation at the DESIRS beamline of the SOLEIL synchrotron.[151] *n*-Pentane serves as a well-suited surrogate for diesel and gasoline, as it has a pronounced low-temperature chemistry, representative for that of higher molecular weight fuels.[151-152] Although the low-temperature oxidation of *n*-pentane was studied before utilizing PIMS and gas chromatography, the additional information obtained from ms-TPES helped to determine a more accurate estimate of the branching ratio of the pentene isomers 1-pentene and 2-pentene.[151] Also, an ms-TPES of the alkenylhydroperoxide but-1-enyl-3-hydroperoxide, was measured for the first time in this study. The formation of but-1-enyl-3-hydroperoxide was confirmed by excellent overlap between the calculated and the measured ms-TPES. The authors stated that hot bands or other conformers may be the reason for the earlier onset of the threshold photoelectron signal. Nonetheless, the contribution of the isomer but-2-enyl-1-hydroperoxide could be ruled out as the calculated PES showed an intense electronic band between 10.3 and 10.4 eV which was not observed experimentally.

In their follow-up paper,[150] the group focused on the identification of the isomeric distribution and fragmentation patterns of ketohydroperoxides formed during the low-temperature oxidation of *n*-pentane. The fragmentation patterns, i.e., the specific contributions of every fragment to the signals at the corresponding *m/z* are needed to quantify KHPs using total ionization cross-sections.[148] For the identification of the formed KHPs, the authors calculated the adiabatic ionization energies and the photoelectron spectrum of the 10 possible KHPs and compared them with the experimental ms-TPES at *m/z* 118. Half of the possible KHPs show features above 9.8 eV, whereas the experimental ms-TPES showed a significant signal drop above 9.4 eV due to fragmentation. Consequently, the authors assume that the corresponding cations of these KHPs are unstable and neglected them in the assignment. The best fit of the experimental ms-TPES is represented by the weighted sum of the calculated PES for 1-methyl-2-hydroperoxyfurane, 1,2KHP, and 2,4KHP (see **Figure 18**a) with a branching ratio of 0.3:0.1:1, differing from those obtained by kinetic simulations using the detailed model of Bugler et al.[153] **Figure 18**a shows that the red part of the ms-TPES (below 9.3 eV) cannot be explained by the FC calculated spectrum. The authors mention hot-band contributions as the most likely reason for this deviation. With respect to the fragmentation pattern, the authors identified three major fragments of the C_5 KHP, i.e., *m/z* 85, 57, and 43 by comparing their energy- and temperature-dependent signals (see **Figure 18**(b and c)). **Figure 18**b shows the ms-TPES of the fragments at *m/z* 118 plotted against photon energy and a fixed temperature, indicating the onset of fragmentation at 9.2 eV, corresponding to the onset of the signal drop for *m/z* 118. Additionally, **Figure 18**c shows the same temperature dependence for the ion signal of the assumed fragments at *m/z* 85, 57, and 43 and the C_5 KHP at *m/z* 118. According to the authors, the further signal increase for *m/z* 43 in **Figure 18**b and the shifted maximum of the ion signal for *m/z* 43 in **Figure 18**c are mainly due to the fragmentation of acetone. Considering all these fragments in the evaluation of the KHP mole fraction for the previously published PIMS experiments by Rodriguez et al.,[154] the deviation between

simulations and experiments could be reduced from a factor of 125 to a factor of 12.

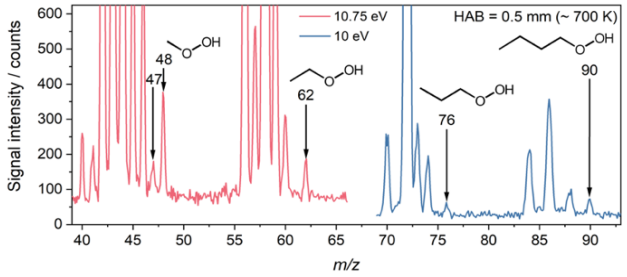

Figure 19 Mass spectrum from the preheat zone of an *n*-butane/H_2 flame measured at two different photoionization energies. Data taken from Ref. [155].

As described above, the first initiation step in the low-temperature chemistry is the fuel radical formation by hydrogen abstraction followed by an oxygen addition to form the peroxy radical (see also **Figure 13**). Peroxy radicals are prone to decomposition at elevated temperatures. For this reason, such species have so far mainly been investigated in reactor experiments.[156] In flames, the steep temperature gradient leads to rapid decomposition. Formation of alkyl hydroperoxides in flames was first observed by Zhang et al. by photoionization mass spectrometry, but the corresponding radicals remained elusive until recently.[157] Bierkandt et al. investigated the low-temperature oxidation in different flames and found compelling evidence for peroxy radical species.

Mass spectra at 10.00 and 10.75 eV from an *n*-butane/hydrogen flame, as measured in the preheat zone at a flame temperature of around 700 K, are presented in **Figure 19**. As the observed signals at *m/z* 48, 62, 76, and 90 are rather atypical for high-temperature chemistry, those were assigned to the alkyl hydroperoxides formed from the corresponding peroxy radicals. The fact that molecular-beam mass spectrometry is very sensitive to radical measurements in flames is shown for mass 47. For the first time, Bierkandt et al. have detected the methylperoxy (H_3C-OO) radical in a flame (see **Figure 20**).[155] Both the photoionization spectrum and the photoelectron spectrum clearly show the presence of this radical (**Figure 20**). Larger alkylperoxy radicals were not detected, but the absence of a mass spectrometric signal does not exclude their presence in the flame. As discussed by Meloni et al.,[158] larger alklylperoxy radicals have unstable cations and evade mass spectrometric detection in the parent mass channel. Most recently, propylperoxy species (C_3H_7OO, m/z 75) were isomer-selectively detected by Tang et al. and FC simulations have been performed and agree well with the TPES of the fragment (C_3H_7 m/z 43).[159]

Based on the literature photoionization spectra of the hydroperoxides and their isomeric species, the C_2 to C_4 alkyl hydroperoxides were clearly identified in flames (**Figure 20**). For example, ethyl hydroperoxide was previously detected during the low-temperature oxidation of *n*-butane by Battin-Leclerc et al.,[160] and the jet-stirred-reactor-sampled photoionization spectrum agreed well with the flame-sampled spectrum confirming that ethyl hydroperoxide is also formed in flames (see **Figure 20**).

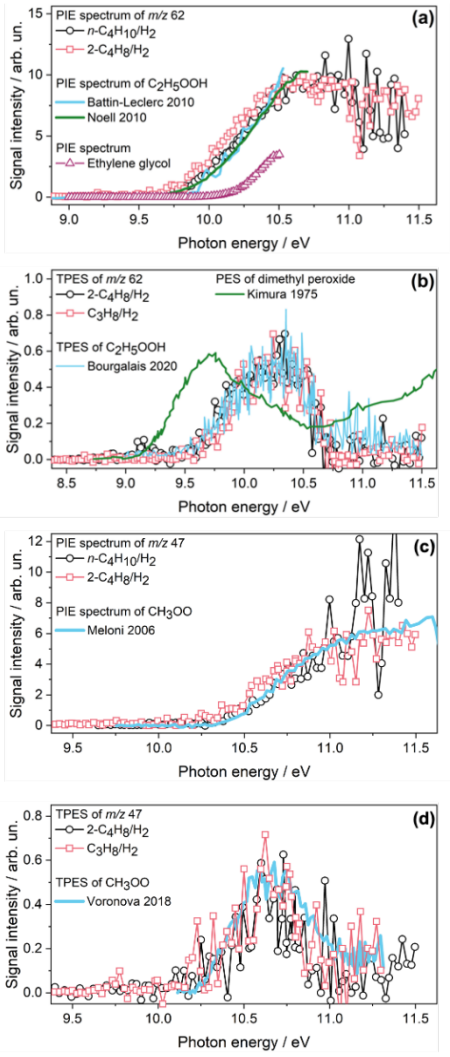

Figure 20 Identification of the ethyl hydroperoxide and the methylperoxy radical in flames by photoelectron spectroscopy. Reproduced from Ref. [155].

The flame-sampled photoelectron spectra of mass 62 also matched the experimental spectrum of the ethyl hydroperoxide from Bourgalais et al.[151] and additionally confirmed the formation of alkyl hydroperoxides in the flame-sampling experiments, which may indicate the presence of ethylperoxy radicals. It is important to note that the TPES are unstructured due to the large change in geometry upon ionization, similar to alkanes and alcohols, and although fitting the band structure does lead to isomer-specific assignment, it is, however, with a lower confidence than for spectra with well-resolved vibrational structure. Other isomers of the composition $C_2H_5O_2H$ (*m/z* 62), such as dimethyl peroxide, could still be excluded.

Observation of low-temperature species in flame environments gives a great opportunity to investigate the transition from low-temperature to high-temperature oxidation chemistry. The presence of such species may influence the formation of other oxygenated species, such as ethanol, as also discussed by Zhang et

al.[161] Studying these processes may aid the development of low-temperature combustion devices, such as HCCI engines.

4.4 Understanding Pollutant Formation

Besides the mechanistic aspects of the initiation chemistry in combustion, as discussed in the previous chapter, understanding the formation of pollutants, such as NO_x, polycyclic aromatic hydrocarbons (PAHs) as well as soot, is a prerequisite for combustion technologies in a sustainable future.

4.4.1 Soot Precursors

During combustion of aliphatic hydrocarbons, e.g., acetylene (C_2H_2) or butadiene (C_4H_6), the formation of the first aromatic ring is the rate-limiting step, i.e., the bottleneck, in soot formation.[162] Radicals are often key reaction species in these reaction routes and are of eminent importance for describing the combustion chemistry. For example, the recombination reaction of the propargyl radical (C_3H_3) always contributes significantly to benzene (C_6H_6) formation during combustion of non-cyclic fuels. Propargyl is a resonance-stabilized radical (RSR) with an unpaired electron delocalized over multiple sites resulting in two resonant electronic structures. RSRs are energetically more stable than non-resonance-stabilized radicals and can accumulate in significantly higher concentrations in a flame environment. Other RSRs, such as allyl (C_3H_5), *i*-C_4H_3, *i*-C_4H_5, and cyclopentadienyl (C_5H_5) radicals are also involved in the first aromatic ring formation step. Thanks to synchrotron-based photoionization mass spectrometry, it is now accepted that the reactions of the *i*-isomers of the C_4H_3 and C_4H_5 radicals with acetylene are important cyclization reactions for the formation of benzene in flames as opposed to those of the *n*-isomers.[163] Experimental investigation of rich acetylene flames with photoelectron spectroscopy also confirmed that *i*-C_4H_3 and *i*-C_4H_5 radicals are dominant, while the concentrations of *n*-isomers are too low for detection and so the n-isomers only play a minor role in the formation of the first aromatic ring.[164] In the presence of an aromatic moiety in the fuel, benzene can be readily formed from decomposition of the fuel in the reaction zone of a flame. Consequently, synthesizing the first aromatic ring is not the rate-limiting step in PAH formation in such cases, as shown in the combustion of *m*-xylene[126] or anisole.[165]

Besides phenol and guaiacol, anisole is a simple molecule that mimics the phenolic structure of lignin and is often used as a model compound for biomass combustion (see chapter 3). Combustion of anisole under rich conditions in flames was investigated by PIMS at the ALS and by iPEPICO at the SLS.[165] As expected from the low bond energy in O–CH_3, the unimolecular decomposition into phenoxy and methyl radicals is the major destruction route in anisole combustion. The resonance-stabilized phenoxy radical is a key species and a source of five-membered ring species by ring-contraction reactions. One of these main intermediates is the cyclopentadienyl radical, which is formed directly from the phenoxy radical over a bicyclic structure and is directly coupled by self-recombination reactions to naphthalene or by addition of methyl radicals to methylcyclopentadienes (C_6H_8). Further differentiation between the methylcyclopentadiene isomers in the anisole flame was only possible by photoelectron spectroscopy. By comparing the *m/z* 80 ms-TPES with Franck–Condon simulations, 1-methyl-1,3-cyclopentadiene (1-MCPD), 2-methyl-1,3-cyclopentadiene (2-MCPD), and 5-methyl-1,3-cyclopentadiene (5-MCPD) were identified as shown in **Error! Reference source not found.**. These isomers were also found in a *m*-xylene flame utilizing the same techniques.[126] They can be dehydrogenated to yield fulvene (c-C_5H_4=CH_2), which isomerizes to benzene and presents another viable reaction pathway towards formation of the first PAH ring.

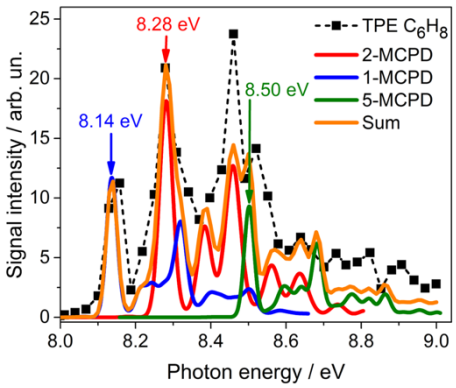

Figure 21 Identification of methylcyclopentadiene isomers by photoelectron spectroscopy in a rich anisole flame. Reprinted from Ref. [165] , Copyright (2017), with permission from Elsevier.

Beyond the formation of typical soot precursors, anisole combustion also involves formation pathways of larger oxygenates and may result in unexpected emissions, especially for biomass derived fuels.[165] For example, guaiacol can be directly formed by *ipso* addition of OH to anisole and was identified by its photoionization spectrum in anisole flames. The unimolecular bond breaking of the O–CH_3 bond in guaiacol leads to reaction pathways that are analogous to those of the phenoxy radical, which explains the presence of fulvenone (c-C_5H_4=C=O) in anisole combustion. The same formation route from guaiacol to fulvenone was previously observed by iPEPICO during the catalytic pyrolysis of guaiacol[166] and is also discussed in chapter 3.2 (see R10). The findings, that lignin-derived fuels, such as anisole with labile C–O bonds, are prone to soot formation at fuel-rich conditions may pose further challenges to optimize the process conditions and reduce PAH and soot formation. Combustion of non-aromatic biomass-derived fuels was also studied by PEPICO spectroscopy, namely methyl propanoate[167] and diethyl ether.[69] Methyl propanoate ($C_4H_8O_2$) is an ester, which may be produced from lignocellulosic biomass as starting material via anaerobic fermentation to 2-butanol and following aerobic biotransformation over butanone.[168] Felsmann et al. demonstrated for a fuel-rich methyl propanoate flame that with fixed-photon-energy PEPICO an itemization of a complex isomeric composition is also possible and additionally enables time saving compared to scanning the photon energy.[69] For example, with a scan at 9.94 eV at 2.25 mm above the burner surface and an acquisition time of 3600 s, the authors separated five combustion intermediates at *m/z* 56 with chemical formula of C_3H_4O and C_4H_8 from the flame-sampled PES. Diethyl ether ($C_4H_{10}O$) is accessible from biomass-derived syngas or by conversion of ethanol. Piper et al. studied combustion of a rich diethyl ether flat flame by double-imaging PEPICO

spectroscopy.[69] They clearly identified ethyl vinyl ether (C_4H_8O) as important combustion intermediate by the measured TPES.

4.4.2 NOx Formation

Nitric oxides, termed NOx, are emitted from practically all combustion sources. The NOx emissions are heavily regulated due to environmental and health concerns.[169-171] The main formation pathways of NO are identified as the thermal, prompt, NNH, and N_2O pathways. They are implemented in almost all reaction mechanisms and have been described or reviewed in several recent publications.[169-173] While the reaction mechanisms already describe many aspects of NOx formation in different combustion situations adequately, there are still subsets of high-temperature nitrogen chemistry where open questions remain.[169] For example, new nitrogen-containing fuels, e.g., ammonia or biomass, are employed as energy carriers and storage to reduce CO_2 emissions. These developments increase the need to understand the interaction between the intermediate species pools formed by complex hydrocarbons and nitrogen compounds at a fundamental level.[169, 171] Chemically detailed validation data under high-pressure conditions as in engines or turbines are scarce but much-needed to improve existing reaction mechanisms. To obtain comprehensive speciation data for combustion experiments with pressures up to 25 bar, a high-pressure plug-flow reactor experiment has been commissioned at the VUV beamline of the SLS recently and is described in chapter 4.3 (Figure 12 d).[77 174-176] It was shown that meaningful ms-TPES data of different isomers and quantitative speciation data can be obtained, regardless of the three-stage differential pumping. This sampling strategy limits the measurements to closed-shell intermediate species, while radicals are lost during the sampling process.[77]

Using this high-pressure plug-flow reactor, the partial oxidation of methane doped with nitric oxide was investigated to understand the reactions of the decomposition products of the fuel with NO and provide isomer-resolved and quantitative data of stable nitrogen-containing reaction intermediates. Theoretical studies suggest that HNO_2 is formed in three distinct and stable isomers under combustion conditions: *trans*-HONO, *cis*-HONO, and H-NO_2, and the subsequent destruction steps of these species should be implemented as isomer-specific pathways in reaction mechanisms.[177-179] Although all three isomers are considered to be important combustion intermediates,[179] nitrous acid (HONO) has mostly evaded spectroscopic detection and experimental evidence of the other isomers is scarce[180-182] A detailed analysis of the threshold photoelectron spectra measured by PEPICO spectroscopy can facilitate future detection strategies. Comparison of calculated Franck–Condon envelopes with the measured data in **Figure 22** shows that only *trans*-HONO contributes to the signal at *m*/*z* 47 at photon energies above the ionization threshold of 10.95 eV. The rapid decline of the signal in the ms-TPES at energies above 11.2 eV can be attributed to fragmentation of the $HONO^+$ to NO^+ on *m*/*z* 30. The *cis*-$HONO^+$ is only very weakly bound and forms almost exclusively OH and NO^+ which is tentatively found in the same mass channel. H–NO_2 is expected to have a stable cation. The fact that it is not detected at these reaction conditions suggests that it is either not present in the sample or, if it is formed, it is consumed more rapidly than expected by current reaction models.

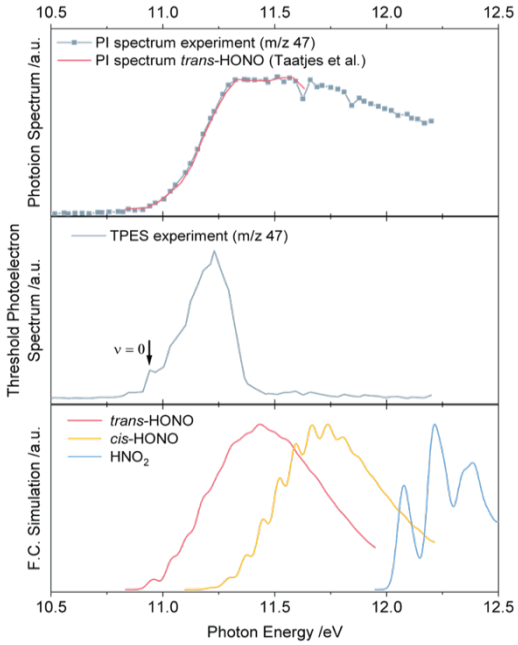

Figure 22 Photoionization (top) and photoion mass-selected threshold photoelectron spectrum (center) of *m*/*z* 47 combustion intermediate shown together with calculated Franck–Condon envelopes (bottom) for the three HNO_2 isomers. Reproduced from Ref. [183] with permission from the PCCP Owner Societies.

This example shows that despite a well-established understanding of the main NOx formation pathways, some details of the nitrogen chemistry have still not been resolved. Moving to systems in which nitrogen (e.g., ammonia combustion) is introduced into the combustion system as the fuel rather than a component of the air, these details have the potential to lead to serious mismatches of predicted and observed NOx emissions. The same is true for the chemical details which underly the formation of hydrocarbon pollutants, the fuel destruction process, and the ignition process – the chemical details will matter for the optimization of these processes.

To summarize, PEPICO detection was implemented as an analysis tool in combustion diagnostics and imaging techniques enable new methods to quantify missing reactive species. Different kinetic tools from reactors to flat flame burners were introduced and used to shine new light on ignition chemistry and pollutant formation.

5. Zooming Into Flame Chemistry

We have discussed the pyrolysis of plant-derived lignin, where MBMS helps to understand the global picture emerging from countless parallel and sequential reactions (top-down approach). Fundamental mechanistic insights are extracted by investigating the elementary reactions of lignin model compounds with and without the influence of a catalyst, as shown in chapter 3 (bottom-up approach). As far as the chemistry of flames is concerned, similar considerations apply, and a combustion model can only be as true as the individual reactions are understood. In this chapter, we will discuss how combustion models can be further refined using advanced PEPICO approaches, illustrated by accurate rate constant measurements of oxidation reactions of radicals, by mechanistic studies elucidating PAH and PANH formation channels as well as by assessment of the organophosphorus flame retardants.

5.1 Rate Constant Measurements

Kinetic combustion models describe the reactive flow from the fuel and oxidizer to the intermediates (radicals) and finally to the products (CO, CO_2, and H_2O) by considering the complex interplay between elementary reactions. Each channel is expressed in a temperature- and pressure-dependent rate constant. Taatjes and Osborn showed that photoionization mass spectrometry combined with a kinetic flow tube reactor is a powerful combination to determine individual rate constants of chemical reactions, ranging from combustion to atmospheric chemistry related topics.[38, 184-186] However, the isomer-specificity of PIMS is limited, as the spectra rarely show sharp isomer-specific resonances. To overcome this limitation, Sztáray, Osborn and co-workers proposed a new PEPICO spectrometer, CRF-PEPICO (**Figure *23*** a), which includes a kinetic flow tube reactor (**Figure *23*** b).[48] In proof of principle experiments, they showed the ms-TPES of propargyl and iodomethyl radicals produced via photolysis and measured the rate-constant of the $CH_2I + O_2$ reaction. Metered flows of argon, oxygen, and CH_2I_2 were mixed at the entrance of the flow tube reactor and a laser at 355 nm dissociates the precursor (**Figure *23*** b). The kinetic time profiles are depicted in **Figure *23*** c, which show that CH_2I radicals are formed at 0 ms, when the laser fires. The radicals effusively leak into the ionization region of the spectrometer via a sampling hole. Kinetic traces are acquired, because CH_2I produced upstream of the sampling hole is detected later than 0 ms and spends more time in the flow tube reactor. The strong decay of CH_2I after 20 ms is due to the replenishment of the reactor with fresh and unphotolyzed CH_2I_2. When the oxygen concentration is increased, the kinetic time (**Figure *23*** d) shortens dramatically as the radicals are consumed faster by reaction with oxygen at pseudo first-order conditions. By plotting the individual decay rates against the oxygen concentration, the bimolecular rate constant can be obtained from a linear fit (***Figure 23*** e) as $k(CH_2I + O_2) = (1.78 \pm 0.19) \times 10^{-12}$ cm^3 s^{-1}, in excellent agreement with the literature.[187-189]

Allyl is one of the most basic reactive intermediates in combustion chemistry. Due to the fact that the radical site is resonantly stabilized between the two CH_2 groups, it is quite unreactive towards oxidation, despite the high reaction exothermicity of −79.7 kJ mol^{-1}.[190] Schleier et al. recently reinvestigated this

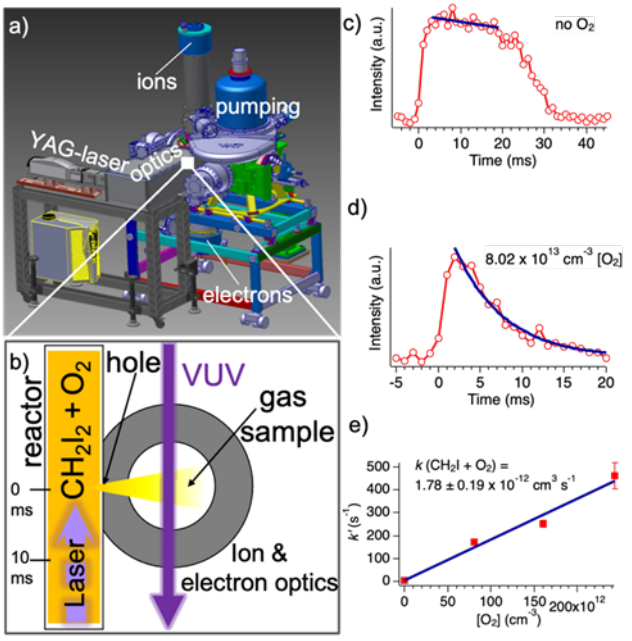

Figure 23 (a) Laser photolysis setup and CRF-PEPICO endstation at the Swiss Light Source. (b) Zoom into the ionization region, with the flow tube and the 100-400 µm sampling hole. The effusive beam expands into the ionization region, where it is intersected with the VUV photon beam. Ions and electrons are accelerated in oposite directions and detected in coincidence. When the laser fires, radicals are generated along the tubular reactor at 0 ms kinetic time (c). The decay at 20 ms is due to the fresh unphotolyzed precursor flowing into the reactor. Upon increasing the oxygen concentration (d) the decay rate of the radicals signal increases, due formation of peroxy radicals. By plotting the individual decay rates (e) against the oxygen concentration the bimolecular rate constant is obtained. Reprinted from Ref. [48], with the permission of AIP Publishing.

reaction using the CRF-PEPICO endstation.[116, 190] Allyl radicals were produced via direct photolysis of allyl iodide at 213 and 266 nm (**Figure *24***a) or via propene hydrogen abstraction by chlorine radicals. The latter were generated by photolysis of oxalyl chloride at 266 nm. The ms-TPES of both precursors showed that exclusively allyl radicals were produced, without contributions from 1-propenyl or cyclopropyl. Sensitivity analysis (**Figure *24***b) showed recombination and wall loss side reactions accounted for less than 5%. Thus, a pseudo first order rate-constant plot could be applied to obtain the bimolecular rate constates of the allyl + oxygen reaction at different pressures, similar to the $CH_2I + O_2$ reaction. Rate constants of 1.35×10^{11} cm^3 mol^{-1} s^{-1} and 1.75×10^{11} cm^3 mol^{-1} s^{-1}, at 0.8 and 3 mbar, respectively were determined.[116]

Schleier et al. also extended their allyl kinetics study to investigating the oxidation of 1- and 2-methyl-allyl isomers as

produced from 213 nm photolysis of the respective halides, according to R13-R15:[191]

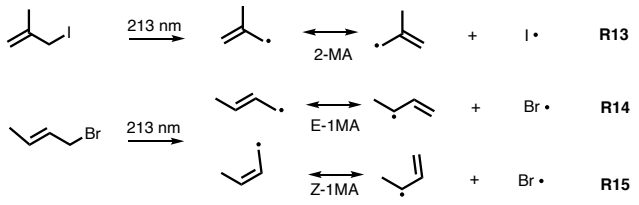

For 2-methylallyl (2-MA), a rate constant of k(2-MA + O2) = (5.1 ± 1.0) × 10^{11} cm^3 mol^{-1} s^{-1} was obtained, which does not show a pressure dependence, as the reaction is already at the high-pressure limit even at 1 mbar. The 1-methylallyl radical, on the other hand, appears as E- (R14) and Z-isomer (R15), which was confirmed by measuring the ms-TPES during the photolysis reaction. Below 7.55 eV, only the E-isomer was ionized and the obtained rate-constant is even conformer dependent. Above this photon energy, both isomers are ionized, and the determined rate constant of the mixture agrees within the error margin of the experiment. In contrast to 2-MA, the 1-MA rate constants are slightly slower and show a little pressure dependence, with values of k(1-MA + O_2) = (3.5 ± 0.7) × 10^{11} cm^3 mol^{-1} s^{-1} at 1 mbar and k(1-MA + O_2) = (4.6 ± 0.9) × 10^{11} cm^3 mol^{-1} s^{-1} at 3 mbar. Comparing the high-pressure limits of allyl and methylallyl radicals the following correlation is found: $k_{allyl} < k_{2\text{-MA}} < k_{1\text{-MA}}$. Schleier et al. explained this trend by the slight increase of the bond dissociation energy of the corresponding allylperoxy radicals. Furthermore, this study confirms the previously found relationship of alkyl radical + oxygen reactions, which show a correlation between the high-pressure limiting rate constants, the size of the radical, and the bond dissociation energy.

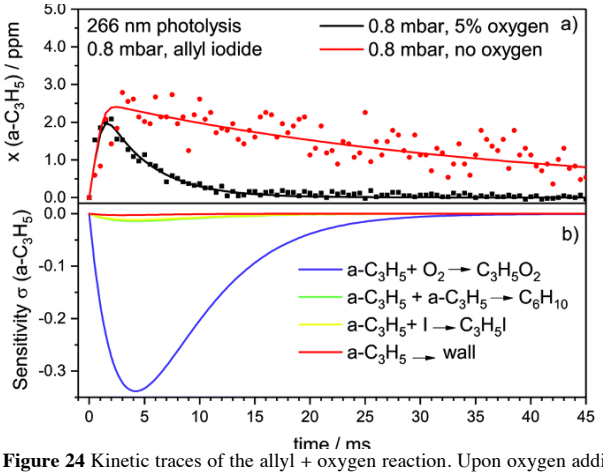

Figure 24 Kinetic traces of the allyl + oxygen reaction. Upon oxygen addition, allyl depletes faster. Sensitivity analysis shows that the allyl oxidation reaction exhibits the largest rate constants. Reproduced from Ref. [116] with permission from the PCCP Owner Societies.

5.2 Understanding PAH and PANH Formation Chemistry

The oxidation rate constant increases significantly upon methylation of the allyl radicals. Especially at fuel-rich conditions, the complete oxidation of radicals to yield CO or CO_2 is not the most prominent reaction and other channels may efficiently compete. It is known that resonance-stabilized radicals, such as allyl or propargyl, are prone to dimerization yielding, e.g., benzene or other aromatics. These are PAH precursors par excellence, which will form soot, lowering the combustion efficiency. Thus, there is a need for understanding these fundamental channels of the PAH and soot formation to avoid unwanted side reactions.

As discussed earlier, PEPICO spectroscopy is distinguished from conventional PIMS methods by utilizing threshold photoelectron spectra as second analytical dimension for isomer-selective identification of products and transients. Here, we focus on two examples of how five-membered rings can be formed by allyl radicals' reaction with acetylene or benzyne mimicking two important PAH formation channels:

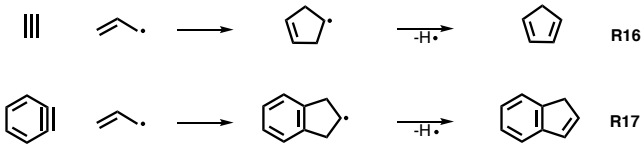

Bouwman et al. utilized a Chen-type pyrolysis reactor, as described in chapter 3 to generate allyl radicals from allyl-iodide in situ.[192] Instead of argon as buffer gas, acetylene was used to study the allyl + acetylene reaction. Mass spectra show that at reactor temperatures as high as 900 K, m/z 66 is the only product of reaction R16. Increasing the temperature further leads to a decomposition of C_5H_6 by dehydrogenation. Thanks to ms-TPES detection, cyclopentadiene was identified as the sole isomer of the composition C_5H_6 (m/z 66), while acyclic species such as pentenynes or pentatrienes were completely absent. This result was rationalized with the help of a computed C_5H_7 potential energy surface, which showed that the allyl + acetylene addition proceeds over an entrance barrier of 59 kJ mol^{-1} to form an adduct, which ring closes to yield cyclopentenyl (C_5H_7, R16). The importance of the C_3H_5 + C_2H_2 reaction is mirrored by the fact that cyclopentadienyl c-C_5H_5 radicals are also produced at elevated temperatures. They can dimerize to form $C_{10}H_{10}$ intermediates, which dehydrogenate to form naphthalene ($C_{10}H_8$) a well-known precursor for larger PAHs and soot.[193]

In a recent review, Kaiser and Hansen summarized PAH formation channels,[194] which can proceed along the hydrogen abstraction acetylene addition (HACA),[195] hydrogen abstraction vinylacetylene addition (HAVA),[196] phenyl addition dehydrocyclization (PAC),[197] methylidyne addition cyclization aromatization (MACA),[198] and radical–radical reaction (RRR) routes.[199] Especially the last one represents an interesting avenue towards ring species, as recently shown by McCabe et al., who investigated the allyl + ortho-benzyne reaction (R17). Benzyne has an interesting electronic structure as it has both aryne and biradical character. While the neutral is planar it has recently been shown that the cation has a twisted C_2 geometry.[200] Benzyne and allyl were in situ produced from benzocyclobutenedione (1% in argon) and allyliodide (16% in argon), respectively, in a Chen-type pyrolysis reactor. The mass spectra show clean formation of m/z 116, if both reactants are present. The m/z 116 ms-TPES in **Figure 25**a shows a strong resonance at 8.14 eV, which can be assigned to the adiabatic ionization energy of indene.[201] The signal at 8.1 eV is associated with hot and

sequence band transitions, which are expected, as the product is generated in a 900 K hot reactor and cooling is less efficient upon expansion into the vacuum chamber.[68] Nonetheless, the spectrum agrees very well with that of indene and other C_9H_8 isomers, such as phenylallene (AIE = 8.29 eV),[202] 3-phenyl-1-propyne (AIE = 8.99 eV), or 1-phenyl-1-propyne (AIE = 8.42 eV) are absent.[203]

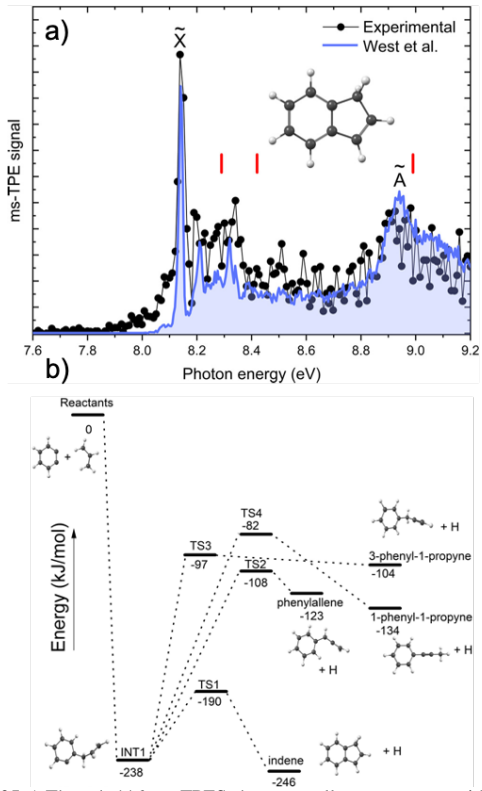

Figure 25 a) The *m/z* 116 ms-TPES shows excellent agreement with the indene reference spectrum. Other C_9H_8 isomers, such as phenylallene (8.29 eV), 3-phenyl-1-propyne (8.99 eV), or 1-phenyl-1-propyne (8.42 eV, indicated as red sticks) were not observed. b) Potential energy surface of the allyl + o-benzyne reaction. Typically for a radical–radical reaction, no entrance barrier is observed, and the indene formation is highly exothermic, while the other reaction channels are higher in energy. Reprinted with permission from Ref. [68]. Copyright 2020 American Chemical Society

This was further investigated by calculating the C_9H_9 potential energy surface, as depicted in **Figure 25**b. In contrast to the allyl + acetylene reaction, no entrance barrier is observed for allyl + benzyne, forming the association complex INT1. Ring closure through TS1 and subsequent hydrogen loss (not shown here) yields indene. The rate-limiting transition states (TS2, TS3 and TS4) for the formation of phenylallene, 1-phenyl-1-propyne, and 1-phenyl-1-propyne are also depicted in **Figure 25**, but the reactions are less exothermic by more than 100 kJ mol^{-1}. McCabe et al. also calculated the reaction rates for the formation of the four products and found that indene dominates the overall products by more than 99%, which agrees with the experimental findings. At higher reactor temperatures, indene loses hydrogen to form the indenyl radical, which is known to impact aromatic growth.[199] This finding suggests that the reaction of benzyne + allyl may also contribute to the initial formation of five-ring PAHs especially considering the abundance of benzyne in combustion reactions.[204]

While this reaction shows the clean formation of PAHs, there are systems with multiple competing reaction channels, which poses a challenge to spectroscopic technique to identify reactive species. While in the phenyl + vinylacetylene reaction at least 50% of the reactive flux goes towards the formation of naphthalene as recently reported by Zhao et al.,[199] the situation changes if vinylacetylene is substituted by isoelectronic acrylonitrile, which does not yield quinoline according to R18.

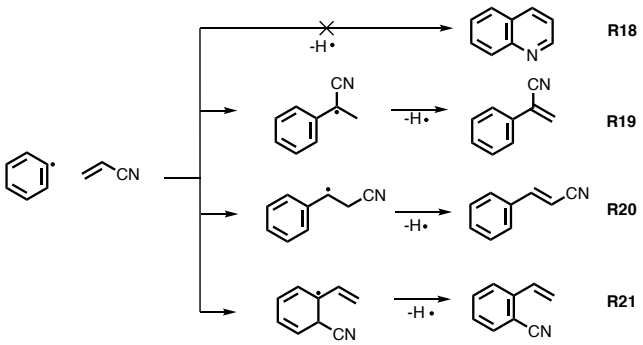

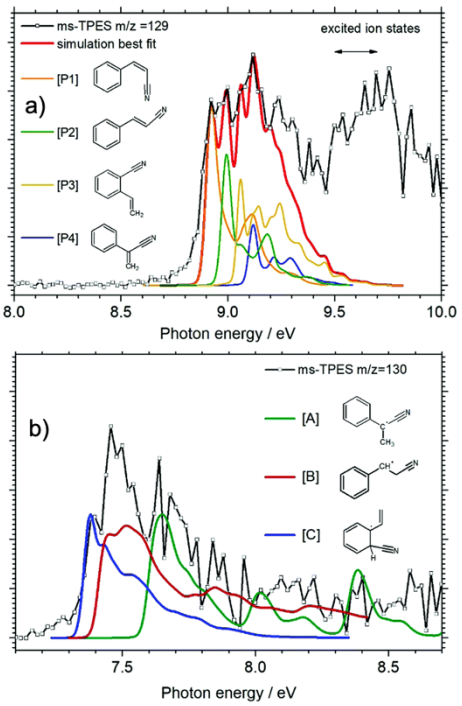

Figure 26 ms-TPE spectra of the products (a) and intermediates (b) of the acrylonitrile + phenyl radical reaction. Reproduced from Ref.[205] with permission from the PCCP Owner Societies.

Bouwman et al. found that the nitrile group inhibits ring-closure in R18, due to a high-lying barrier and is thus kinetically controlled.[205] Formation of the less thermodynamically stable 2-phenyl acrylonitrile (R19), 3-phenylacrylonitriles (R20), and *ortho*-cyanostyrene (R21) are favored, as shown by comprehensive potential energy surface calculations and Franck–Condon spectral modeling (**Figure *26***). Most notably, from the 40 evaluated open-shell adduct isomers at *m*/*z* 130, three radicals describe the ms-TPES best (**Figure *26***b). Among the 17 evaluated *m*/*z* 129 product candidates, four may contribute to the experimental TPES. This shows that photoion mass-selected threshold photoelectron spectroscopy with FC spectral modeling can elucidate even complex combustion reactions even if numerous isomers are present in the sample simultaneously.

5.3 Understanding Flame Inhibition

As discussed in the previous chapter, kinetic measurements of elementary reactions and advanced mechanisms to unveil combustion chemistry are important to develop predictive combustion models. Active strategies utilizing organophosphorus compounds (OPCs) can be utilized to control, lower or even stop combustion. Efforts have been undertaken to understand the chemistry of OPCs. While they are responsible for flame inhibition, they can also increase or catalyze the combustion efficiency of hydrogen fuels, which is utilized during supersonic combustion in scramjet engines.[206-207] It is hypothesized, that phosphoryl species, such as PO, PO_2, and HOPO are the key reactive species during the inhibition or catalytic combustion mechanism, as they can quench H or OH radicals according to R22-R24:

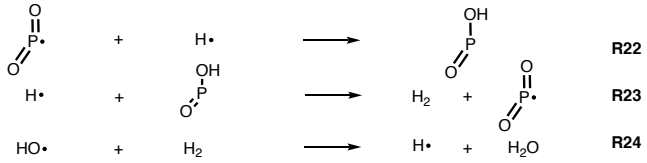

However, due to the lack of sensitive methods to detect these elusive species, their origin and fate poses a major challenge. Korobeinichev and co-workers observed PO_x species in burner studies utilizing molecular beam sampling techniques and electron ionization.[208-209] Nonetheless, the elementary reactions of how PO and PO_2 are formed from stable precursors were still not fully understood. In 2014, Liang et al. utilized a Chen-type microreactor by combining it with the PEPICO system at the SLS to investigate the pyrolysis of dimethyl methyl phosphonate (DMMP).[74]

The unimolecular decomposition of DMMP is initiated by a subsequent methanol and formaldehyde loss to produce three tautomers of the composition $OPCH_3$ (R25).

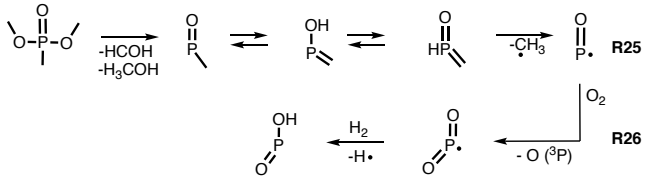

While the $HPO{=}CH_2$ and $P(OH){=}CH_2$ tautomers could be assigned, the $P(=O)CH_3$ intermediate evaded detection, as it rapidly decompose to yield PO and methyl radicals, as proven by the ms-TPES in **Figure *27***a. The PO_2 radical was absent during the unimolecular decomposition of DMMP and it was hypothesized that an oxidative environment is needed. Also other OPCs such as dimethyl phosphoramidate (DMPR) did not yield PO_2, but rather PO and PN species.[210] Only recently Liang et al. showed that oxygen is indeed needed to produce PO_2 in the gas phase, as proven by TPES detection of PO_2 (see **Figure *27***b) and O (^{3}P) .[211] In addition, the hypophosphorous acid (HOPO) signal increased in the mass spectrum when hydrogen and oxygen were cofed. The decomposition and oxidation of DMMP to yield PO, PO_2 and HOPO can thus be summarized according to R26 and sheds new light on the underlying mechanisms to control combustion processes.

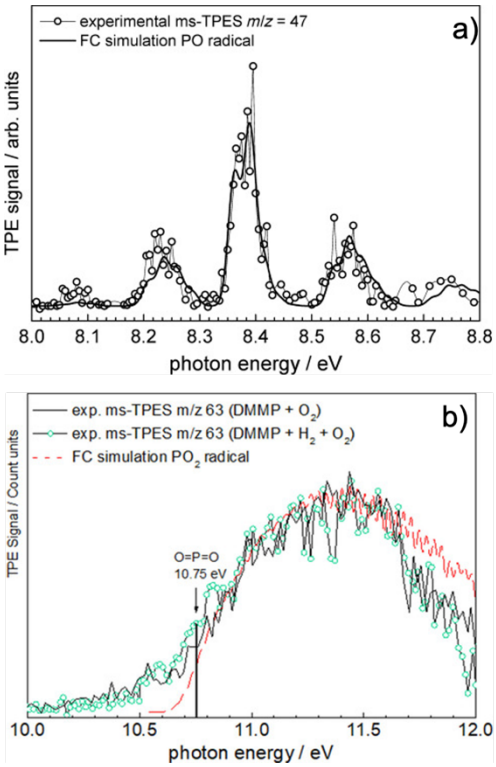

Figure 27 ms-TPES spectrum of key phosphoryl species. Both the PO and PO_2 radicals could be unequivocally assigned thanks to Franck–Condon spectral modeling. While PO is the unimolecular reaction product of DMMP, PO_2 could only be observed upon addition of oxygen to the reaction mixture. Taken with permission from Refs. [74] and [211] copyright John Wiley and Sons.

In summary, in this chapter we have measured rate constants of the (methyl)-allyl + oxygen reactions even conformer-selectively. Furthermore, the mechanism of PAH and PANH formation channels were refined thanks to ms-TPE spectroscopy and quantum chemical calculations. Intense transitions from the neutral into the cation aid species assignment to narrow down potential contributors from 40 species to only three. In the last example, we shed light on the gas-phase formation of active flame retardants, such as on phosphoryl species. These deep

mechanistic insights may be utilized to optimize combustion models or to control this process in a more targeted way.

6. Challenges and Perspectives

What are the future challenges for photoelectron photoion coincidence techniques? How can this technique address novel reactive environments? How can species be quantified to develop predictive models? Are there new reactors and sources to be combined with PEPICO?

6.1 Instrumentational Developments

Coincidence detection inherently limits the dynamic range of an experiment as false coincidences, i.e., detector events belonging to independent ionization events, lead to a non-zero background, which needs to be subtracted. If the Poisson noise of the background is comparable with the true coincidence signal, the true signal is lost. A high-frequency deflection field of the focused ion beam can be used to increase the dynamic range of detection of PEPICO from 10^3:1 to 10^5:1.[212] Here, the recorded ion TOF and the temporal phase of the deflection field the ion passes determines the (x,y) position where the ion should arrive on the detector. If the position of the ion deviates from this location, the ion originated from a different ionization event and can thus be discarded as false coincidence. With the help of this feature argon clusters as large as Ar_9^+ could be detected in an argon molecular beam after background suppression. It is yet to be shown how these new deflection techniques are compatible with sampling from reactors, furnaces, and burners.

Further improvements address spectral broadening and mass resolution, which represent the main challenges of identifying larger aromatic molecules such as PAHs in the complex gas mixtures of a flame environment with PEPICO. The mass resolution may not be sufficient to separate the signals of pure hydrocarbon species from oxygenated hydrocarbons, as pointed out in chapter 4.4.1. In addition, the TPE spectra can overlap substantially if several isomers are present. Simply increasing the VUV radiation or the threshold electron resolution to resolve more features of the molecule–ion transitions is not enough to solve this issue because the sample is often rotationally and even vibrationally excited. Molecular-beam sampling as implemented in typical MBMS instruments will only cool the gas sample from the flame temperatures to approximately room temperature.[213] The cooling process can be improved by microprobe sampling. In 2020, Mercier et al. presented highly resolved TPE spectra of PAH measured with the VUV-PEPICO instrument at SOLEIL.[214] With this development, the authors have substantially advanced the detection options for PAH in flames and show that PEPICO detection has a high potential for investigating the in-situ mechanisms of soot and PAH formation in laboratory flames, however, at the expense of quenching reactive intermediates.

6.2 Quantification Strategies & Databases

The development of predictive catalytic and combustion models relies on a solid quantification strategy of the reactive environment. Here, the photon energy dependent ionization cross sections are needed. While these data are available for stable molecules, they often remain elusive for reactive intermediates, such as radicals and carbenes.[215] On the one hand, attempts have been made to experimentally determine ionization cross sections by relying on mass balance strategies, where both the species of interest and an internal standard have to be synthesized in-situ in a 1:1 ratio.[216-217] Careful calibration of, e.g., the mass discrimination factor and a well-understood chemistry are prerequisites for accurate cross sections. On the other hand, calculated ionization cross sections depend on how the wave function of the leaving electron is treated,[218] as well as how accurate the theoretical description of photoionization is.[219] In addition, questions arise how strategies can be developed to use the isomer-selective TPES signal for the quantification. The threshold ionization cross section may depend on apparatus functions, such as electric fields (Stark effects), scan steps, energy resolution etc., which represent further challenges. Linking PEPICO measurements with complementary diagnostic methods, such as laser spectroscopy, may also provide quantitative data and allow conclusions about ionization cross sections. These experiments often suffer from lack of reproducibility. To help reliable, isomer-selective detection and quantification, there is a demand for a database collecting both (threshold) photoelectron spectra as well as ionization cross section data for stable as well as reactive intermediates.

6.3 New Sources and Reactions

Kinetic measurements are often performed in long shock tubes (up to 12 m) at very high pressures. Due to the low repetition rate (1 experiment in minutes or hours) and short detection window, photoionization with photon energy scans is impractical. In 2014, Tranter and Lynch introduced a miniature high repetition rate shock tube, capable of experiments above 600 K and 100 bar at a repetition rate of up to 4 Hz and combined them with x-ray and VUV-PIMS detection.[42] Most recently, Nagaraju et al. combined a similar shock tube experiment with the DELICIOUS-III i^2PEPICO spectrometer at the DESIRS beamline at SOLEIL Synchrotron in France.[76] Experiments of up to 1.5 Hz were possible at up to 7.5 bar and 1525 K, and impressive isomer-selective detection capabilities were presented. However, the authors pointed out that the signal-to-noise (S/N) ratios had to be improved to obtain kinetic data.[76]

For room and low-temperature kinetic studies at conditions relevant to the interstellar medium, a fluorine discharge source and a Laval nozzle instrument (CRESU) were successfully combined with PEPICO and commissioned at the DESIRS beamline at SOLEIL.[75, 220] Impressive radical generation capabilities were demonstrated and numerous well-resolved ms-TPES of highly reactive intermediates have been recorded, which are partially inaccessible in hot pyrolysis reactors.[75, 159, 221-223] By changing the fluorine discharge position in the reactor, kinetic measurements are theoretically possible, but proof-of-principle experiments are pending. Apart from these setups, a photolysis PEPICO experiment is being developed at Sandia National Laboratories to be used at the ALS in Berkeley.[41]

All experiments discussed in this review are carried out in the gas phase. However, most industrial processes rely on the solvent phase. Currently, these approaches are difficult to probe as liquid sampling and high vacuum detection are often incompatible. Recently, Komorek et al. introduced an elegant technique, which combines a microfluidic cell to evaporate directly from

the liquid phase and combined this with ReTOF-PIMS at the ALS to study sulfur clusters in an electrochemical cell and to study the generation of secondary organic aerosol formation.[224-225] This device is based on the System for Analysis at the Liquid Vacuum Interface (SALVI) approach, introduced in 2011 by Yang et al.[226] Further thermal vaporization techniques have potential to be combined with photoion and/or photoelectron detection at VUV beamlines, to study reactions in the liquid phase.[227-228]

Heterogeneous catalysis is a growing field for the utilization of mass spectrometry, velocity map imaging, and photoelectron spectroscopy to study reactive intermediates and reaction mechanisms, as reviewed recently.[40] Alkane activation, methanol-to-olefin/hydrocarbon processes, or catalyst deactivation by fouling, poisoning, ageing, and coking often involve gas-phase intermediates or intermediates that readily desorb from the catalyst surface and are, thus, amenable to mass spectrometric detection. Furthermore, efforts must be made to model the mass transport and chemical reactivity including the catalyst surface to extract kinetic information. This will allow to generate predictive models, which can be evaluated against experimental data.

6.4 Laser-based Ionization Schemes

The scarcity of beamtime at synchrotron beamlines makes laboratory-based VUV-light sources attractive. Noble gas lamps deliver limited photon flux, especially when combined with a monochromator. If operated at a fixed wavelength, the photon energy may also be too high to suppress fragmentation or too low to ionize all species of interest, compromising the mass balance. After the advent of high harmonic generation (HHG), relying on high peak power femtosecond lasers, tunable and intense VUV radiation are now within reach in laser laboratories. They typically run at 10 kHz to 1 MHz and allow for coarse tunability along the odd harmonics of the driving laser centered at $\omega = 780$ nm. First attempts have been made to combine these VUV lasers with PEPICO detection investigating pyrolysis reactions.[229] There are, however, a few drawbacks when compared to VUV synchrotron light sources. The photon flux at 10.8 eV (7 ω), a central wavelength for combustion studies, is approximately two orders of magnitude lower than at typical bending magnet beamlines, limiting the sensitivity of the experiments. Due to the transform-limited ultrashort laser pulses, the minimum bandwidth is 50 meV, which impedes spectral resolution in TPES measurements making it difficult to isomer-selectively detect isomers. Further developments may address the flux or the resolution of laboratory-based VUV light sources, but synchrotron light is likely to stay best-suited for coincidence studies in the foreseeable future.

6.5 FEL and PEPICO detection

In the light of the high peak brilliance and ultrashort pulse duration of free electron lasers (FEL) currently available around the globe, it is worth discussing these opportunities for coincidence detection schemes. To ultimately profit from the short pulses, the reaction to be investigated has to proceed in less than a few hundred picoseconds. Currently PEPICO[230-231] detection schemes utilize UV or IR-multiphoton schemes, which may complicate the assignment of photoelectron bands, as the exact numbers of photons is difficult to determine.[232] VUV single photoionization as probe pulse has the great advantage of being universal and not limited by dipole forbidden excitations into intermediate (Rydberg) states. Nevertheless, high repetition rates (> 1 MHz) at a moderately high peak power may be used to suppress multi-photon ionization and enable coincidence detection while controlling the energy balance and, thus, allowing for spectroscopic and analytical applications. This combination may be uniquely able to probe complex ultrafast reactions with multiple products. By utilizing photoion mass-selection of photoelectrons, isomer-selective speciation data can be obtained.

7. Conclusions

In this review, we discuss two aspects of clean combustion, namely the catalytic synthesis of sustainable fuels and the process optimization of combustion to reduce harmful emissions. An advanced mechanistic understanding of these chemical processes is obligatory, which is why state-of-the-art spectroscopic methods are called for. We summarize recent advances in PEPICO spectroscopy as a universal, multiplexed, and sensitive detection tool to obtain insights into sustainable catalytic fuel synthesis and conversion, by detection of reactive intermediates. We discuss how highly reactive and elusive intermediates are isomer-selectively detected by vibrationally resolved photoelectron spectroscopic fingerprints and how ion velocity map imaging helps increase radical detection efficiency and species quantification.

We discuss biomass valorization routes, investigated by wood and lignin pyrolysis using photoionization molecular-beam mass spectrometry. The top-down approach delivers valuable mechanistic insights, such as depolymerization to lignin or hemicellulose marker molecules, which support the chemical engineering approach of the biomass valorization process. Via pyrolysis of lignin model compounds in the bottom-up approach, elementary reactions, such as the initial radical formation, could be investigated with PEPICO detection. Isomer-specific reactions could be unveiled and further refined by increasing the complexity of the probed species. We show that both top-down and bottom-up approaches deliver important mechanistic insights to be combined. Furthermore, we report on catalytic fast pyrolysis of guaiacol and benzenediol isomers, which yield fulvenone, a highly reactive intermediate, responsible for the formation of prototypical sustainable fuels (benzene) and fine chemicals (phenols). The discussion of mechanistic insights and the importance of PEPICO detection is concluded by reviewing studies on alkane valorization strategies via oxyhalogenation reactions. These did not only reveal reaction mechanisms by detection of rate-limiting radicals, but also unveiled side channels yielding, e.g., early coke formation intermediates (PAHs), responsible for catalyst deactivation.

After reviewing the PEPICO spectroscopy insights into catalytic fuel production, the economic and ecologic use of the stored energy represents the next stage in ensuring a sustainable future. Fuel destruction reactions, such as xylyl radical formation in a xylene flame and in a pyrolysis reactor give reveal initial combustion reactions and the fate of the primary fuel radicals. Further details are revealed by sampling reactive species from butane and butene flames to determine relative H-abstraction ratios. Clear trends could be established in systematic studies for the rates as tertiary > primary; secondary > primary;

allylic > non-resonance-stabilized form. PEPICO spectroscopy also provided insights into the formation of peroxides and ketohydroperoxides to better understand low-temperature combustion, relevant in HCCI engines. Peroxy radicals, produced by the reaction of fuel radicals with oxygen, were only recently detected in low-temperature hydrogen flames doped with alkanes. These data are much-needed to develop predictive, chemically correct combustion models to predict ideal combustion conditions for next-generation biofuels.

PEPICO approaches coupled with novel reactors can detect new reaction pathways during pollutant formation. Isomeric methylcyclopentadienes were selectively detected in *m*-xylene as well as in anisole flames, thanks to vibrational fingerprints in the TPE spectrum. They can dehydrogenate to fulvene, which forms benzene at later stages of the combustion process and initiates PAH formation channels. NOx formation was probed by sampling directly from a high-pressure reactor, detecting nitrous acid as intermediate. Here, the fate of HNO_2 isomers is discussed.

Combustion models are comprised of a multitude of chemical reactions. Their individual rate constants describe the reactive flux of the fuel and oxygen to the final products. Thus, the model can only be as accurate as the underlying chemistry is understood. The last chapter zooms into individual elementary reactions of the combustion process. We describe how PEPICO detection can help determine isomer-selective rate constants of fuel radical + oxygen reactions. PAH formation channels are investigated in pyrolysis reactors by probing, e.g., reactions between allyl radicals and acetylene or benzyne, or phenyl + acrylonitrile. Especially the latter case shows how selective TPES detection in combination with quantum chemical methods helped narrow down the isomeric contribution from 30 potential species to only three carriers of the ms-TPES signal.

A perspective on PEPICO instrumental developments conclude this review with the aim to quantify reactive species in harsh environments. We elaborate on current and future VUV light sources, reactors, and sample sources and their combination with novel coincidence methods.

AUTHOR INFORMATION

Corresponding Author

*Patrick Hemberger, Laboratory for Synchrotron Radiation and Femtochemistry, Paul Scherrer Institute, CH-5232 Villigen PSI, Switzerland. patrick.hemberger@psi.ch

Author Contributions

The manuscript was written through contributions of all authors. All authors have given approval to the final version of the manuscript.

Funding Sources

Swiss Federal Office of Energy (SFOE, SI/501269-01) Swiss National Science Foundation (SNSF, 200021_178952). Deutsche Forschungsgemeinschaft KA3871/3-2, KA3871/1-3 and KO4786/2-2.

ACKNOWLEDGMENT

This review is dedicated to Dr. Peter Radi on the occasion of his 65th birthday. P.H. and A.B are grateful funding by the Swiss Federal Office of Energy (SFOE, SI/501269-01) and by the Swiss National Science Foundation (SNSF, 200021_178952). A.B. and P.H. thank Patrick Ascher for technical assistance and Zeyou Pan for providing material for some of the figures. All authors thank the Deutsche Forschungsgemeinschaft for financial support under contracts KA3871/3-2, KA3871/1-3 and KO4786/2-2.

ABBREVIATIONS

1-MA	1-methylallyl
1-MCPD	1-methyl-1,3-cyclopentadiene
2-MA	2-methylallyl
2-MCPD	2-methyl-1,3-cyclopentadiene
5-MCPD	5-methyl-1,3-cyclopentadiene
AIE	adiabatic ionization energy
ALS	Advanced Light Source
BTEX	benzene, toluene, ethylbenzene, and xylenes
BTX	benzene, toluene, and xylenes
CFP	catalytic fast pyrolysis
CRF-PEPICO	combustion reactions followed by photoelectron photoion coincidence
DFT	density functional theory
DMMP	dimethyl methyl phosphonate
DMPR	dimethyl phosphoramidate
DPI	dissociative photoionization
EI	electron ionization
EI-MBMS	electron ionization molecular-beam mass spectrometry
EKE	electron kinetic energy
FC	Franck–Condon
FRL	fuel readiness level
GC/MS	gas chromatrography mass spectrometry
HAB	height above the burner
HACA	hydrogen abstraction acetylene addition
HAVA	hydrogen abstraction vinylacetylene addition
HCCI	homogeneous charge compression ignition
HHG	high harmonic generation
i^2PEPICO	double-imaging photoelectron photoion coincidence
IE	ionization energy
iPEPICO	imaging photoelectron photoion coincidence
IR	infrared
JSR	jet-stirred reactor
KHPs	ketohydroperoxides
LIF	laser-induced fluorescence
m/*z*	mass-to-charge
MACA	methylidyne addition cyclization aromatization
MBMS	molecular-beam mass spectrometry
MPIMS	multiplexed photoionization mass spectrometry
MS	mass spectrometer
ms-TPES	mass-selected threshold photoelectron spectrum/spectra
OCM	oxidative coupling of methane
OPCs	organophosphorus compounds
PAC	phenyl addition dehydrocyclization
PAH	polycyclic aromatic hydrocarbon
PAHs	polycyclic aromatic hydrocarbons
PANH	polycyclic aromatic nitrogen containing hydrocarbon
PCCI	premixed charge compression ignition
PEPICO	photoelectron photoion coincidence
PES	photoelectron spectrum/spectra
PI	photoionization
PI-MBMS	photoionization molecular-beam mass spectrometry
PIMS	photoionization mass spectrometry
py-GC/MS	pyrolysis gas chromatrography mass spectrometry
py-iPEPICO	pyrolysis imaging photoelectron photoion coincidence
REMPI	resonance-enhanced multiphoton ionization
ReTOF-PIMS	reflectron time-of-flight photoionization mass spectrometry
RRR	radical-radical reaction
RSR	resonance-stabilized radical
SALVI	system for snalysis at the liquid vacuum interface
SLS	Swiss Light Source
SPES	slow photoelectron spectroscopy

SVUV-PIMS synchrotron vacuum ultraviolet photoionization mass spectrometry
TOF time of flight
TPES threshold photoelectron spectrum/spectra
TS transition state
UV ultraviolet
VM velocity map
VUV vacuum ultraviolet.

Biographies

Patrick Hemberger

Patrick Hemberger is a principal investigator and beamline scientist at Paul Scherrer Institute (Switzerland). He obtained his PhD in physical chemistry from university of Wurzburg (Germany). Patrick develops and applies PEPICO techniques utilizing VUV synchrotron radiation to unveil reaction mechanisms at all states, timescales and phases, with focus on combustion and catalysis. He received the Ružička Prize in Chemistry from ETH Zurich and is a Mercator fellow from the German Science Foundation (DFG).

Andras Bodi

Andras Bodi received his PhD from Eötvös University, Budapest under the auspices of Profs. B. Sztáray and T. Baer. He worked at the University of Iceland before joining the Paul Scherrer Institut in 2006. He constructed single and double imaging PEPICO endstations at the VUV beamline, where has been leading the Reaction Dynamics Group since 2016. He focuses on single-photon ionization and is excited to see PEPICO applications flourish at synchrotrons all over the world.

Thomas Bierkandt

Thomas Bierkandt is a researcher at the Institute of Combustion Technology of the German Aerospace Center in Stuttgart, Germany. He received the B.S. and M.S. degrees in chemistry and the Ph.D. degree in engineering from the University of Duisburg-Essen. His research expertise is the in-depth analysis of fuel decomposition and pollutant formation pathways in reacting flows, such as in flat low-pressure flames and tubular flow reactors, by molecular-beam mass spectrometry.

Markus Köhler

Markus Köhler is head of the department Chemical Kinetics and Analytics at the Institute of Combustion Technology of the German Aerospace Center in Stuttgart, Germany. He studied chemistry and received his Ph.D. degree in physical chemistry at the University of Bielefeld. His research expertise is deeply rooted in the field of alternative fuels. Understanding the combustion chemistry and pollutant formation from fuel composition all the way to emissions cover his current research.

Dennis Kaczmarek

Dennis Kaczmarek received his M.Sc. degree in mechanical engineering from Ruhr-Universität Bochum and recently his Ph.D. degree in mechanical engineering from the University of Duisburg-Essen in Germany. He is currently working in the DFG research unit FOR1993 with a research focus on experiments on fuel-rich conversion processes using different reactor types and analytical methods such as mass spectrometry and gas chromatography.

Tina Kasper

Tina Kasper has been a professor at the Institute of Combustion and Gas Dynamics at the University of Duisburg-Essen, Germany since 2011. She obtained her Ph.D. degree at Bielefeld University in Germany and was a researcher at Sandia National Laboratories and SRI International in the US. Her expertise is in diagnostics, reaction kinetics, renewable energy carriers, and flame synthesis.

(1) Commission, E. A European Green Deal. https://ec.europa.eu/info/strategy/priorities-2019-2024/european-green-deal_en.

(2) Nations, U. The Paris Agreement. https://unfccc.int/process-and-meetings/the-paris-agreement/the-paris-agreement.

(3) Tracker, C. A. Climate Action Tracker. https://climateactiontracker.org.

(4) Schlögl, R.; Abanades, C.; Aresta, M.; Azapagic, A.; Blekkan, E. A.; Cantat, T.; Centi, G.; Duic, N.; Khamlichi, A. c. E.; Hutchings, G., et al. *Novel carbon capture and utilisation technologies Research and climate aspects*; 2018.

(5) Minx, J. C.; Lamb, W. F.; Callaghan, M. W.; Fuss, S.; Hilaire, J.; Creutzig, F.; Amann, T.; Beringer, T.; de Oliveira Garcia, W.; Hartmann, J., et al. Negative emissions—Part 1: Research landscape and synthesis. *Environ. Res. Lett.* **2018,** *13* (6), 063001.

(6) Schlogl, R. Put the Sun in the Tank: Future Developments in Sustainable Energy Systems. *Angew. Chem. Int. Ed. Engl.* **2019,** *58* (1), 343-348.

(7) Gray, N.; McDonagh, S.; O'Shea, R.; Smyth, B.; Murphy, J. D. Decarbonising ships, planes and trucks: An analysis of suitable low-carbon fuels for the maritime, aviation and haulage sectors. *Adv. Appl. Energy* **2021,** *1*, 100008.

(8) Pregger, T.; Schiller, G.; Cebulla, F.; Dietrich, R.-U.; Maier, S.; Thess, A.; Lischke, A.; Monnerie, N.; Sattler, C.; Clercq, P. L., et al. Future Fuels—Analyses of the Future Prospects of Renewable Synthetic Fuels. *Energies* **2020,** *13* (1), 138.

(9) Schlögl, R. Chemical energy storage enables the transformation of fossil energy systems to sustainability. *Green Chemistry* **2021,** *23* (4), 1584-1593.

(10) Mawhood, R.; Gazis, E.; de Jong, S.; Hoefnagels, R.; Slade, R. Production pathways for renewable jet fuel: a review of commercialization status and future prospects. *Biofuels, Bioproducts and Biorefining* **2016,** *10* (4), 462-484.

(11) Jürgens, S.; Oßwald, P.; Selinsek, M.; Piermartini, P.; Schwab, J.; Pfeifer, P.; Bauder, U.; Ruoff, S.; Rauch, B.; Köhler, M. Assessment of combustion properties of non-hydroprocessed Fischer-Tropsch fuels for aviation. *Fuel Process. Technol.* **2019,** *193*, 232-243.

(12) Kobayashi, H.; Hayakawa, A.; Somarathne, K. D. Kunkuma A.; Okafor, Ekenechukwu C. Science and technology of ammonia combustion. *Proc. Combust. Inst.* **2019,** *37* (1), 109-133.

(13) Kaczmarek, D.; Shaqiri, S.; Atakan, B.; Kasper, T. The influence of pressure and equivalence ratio on the NTC behavior of methane. *Proc. Combust. Inst.* **2021,** *38* (1), 233-241.

(14) Kohse-Hoinghaus, K. *Applied Combustion Diagnostics*. CRC Press: 2002; Vol. 1.

(15) Taatjes, C. A.; Hansen, N.; Osborn, D. L.; Kohse-Höinghaus, K.; Cool, T. A.; Westmoreland, P. R. "Imaging" combustion chemistry via multiplexed synchrotron-photoionization mass spectrometry. *Phys. Chem. Chem. Phys.* **2008,** *10* (1), 20-34.

(16) Hansen, N.; Cool, T. A.; Westmoreland, P. R.; Kohse-Höinghaus, K. Recent contributions of flame-sampling molecular-beam mass spectrometry to a fundamental understanding of combustion chemistry. *Prog. Energy Combust. Sci.* **2009,** *35* (2), 168-191.

(17) Leone, S. R.; Ahmed, M.; Wilson, K. R. Chemical dynamics, molecular energetics, and kinetics at the synchrotron. *Phys. Chem. Chem. Phys.* **2010,** *12* (25), 6564-6578.

(18) Li, Y.; Qi, F. Recent Applications of Synchrotron VUV Photoionization Mass Spectrometry: Insight into Combustion Chemistry. *Acc. Chem. Res.* **2010,** *43* (1), 68-78.

(19) Dyke, J. M. Photoionization studies of reactive intermediates using synchrotron radiation. *Phys Chem Chem Phys* **2019,** *21* (18), 9106-9136.

(20) Baer, T.; Tuckett, R. P. Advances in threshold photoelectron spectroscopy (TPES) and threshold photoelectron photoion coincidence (TPEPICO). *Phys Chem Chem Phys* **2017,** *19* (15), 9698-9723.
(21) Steglich, M.; Custodis, V. B. F.; Trevitt, A. J.; daSilva, G.; Bodi, A.; Hemberger, P. Photoelectron Spectrum and Energetics of the meta-Xylylene Diradical. *J. Am. Chem. Soc.* **2017,** *139* (41), 14348-14351.
(22) Hemberger, P.; Trevitt, A. J.; Gerber, T.; Ross, E.; da Silva, G. Isomer-specific product detection of gas-phase xylyl radical rearrangement and decomposition using VUV synchrotron photoionization. *J. Phys. Chem. A* **2014,** *118* (20), 3593-604.
(23) Hemberger, P.; Custodis, V. B. F.; Bodi, A.; Gerber, T.; van Bokhoven, J. A. Understanding the mechanism of catalytic fast pyrolysis by unveiling reactive intermediates in heterogeneous catalysis. *Nat Commun* **2017,** *8*, 15946.
(24) Pan, Z.; Puente-Urbina, A.; Bodi, A.; van Bokhoven, J. A.; Hemberger, P. Isomer-dependent catalytic pyrolysis mechanism of the lignin model compounds catechol, resorcinol and hydroquinone. *Chem. Sci.* **2021,** *12* (9), 3161-3169.
(25) Jiao, F.; Li, J.; Pan, X.; Xiao, J.; Li, H.; Ma, H.; Wei, M.; Pan, Y.; Zhou, Z.; Li, M., et al. Selective conversion of syngas to light olefins. *Science* **2016,** *351* (6277), 1065-8.
(26) Zack, L. N.; Maier, J. P. Laboratory spectroscopy of astrophysically relevant carbon species. *Chem. Soc. Rev.* **2014,** *43* (13), 4602-14.
(27) Ryazantsev, S. V.; Feldman, V. I. Matrix-isolation studies on the radiation-induced chemistry in H(2)O/CO(2) systems: reactions of oxygen atoms and formation of HOCO radical. *J. Phys. Chem. A* **2015,** *119* (11), 2578-86.
(28) Novelli, A.; Hens, K.; Tatum Ernest, C.; Kubistin, D.; Regelin, E.; Elste, T.; Plass-Dülmer, C.; Martinez, M.; Lelieveld, J.; Harder, H. Characterisation of an inlet pre-injector laser-induced fluorescence instrument for the measurement of atmospheric hydroxyl radicals. *Atmos. Meas. Tech.* **2014,** *7* (10), 3413-3430.
(29) Bruneaux, G. Combustion structure of free and wall-impinging diesel jets by simultaneous laser-induced fluorescence of formaldehyde, poly-aromatic hydrocarbons, and hydroxides. *Int. J. Engine Res.* **2008,** *9* (3), 249-265.
(30) Yoon, M.-C.; Choi, Y. S.; Kim, S. K. The OH production from the π–π* transition of acetylacetone. *Chem. Phys. Lett.* **1999,** *300* (1-2), 207-212.
(31) Antonov, I.; Voronova, K.; Chen, M. W.; Sztaray, B.; Hemberger, P.; Bodi, A.; Osborn, D. L.; Sheps, L. To Boldly Look Where No One Has Looked Before: Identifying the Primary Photoproducts of Acetylacetone. *J. Phys. Chem. A* **2019,** *123* (26), 5472-5490.
(32) Osborn, D. L. Reaction Mechanisms on Multiwell Potential Energy Surfaces in Combustion (and Atmospheric) Chemistry. *Annu. Rev. Phys. Chem.* **2017,** *68*, 233-260.
(33) Jones, I. T. N.; Bayes, K. D. Detection of steady-state free-radical concentrations by photoionization. *J. Am. Chem. Soc.* **1972,** *94* (19), 6869-6871.
(34) Slagle, I. R.; Gutman, D. Kinetics of polyatomic free radicals produced by laser photolysis. 5. Study of the equilibrium methyl + oxygen .dblarw. CH3O2 between 421 and 538.degree. *J. Am. Chem. Soc.* **1985,** *107* (19), 5342-5347.
(35) Heringa, M. F.; DeCarlo, P. F.; Chirico, R.; Tritscher, T.; Clairotte, M.; Mohr, C.; Crippa, M.; Slowik, J. G.; Pfaffenberger, L.; Dommen, J., et al. A new method to discriminate secondary organic aerosols from different sources using high-resolution aerosol mass spectra. *Atmos. Chem. Phys.* **2012,** *12* (4), 2189-2203.
(36) Qi, F. Combustion chemistry probed by synchrotron VUV photoionization mass spectrometry. *Proc. Combust. Inst.* **2013,** *34* (1), 33-63.
(37) Kostko, O.; Bandyopadhyay, B.; Ahmed, M. Vacuum Ultraviolet Photoionization of Complex Chemical Systems. *Annu. Rev. Phys. Chem.* **2016,** *67* (1), 19-40.
(38) Osborn, D. L.; Zou, P.; Johnsen, H.; Hayden, C. C.; Taatjes, C. A.; Knyazev, V. D.; North, S. W.; Peterka, D. S.; Ahmed, M.; Leone, S. R. The multiplexed chemical kinetic photoionization mass

spectrometer: a new approach to isomer-resolved chemical kinetics. *Rev. Sci. Instrum.* **2008,** *79* (10), 104103.

(39) You, R.; Huang, W. Photoionization Mass Spectrometry for Online Detection of Reactive and Unstable Gas-Phase Intermediates in Heterogeneous Catalytic Reactions. *ChemCatChem* **2019,** *12* (3), cctc.201901639-cctc.201901639.

(40) Hemberger, P.; van Bokhoven, J. A.; Pérez-Ramírez, J.; Bodi, A. New analytical tools for advanced mechanistic studies in catalysis: photoionization and photoelectron photoion coincidence spectroscopy. *Cat. Sci. Technol.* **2020,** *10* (7), 1975-1990.

(41) Sheps, L.; Antonov, I.; Au, K. Sensitive Mass Spectrometer for Time-Resolved Gas-Phase Chemistry Studies at High Pressures. *J. Phys. Chem. A* **2019,** *123* (50), 10804-10814.

(42) Tranter, R. S.; Lynch, P. T. A miniature high repetition rate shock tube. *Rev. Sci. Instrum.* **2013,** *84* (9), 094102.

(43) Eppink, A. T. J. B.; Parker, D. H. Velocity map imaging of ions and electrons using electrostatic lenses: Application in photoelectron and photofragment ion imaging of molecular oxygen. *Rev. Sci. Instrum.* **1997,** *68* (9), 3477-3484.

(44) Bodi, A.; Hemberger, P.; Osborn, D. L.; Sztáray, B. Mass-Resolved Isomer-Selective Chemical Analysis with Imaging Photoelectron Photoion Coincidence Spectroscopy. *J. Phys. Chem. Lett.* **2013,** *4* (17), 2948-2952.

(45) Tang, X.; Zhou, X.; Niu, M.; Liu, S.; Sun, J.; Shan, X.; Liu, F.; Sheng, L. A threshold photoelectron-photoion coincidence spectrometer with double velocity imaging using synchrotron radiation. *Rev. Sci. Instrum.* **2009,** *80* (11), 113101-113101.

(46) Bodi, A.; Hemberger, P.; Gerber, T.; Sztáray, B. A new double imaging velocity focusing coincidence experiment: i2PEPICO. *Rev. Sci. Instrum.* **2012,** *83* (8), 083105-083105.

(47) Garcia, G. A.; Cunha de Miranda, B. K.; Tia, M.; Daly, S.; Nahon, L. DELICIOUS III: A multipurpose double imaging particle coincidence spectrometer for gas phase vacuum ultraviolet photodynamics studies. *Rev. Sci. Instrum.* **2013,** *84* (5), 053112-053112.

(48) Sztáray, B.; Voronova, K.; Torma, K. G.; Covert, K. J.; Bodi, A.; Hemberger, P.; Gerber, T.; Osborn, D. L. CRF-PEPICO: Double velocity map imaging photoelectron photoion coincidence spectroscopy for reaction kinetics studies. *J. Chem. Phys.* **2017,** *147* (1), 013944-013944.

(49) Jarvis, G. K.; Weitzel, K.-M.; Malow, M.; Baer, T.; Song, Y.; Ng, C. Y. High-resolution pulsed field ionization photoelectron-photoion coincidence spectroscopy using synchrotron radiation. *Rev. Sci. Instrum.* **1999,** *70* (10), 3892-3906.

(50) Bodi, A.; Csontos, J.; Kállay, M.; Borkar, S.; Sztáray, B. On the protonation of water. *Chemical Science* **2014,** *5* (8), 3057-3063.

(51) Matthiasson, K.; Kvaran, A.; Garcia, G. A.; Weidner, P.; Sztaray, B. Resolving the F2 bond energy discrepancy using coincidence ion pair production (cipp) spectroscopy. *Phys Chem Chem Phys* **2021,** *23* (14), 8292-8299.

(52) Bodi, A.; Sztaray, B.; Baer, T.; Johnson, M.; Gerber, T. Data acquisition schemes for continuous two-particle time-of-flight coincidence experiments. *Rev. Sci. Instrum.* **2007,** *78* (8), 084102.

(53) Wu, X.; Zhou, X.; Hemberger, P.; Bodi, A. Dissociative Photoionization of Dimethyl Carbonate: The More It Is Cut, the Bigger the Fragment Ion. *J. Chem. Phys. A* **2017,** *121* (14), 2748-2759.

(54) Steglich, M.; Wu, X.; Bodi, A.; Hemberger, P. Double-Imaging Photoelectron Photoion Coincidence Spectroscopy Reveals the Unimolecular Thermal Decomposition Mechanism of Dimethyl Carbonate. *J. Phys. Chem. A* **2021,** *125* (14), 2895-2904.

(55) Osterwalder, A.; Nee, M. J.; Zhou, J.; Neumark, D. M. High resolution photodetachment spectroscopy of negative ions via slow photoelectron imaging. *J. Chem. Phys.* **2004,** *121* (13), 6317-22.

(56) Sztáray, B.; Baer, T. Suppression of hot electrons in threshold photoelectron photoion coincidence spectroscopy using velocity focusing optics. *Rev. Sci. Instrum.* **2003,** *74* (8), 3763-3768.

(57) Bodi, A.; Hemberger, P. Imaging breakdown diagrams for bromobutyne isomers with photoelectron-photoion coincidence. *Phys Chem Chem Phys* **2014,** *16* (2), 505-15.

(58) Reusch, E.; Holzmeier, F.; Constantinidis, P.; Hemberger, P.; Fischer, I. Isomer-Selective Generation and Spectroscopic Characterization of Picolyl Radicals. *Angew. Chem. Int. Ed.* **2017,** *56* (27), 8000-8003.

(59) Zhao, L.; Doddipatla, S.; Kaiser, R. I.; Lu, W.; Kostko, O.; Ahmed, M.; Tuli, L. B.; Morozov, A. N.; Howlader, A. H.; Wnuk, S. F., et al. Gas-phase synthesis of corannulene - a molecular building block of fullerenes. *Phys Chem Chem Phys* **2021,** *23* (10), 5740-5749.

(60) Wu, X.; Zhou, X.; Hemberger, P.; Bodi, A. The ionization energy of the vinyl radical: a Mexican standoff with a happy ending. *Phys Chem Chem Phys* **2019,** *21* (40), 22238-22247.

(61) Garcia, G. A.; Loison, J.-C.; Holzmeier, F.; Gans, B.; Alcaraz, C.; Nahon, L.; Wu, X.; Zhou, X.; Bodi, A.; Hemberger, P. Characterisation of the first electronically excited state of protonated acetylene $C_2H_3^+$ by coincident imaging photoelectron spectroscopy. *Mol. Phys.* **2020,** *119* (1-2).

(62) Barone, V.; Bloino, J.; Biczysko, M.; Santoro, F. Fully Integrated Approach to Compute Vibrationally Resolved Optical Spectra: From Small Molecules to Macrosystems. *J. Chem. Theory Comput.* **2009,** *5* (3), 540-554.

(63) Koziol, L.; Mozhayskiy, V. A.; Braams, B. J.; Bowman, J. M.; Krylov, A. I. Ab initio calculation of the photoelectron spectra of the hydroxycarbene diradicals. *J. Phys. Chem. A* **2009,** *113* (27), 7802-9.

(64) Garcia, G. A.; Nahon, L.; Powis, I. Two-dimensional charged particle image inversion using a polar basis function expansion. *Rev. Sci. Instrum.* **2004,** *75* (11), 4989-4996.

(65) Poully, J. C.; Schermann, J. P.; Nieuwjaer, N.; Lecomte, F.; Grégoire, G.; Desfrançois, C.; Garcia, G. A.; Nahon, L.; Nandi, D.; Poisson, L., et al. Photoionization of 2-pyridone and 2-hydroxypyridine. *Phys. Chem. Chem. Phys.* **2010,** *12* (14), 3566-72.

(66) Pastoors, J. I. M.; Bodi, A.; Hemberger, P.; Bouwman, J. Dissociative Ionization and Thermal Decomposition of Cyclopentanone. *Chem. Europ. J.* **2017,** *23* (53), 13131-13140.

(67) Bouwman, J.; Hrodmarsson, H. R.; Ellison, G. B.; Bodi, A.; Hemberger, P. Five Birds with One Stone: Photoelectron Photoion Coincidence Unveils Rich Phthalide Pyrolysis Chemistry. *J. Phys. Chem. A* **2021,** *125* (8), 1738-1746.

(68) McCabe, M. N.; Hemberger, P.; Reusch, E.; Bodi, A.; Bouwman, J. Off the Beaten Path: Almost Clean Formation of Indene from the ortho-Benzyne + Allyl Reaction. *J Phys Chem Lett* **2020,** *11* (8), 2859-2863.

(69) Pieper, J.; Schmitt, S.; Hemken, C.; Davies, E.; Wullenkord, J.; Brockhinke, A.; Krüger, J.; Garcia, G. A.; Nahon, L.; Lucassen, A., et al. Isomer Identification in Flames with Double-Imaging Photoelectron/Photoion Coincidence Spectroscopy (i2PEPICO) using Measured and Calculated Reference Photoelectron Spectra. *Z. Phys. Chem.* **2018,** *232* (2), 153-187.

(70) Felsmann, D.; Moshammer, K.; Krüger, J.; Lackner, A.; Brockhinke, A.; Kasper, T.; Bierkandt, T.; Akyildiz, E.; Hansen, N.; Lucassen, A., et al. Electron ionization, photoionization and photoelectron/photoion coincidence spectroscopy in mass-spectrometric investigations of a low-pressure ethylene/oxygen flame. *Proc. Combust. Inst.* **2015,** *35* (1), 779-786.

(71) Biordi, J. C. Molecular beam mass spectrometry for studying the fundamental chemistry of flames. *Prog. Energy Combust. Sci.* **1977,** *3* (3), 151-173.

(72) Krüger, D.; Oßwald, P.; Köhler, M.; Hemberger, P.; Bierkandt, T.; Kasper, T. The fate of the OH radical in molecular beam sampling experiments. *Proc. Combust. Inst.* **2019,** *37* (2), 1563-1570.

(73) Yoder, B. L.; Bravaya, K. B.; Bodi, A.; West, A. H. C.; Sztáray, B.; Signorell, R. Barrierless proton transfer across weak CH···O hydrogen bonds in dimethyl ether dimer. *J. Chem. Phys.* **2015,** *142* (11), 114303-114303.

(74) Liang, S.; Hemberger, P.; Neisius, N. M.; Bodi, A.; Grützmacher, H.; Levalois-Grützmacher, J.; Gaan, S. Elucidating the Thermal Decomposition of Dimethyl Methylphosphonate by Vacuum Ultraviolet (VUV) Photoionization: Pathways to the PO Radical, a Key Species in Flame-Retardant Mechanisms. *Chemistry – A European Journal* **2015,** *21* (3), 1073-1080.

(75) Garcia, G. A.; Tang, X.; Gil, J. F.; Nahon, L.; Ward, M.; Batut, S.; Fittschen, C.; Taatjes, C. A.; Osborn, D. L.; Loison, J. C. Synchrotron-based double imaging photoelectron/photoion coincidence spectroscopy of radicals produced in a flow tube: OH and OD. *J. Chem. Phys.* **2015,** *142* (16), 164201.
(76) Nagaraju, S.; Tranter, R. S.; Cano Ardila, F. E.; Abid, S.; Lynch, P. T.; Garcia, G. A.; Gil, J. F.; Nahon, L.; Chaumeix, N.; Comandini, A. Reprint of: Pyrolysis of ethanol studied in a new high-repetition-rate shock tube coupled to synchrotron-based double imaging photoelectron/photoion coincidence spectroscopy. *Combust. Flame* **2021,** *224*, 150-165.
(77) Hoener, M.; Kaczmarek, D.; Bierkandt, T.; Bodi, A.; Hemberger, P.; Kasper, T. A pressurized flow reactor combustion experiment interfaced with synchrotron double imaging photoelectron photoion coincidence spectroscopy. *Rev. Sci. Instrum.* **2020,** *91* (4), 045115.
(78) Dufour, A.; Weng, J.; Jia, L.; Tang, X.; Sirjean, B.; Fournet, R.; Gall, H. L.; Brosse, N.; Billaud, F.; Mauviel, G., et al. Revealing the chemistry of biomass pyrolysis by means of tunable synchrotron photoionisation-mass spectrometry. *RSC Advances* **2013,** *3* (14), 4786-4792.
(79) Gerlach, M.; Bodi, A.; Hemberger, P. Metamorphic meta isomer: carbon dioxide and ketenes are formed via retro-Diels-Alder reactions in the decomposition of meta-benzenediol. *Phys Chem Chem Phys* **2019,** *21* (35), 19480-19487.
(80) Custodis, V. B. F.; Hemberger, P.; Ma, Z.; van Bokhoven, J. A. Mechanism of Fast Pyrolysis of Lignin: Studying Model Compounds. *J. Phys. Chem. B* **2014,** *118* (29), 8524-8531.
(81) Rathmann, R.; Szklo, A.; Schaeffer, R. Land use competition for production of food and liquid biofuels: An analysis of the arguments in the current debate. *Renewable Energy* **2010,** *35* (1), 14-22.
(82) Cao, L.; Yu, I. K. M.; Liu, Y.; Ruan, X.; Tsang, D. C. W.; Hunt, A. J.; Ok, Y. S.; Song, H.; Zhang, S. Lignin valorization for the production of renewable chemicals: State-of-the-art review and future prospects. *Bioresour. Technol.* **2018,** *269*, 465-475.
(83) Jablonski, W.; Gaston, K. R.; Nimlos, M. R.; Carpenter, D. L.; Feik, C. J.; Phillips, S. D. Pilot-Scale Gasification of Corn Stover, Switchgrass, Wheat Straw, and Wood: 2. Identification of Global Chemistry Using Multivariate Curve Resolution Techniques. *Ind. Eng. Chem. Res.* **2009,** *48* (23), 10691-10701.
(84) Fendt, A.; Streibel, T.; Sklorz, M.; Richter, D.; Dahmen, N.; Zimmermann, R. On-Line Process Analysis of Biomass Flash Pyrolysis Gases Enabled by Soft Photoionization Mass Spectrometry. *Energy & Fuels* **2012,** *26* (1), 701-711.
(85) Weng, J.; Jia, L.; Wang, Y.; Sun, S.; Tang, X.; Zhou, Z.; Kohse-Höinghaus, K.; Qi, F. Pyrolysis study of poplar biomass by tunable synchrotron vacuum ultraviolet photoionization mass spectrometry. *Proc. Combust. Inst.* **2013,** *34* (2), 2347-2354.
(86) Evans, R. J.; Milne, T. A. Molecular characterization of the pyrolysis of biomass. *Energy & Fuels* **1987,** *1* (2), 123-137.
(87) Weng, J.; Jia, L.; Sun, S.; Wang, Y.; Tang, X.; Zhou, Z.; Qi, F. On-line product analysis of pine wood pyrolysis using synchrotron vacuum ultraviolet photoionization mass spectrometry. *Anal. Bioanal. Chem* **2013,** *405* (22), 7097-7105.
(88) Jia, L.; Le Brech, Y.; Mauviel, G.; Qi, F.; Bente-von Frowein, M.; Ehlert, S.; Zimmermann, R.; Dufour, A. Online Analysis of Biomass Pyrolysis Tar by Photoionization Mass Spectrometry. *Energy & Fuels* **2016,** *30* (3), 1555-1563.
(89) He, T.; Zhang, Y.; Zhu, Y.; Wen, W.; Pan, Y.; Wu, J.; Wu, J. Pyrolysis Mechanism Study of Lignin Model Compounds by Synchrotron Vacuum Ultraviolet Photoionization Mass Spectrometry. *Energy & Fuels* **2016,** *30* (3), 2204-2208.
(90) Kohn, D. W.; Clauberg, H.; Chen, P. Flash pyrolysis nozzle for generation of radicals in a supersonic jet expansion. *Rev. Sci. Instrum.* **1992,** *63* (8), 4003-4005.
(91) Robichaud, D. J.; Scheer, A. M.; Mukarakate, C.; Ormond, T. K.; Buckingham, G. T.; Ellison, G. B.; Nimlos, M. R. Unimolecular thermal decomposition of dimethoxybenzenes. *J. Chem. Phys.* **2014,** *140* (23), 234302.

(92) Scheer, A. M.; Mukarakate, C.; Robichaud, D. J.; Nimlos, M. R.; Carstensen, H.-H.; Ellison, G. B. Unimolecular thermal decomposition of phenol and d5-phenol: Direct observation of cyclopentadiene formation via cyclohexadienone. *J. Chem. Phys.* **2012,** *136* (4), 044309.
(93) Scheer, A. M.; Mukarakate, C.; Robichaud, D. J.; Nimlos, M. R.; Carstensen, H. H.; Ellison, G. B. Unimolecular thermal decomposition of phenol and d5-phenol: direct observation of cyclopentadiene formation via cyclohexadienone. *J. Chem. Phys.* **2012,** *136* (4), 044309.
(94) Vasiliou, A. K.; Kim, J. H.; Ormond, T. K.; Piech, K. M.; Urness, K. N.; Scheer, A. M.; Robichaud, D. J.; Mukarakate, C.; Nimlos, M. R.; Daily, J. W., et al. Biomass pyrolysis: Thermal decomposition mechanisms of furfural and benzaldehyde. *J. Chem. Phys.* **2013,** *139* (10), 104310.
(95) Guan, Q.; Urness, K. N.; Ormond, T. K.; David, D. E.; Barney Ellison, G.; Daily, J. W. The properties of a micro-reactor for the study of the unimolecular decomposition of large molecules. *Int. Rev. Phys. Chem.* **2014,** *33* (4), 447-487.
(96) Grimm, S.; Baik, S.-J.; Hemberger, P.; Bodi, A.; Kempf, A. M.; Kasper, T.; Atakan, B. Gas-phase aluminium acetylacetonate decomposition: revision of the current mechanism by VUV synchrotron radiation. *Phys. Chem. Chem. Phys.* **2021**.
(97) Zagidullin, M. V.; Kaiser, R. I.; Porfiriev, D. P.; Zavershinskiy, I. P.; Ahmed, M.; Azyazov, V. N.; Mebel, A. M. Functional Relationships between Kinetic, Flow, and Geometrical Parameters in a High-Temperature Chemical Microreactor. *J. Chem. Phys. A* **2018,** *122* (45), 8819-8827.
(98) Ormond, T. K.; Hemberger, P.; Troy, T. P.; Ahmed, M.; Stanton, J. F.; Ellison, G. B. The ionisation energy of cyclopentadienone: a photoelectron–photoion coincidence study. *Mol. Phys.* **2015,** *113* (15-16), 2350-2358.
(99) Hemberger, P.; Pan, Z.; Bodi, A.; van Bokhoven, J. A.; Ormond, T. K.; Ellison, G. B.; Genossar, N.; Baraban, J. H. The Threshold Photoelectron Spectrum of Fulvenone: A Reactive Ketene Derivative in Lignin Valorization. *ChemPhysChem* **2020,** *21* (19), 2217-2222.
(100) Ormond, T. K.; Baraban, J. H.; Porterfield, J. P.; Scheer, A. M.; Hemberger, P.; Troy, T. P.; Ahmed, M.; Nimlos, M. R.; Robichaud, D. J.; Daily, J. W., et al. Thermal Decompositions of the Lignin Model Compounds: Salicylaldehyde and Catechol. *J. Chem. Phys. A* **2018,** *122* (28), 5911-5924.
(101) Custodis, V. B. F.; Hemberger, P.; van Bokhoven, J. A. How Inter- and Intramolecular Reactions Dominate the Formation of Products in Lignin Pyrolysis. *Chemistry – A European Journal* **2017,** *23* (36), 8658-8668.
(102) Mante, O. D.; Dayton, D. C.; Carpenter, J. R.; Wang, K.; Peters, J. E. Pilot-scale catalytic fast pyrolysis of loblolly pine over γ-Al2O3 catalyst. *Fuel* **2018,** *214*, 569-579.
(103) Scheer, A. M.; Mukarakate, C.; Robichaud, D. J.; Nimlos, M. R.; Ellison, G. B. Thermal Decomposition Mechanisms of the Methoxyphenols: Formation of Phenol, Cyclopentadienone, Vinylacetylene, and Acetylene. *J. Chem. Phys. A* **2011,** *115* (46), 13381-13389.
(104) Chowdhury, A. D.; Gascon, J. The Curious Case of Ketene in Zeolite Chemistry and Catalysis. *Angew. Chem. Int. Ed.* **2018,** *57* (46), 14982-14985.
(105) Anderson, J. R.; Chang, Y.-F.; Western, R. J. Retained and desorbed products from reaction of 1-hexene over H-ZSM5 zeolite: Routes to coke precursors. *J. Catal.* **1989,** *118* (2), 466-482.
(106) Zichittella, G.; Pérez-Ramírez, J. Status and prospects of the decentralised valorisation of natural gas into energy and energy carriers. *Chem. Soc. Rev.* **2021,** *50* (5), 2984-3012.
(107) Luo, L.; You, R.; Liu, Y.; Yang, J.; Zhu, Y.; Wen, W.; Pan, Y.; Qi, F.; Huang, W. Gas-Phase Reaction Network of Li/MgO-Catalyzed Oxidative Coupling of Methane and Oxidative Dehydrogenation of Ethane. *ACS Catalysis* **2019,** *9* (3), 2514-2520.
(108) Lunsford, J. H. The Catalytic Oxidative Coupling of Methane. *Angew. Chem. Int. Ed.* **1995,** *34* (9), 970-980.
(109) Driscoll, D. J.; Martir, W.; Wang, J. X.; Lunsford, J. H. Formation of gas-phase methyl radicals over magnesium oxide. *J. Am. Chem. Soc.* **1985,** *107* (1), 58-63.
(110) Paunović, V.; Hemberger, P.; Bodi, A.; López, N.; Pérez-Ramírez, J. Evidence of radical chemistry in catalytic methane oxybromination. *Nat. Catal.* **2018,** *1* (5), 363-370.

(111) Paunović, V.; Zichittella, G.; Hemberger, P.; Bodi, A.; Pérez-Ramírez, J. Selective Methane Functionalization via Oxyhalogenation over Supported Noble Metal Nanoparticles. *ACS Catalysis* **2019,** *9* (3), 1710-1725.
(112) Zichittella, G.; Scharfe, M.; Puértolas, B.; Paunović, V.; Hemberger, P.; Bodi, A.; Szentmiklósi, L.; López, N.; Pérez-Ramírez, J. Halogen-Dependent Surface Confinement Governs Selective Alkane Functionalization to Olefins. *Angew. Chem. Int. Ed.* **2019,** *58* (18), 5877-5881.
(113) Zichittella, G.; Hemberger, P.; Holzmeier, F.; Bodi, A.; Pérez-Ramírez, J. Operando Photoelectron Photoion Coincidence Spectroscopy Unravels Mechanistic Fingerprints of Propane Activation by Catalytic Oxyhalogenation. *J. Phys. Chem. Lett.* **2020,** *11* (3), 856-863.
(114) Holzmeier, F.; Herbert, M.-P.; Fischer, I.; Steglich, M.; Bodi, A.; Hemberger, P. A photoionization study of 2-propyl and t-butyl radicals. *J. Anal. Appl. Pyrolysis* **2017,** *124*, 454-460.
(115) Dyke, J. M.; Jonathan, N.; Lewis, A. E.; Mills, J. D.; Morris, A. Vacuum ultraviolet photoelectron spectroscopy of transient species. *Mol. Phys.* **1983,** *50* (1), 77-89.
(116) Schleier, D.; Constantinidis, P.; Faßheber, N.; Fischer, I.; Friedrichs, G.; Hemberger, P.; Reusch, E.; Sztáray, B.; Voronova, K. Kinetics of the a-C3H5 + O2 reaction, investigated by photoionization using synchrotron radiation. *Phys. Chem. Chem. Phys.* **2018,** *20* (16), 10721-10731.
(117) IEA, I. E. A. World Energy Outlook 2020. https://www.iea.org/reports/world-energy-outlook-2020.
(118) Kohse-Höinghaus, K. A new era for combustion research. *Pure Appl. Chem.* **2019,** *91* (2), 271-288.
(119) Yuan, W.; Li, T.; Li, Y.; Zeng, M.; Zhang, Y.; Zou, J.; Cao, C.; Li, W.; Yang, J.; Qi, F. Experimental and kinetic modeling investigation on anisole pyrolysis: Implications on phenoxy and cyclopentadienyl chemistry. *Combust. Flame* **2019,** *201*, 187-199.
(120) Taatjes, C. A.; Hansen, N.; McIlroy, A.; Miller, J. A.; Senosiain, J. P.; Klippenstein, S. J.; Qi, F.; Sheng, L.; Zhang, Y.; Cool, T. A., et al. Enols are common intermediates in hydrocarbon oxidation. *Science* **2005,** *308* (5730), 1887-9.
(121) Kathrotia, T.; Naumann, C.; Oßwald, P.; Köhler, M.; Riedel, U. Kinetics of Ethylene Glycol: The first validated reaction scheme and first measurements of ignition delay times and speciation data. *Combust. Flame* **2017,** *179*, 172-184.
(122) Kruger, J.; Garcia, G. A.; Felsmann, D.; Moshammer, K.; Lackner, A.; Brockhinke, A.; Nahon, L.; Kohse-Hoinghaus, K. Photoelectron-photoion coincidence spectroscopy for multiplexed detection of intermediate species in a flame. *Phys Chem Chem Phys* **2014,** *16* (41), 22791-804.
(123) Oßwald, P.; Hemberger, P.; Bierkandt, T.; Akyildiz, E.; Köhler, M.; Bodi, A.; Gerber, T.; Kasper, T. In situ flame chemistry tracing by imaging photoelectron photoion coincidence spectroscopy. *Rev. Sci. Instrum.* **2014,** *85* (2), 025101-025101.
(124) D., S.; D., P.; M.J., C. Use of laser-induced fluorescence of OH to study the perturbation of a flame by a probe. *Symposium (International) on Combustion* **1981,** *18*, 1567-1573.
(125) Egolfopoulos, F. N.; Hansen, N.; Ju, Y.; Kohse-Höinghaus, K.; Law, C. K.; Qi, F. Advances and challenges in laminar flame experiments and implications for combustion chemistry. *Prog. Energy Combust. Sci.* **2014,** *43*, 36-67.
(126) Bierkandt, T.; Hemberger, P.; Oßwald, P.; Köhler, M.; Kasper, T. Insights in m-xylene decomposition under fuel-rich conditions by imaging photoelectron photoion coincidence spectroscopy. *Proc. Combust. Inst.* **2017,** *36* (1), 1223-1232.
(127) Kasper, T.; Oßwald, P.; Struckmeier, U.; Kohse-Höinghaus, K.; Taatjes, C. A.; Wang, J.; Cool, T. A.; Law, M. E.; Morel, A.; Westmoreland, P. R. Combustion chemistry of the propanol isomers — investigated by electron ionization and VUV-photoionization molecular-beam mass spectrometry. *Combust. Flame* **2009,** *156* (6), 1181-1201.
(128) Matras, D.; Villermaux, J. Un réacteur continu parfaitement agité par jets gazeux pour l'étude cinétique de réactions chimiques rapides. *Chem. Eng. Sci.* **1973,** *28* (1), 129-137.
(129) Wang, Z.; Herbinet, O.; Hansen, N.; Battin-Leclerc, F. Exploring hydroperoxides in combustion: History, recent advances and perspectives. *Prog. Energy Combust. Sci.* **2019,** *73*, 132-181.

(130) N. Gaiser, T. B., P. Oßwald, J. Zinsmeister, P. Hemberger, S. Shaqiri, T. Kasper, M. Köhler, M. Aigner. In *Disentangling of linear and branched ethers: Flow reactor study of OME2 and trimethoxymethane using molecular beam mass spectrometry and synchrotron photoionization*, Proceedings of the 10th European Combustion Meeting, , Virtual Edition, Virtual Edition, 2021.

(131) Rasmussen, C. L.; Rasmussen, A. E.; Glarborg, P. Sensitizing effects of NOx on CH4 oxidation at high pressure. *Combust. Flame* **2008,** *154* (3), 529-545.

(132) Rasmussen, C. L.; Glarborg, P. Direct Partial Oxidation of Natural Gas to Liquid Chemicals: Chemical Kinetic Modeling and Global Optimization. *Ind. Eng. Chem. Res.* **2008,** *47* (17), 6579-6588.

(133) Rasmussen, C. L.; Jakobsen, J. G.; Glarborg, P. Experimental measurements and kinetic modeling of CH4/O2and CH4/C2H6/O2conversion at high pressure. *Int. J. Chem. Kinet.* **2008,** *40* (12), 778-807.

(134) Osswald, P.; Kohler, M. An atmospheric pressure high-temperature laminar flow reactor for investigation of combustion and related gas phase reaction systems. *Rev. Sci. Instrum.* **2015,** *86* (10), 105109.

(135) Bierkandt, T.; Oßwald, P.; Gaiser, N.; Krüger, D.; Köhler, M.; Hoener, M.; Shaqiri, S.; Kaczmarek, D.; Karakaya, Y.; Hemberger, P., et al. Observation of low-temperature chemistry products in laminar premixed low-pressure flames by molecular-beam mass spectrometry. *Int. J. Chem. Kinet.* *n/a* (n/a).

(136) Nuss, E.; Wick, M.; Andert, J.; De Schutter, J.; Diehl, M.; Abel, D.; Albin, T. Nonlinear model predictive control of a discrete-cycle gasoline-controlled auto ignition engine model: Simulative analysis. *Int. J. Engine Res.* **2019,** *20* (10), 1025-1036.

(137) Hansen, N.; Li, W.; Law, M. E.; Kasper, T.; Westmoreland, P. R.; Yang, B.; Cool, T. A.; Lucassen, A. The importance of fuel dissociation and propargyl + allyl association for the formation of benzene in a fuel-rich 1-hexene flame. *Phys Chem Chem Phys* **2010,** *12* (38), 12112-22.

(138) Bierkandt, T.; Hoener, M.; Gaiser, N.; Hansen, N.; Köhler, M.; Kasper, T. Experimental flat flame study of monoterpenes: Insights into the combustion kinetics of α-pinene, β-pinene, and myrcene. *Proc. Combust. Inst.* **2021,** *38* (2), 2431-2440.

(139) Zádor, J.; Taatjes, C. A.; Fernandes, R. X. Kinetics of elementary reactions in low-temperature autoignition chemistry. *Prog. Energy Combust. Sci.* **2011,** *37* (4), 371-421.

(140) da Silva, G.; Moore, E. E.; Bozzelli, J. W. Decomposition of methylbenzyl radicals in the pyrolysis and oxidation of xylenes. *J. Phys. Chem. A* **2009,** *113* (38), 10264-78.

(141) Hemberger, P.; Trevitt, A. J.; Ross, E.; da Silva, G. Direct Observation of para -Xylylene as the Decomposition Product of the meta -Xylyl Radical Using VUV Synchrotron Radiation. *J. Phys. Chem. Lett.* **2013,** *4* (15), 2546-2550.

(142) Krüger, D.; Oßwald, P.; Köhler, M.; Hemberger, P.; Bierkandt, T.; Karakaya, Y.; Kasper, T. Hydrogen abstraction ratios: A systematic iPEPICO spectroscopic investigation in laminar flames. *Combust. Flame* **2018,** *191*, 343-352.

(143) Schenk, M.; Leon, L.; Moshammer, K.; Oßwald, P.; Zeuch, T.; Seidel, L.; Mauss, F.; Kohse-Höinghaus, K. Detailed mass spectrometric and modeling study of isomeric butene flames. *Combust. Flame* **2013,** *160* (3), 487-503.

(144) Dias, V.; Vandooren, J. Experimental and modeling study of a lean premixed iso-butene/hydrogen/oxygen/argon flame. *Fuel* **2010,** *89* (9), 2633-2639.

(145) Oßwald, P.; Kohse-Höinghaus, K.; Struckmeier, U.; Zeuch, T.; Seidel, L.; Leon, L.; Mauss, F. Combustion Chemistry of the Butane Isomers in Premixed Low-Pressure Flames. *Z. Phys. Chem.* **2011,** *225* (9-10), 1029-1054.

(146) Battin-Leclerc, F.; Herbinet, O.; Glaude, P. A.; Fournet, R.; Zhou, Z.; Deng, L.; Guo, H.; Xie, M.; Qi, F. Experimental confirmation of the low-temperature oxidation scheme of alkanes. *Angew. Chem. Int. Ed. Engl.* **2010,** *49* (18), 3169-72.

(147) Moshammer, K.; Jasper, A. W.; Popolan-Vaida, D. M.; Lucassen, A.; Dievart, P.; Selim, H.; Eskola, A. J.; Taatjes, C. A.; Leone, S. R.; Sarathy, S. M., et al. Detection and Identification of the

Keto-Hydroperoxide (HOOCH2OCHO) and Other Intermediates during Low-Temperature Oxidation of Dimethyl Ether. *J. Phys. Chem. A* **2015,** *119* (28), 7361-74.
(148) Moshammer, K.; Jasper, A. W.; Popolan-Vaida, D. M.; Wang, Z.; Bhavani Shankar, V. S.; Ruwe, L.; Taatjes, C. A.; Dagaut, P.; Hansen, N. Quantification of the Keto-Hydroperoxide (HOOCH2OCHO) and Other Elusive Intermediates during Low-Temperature Oxidation of Dimethyl Ether. *J. Phys. Chem. A* **2016,** *120* (40), 7890-7901.
(149) Herbinet, O.; Battin-Leclerc, F. Progress in Understanding Low-Temperature Organic Compound Oxidation Using a Jet-Stirred Reactor. *Int. J. Chem. Kinet.* **2014,** *46* (10), 619-639.
(150) Battin-Leclerc, F.; Bourgalais, J.; Gouid, Z.; Herbinet, O.; Garcia, G.; Arnoux, P.; Wang, Z.; Tran, L.-S.; Vanhove, G.; Nahon, L., et al. Chemistry deriving from OOQOOH radicals in alkane low-temperature oxidation: A first combined theoretical and electron-ion coincidence mass spectrometry study. *Proc. Combust. Inst.* **2020**.
(151) Bourgalais, J.; Gouid, Z.; Herbinet, O.; Garcia, G. A.; Arnoux, P.; Wang, Z.; Tran, L. S.; Vanhove, G.; Hochlaf, M.; Nahon, L., et al. Isomer-sensitive characterization of low temperature oxidation reaction products by coupling a jet-stirred reactor to an electron/ion coincidence spectrometer: case of n-pentane. *Phys Chem Chem Phys* **2020,** *22* (3), 1222-1241.
(152) Bugler, J.; Somers, K. P.; Silke, E. J.; Curran, H. J. Revisiting the Kinetics and Thermodynamics of the Low-Temperature Oxidation Pathways of Alkanes: A Case Study of the Three Pentane Isomers. *J. Phys. Chem. A* **2015,** *119* (28), 7510-27.
(153) Bugler, J.; Rodriguez, A.; Herbinet, O.; Battin-Leclerc, F.; Togbé, C.; Dayma, G.; Dagaut, P.; Curran, H. J. An experimental and modelling study of n-pentane oxidation in two jet-stirred reactors: The importance of pressure-dependent kinetics and new reaction pathways. *Proc. Combust. Inst.* **2017,** *36* (1), 441-448.
(154) Rodriguez, A.; Herbinet, O.; Wang, Z.; Qi, F.; Fittschen, C.; Westmoreland, P. R.; Battin-Leclerc, F. Measuring hydroperoxide chain-branching agents during n-pentane low-temperature oxidation. *Proc. Combust. Inst.* **2017,** *36* (1), 333-342.
(155) Bierkandt, T.; Oßwald, P.; Gaiser, N.; Krüger, D.; Köhler, M.; Hoener, M.; Shaqiri, S.; Kaczmarek, D.; Karakaya, Y.; Hemberger, P., et al. Observation of low-temperature chemistry products in laminar premixed low-pressure flames by molecular-beam mass spectrometry. *Int. J. Chem. Kinet.* **2021**.
(156) Voronova, K.; Ervin, K. M.; Torma, K. G.; Hemberger, P.; Bodi, A.; Gerber, T.; Osborn, D. L.; Sztáray, B. Radical Thermometers, Thermochemistry, and Photoelectron Spectra: A Photoelectron Photoion Coincidence Spectroscopy Study of the Methyl Peroxy Radical. *J. Phys. Chem. Lett.* **2018,** *9* (3), 534-539.
(157) Zhang, X.; Zhang, Y.; Li, T.; Li, Y.; Zou, J.; Dagaut, P.; Yang, J.; Li, W.; Zeng, M.; Jin, H., et al. Low-temperature chemistry triggered by probe cooling in a low-pressure premixed flame. *Combust. Flame* **2019,** *204*, 260-267.
(158) Meloni, G.; Zou, P.; Klippenstein, S. J.; Ahmed, M.; Leone, S. R.; Taatjes, C. A.; Osborn, D. L. Energy-resolved photoionization of alkylperoxy radicals and the stability of their cations. *J Am Chem Soc* **2006,** *128* (41), 13559-67.
(159) Tang, X.; Lin, X.; Garcia, G. A.; Loison, J.-C.; Gouid, Z.; Abdallah, H. H.; Fittschen, C.; Hochlaf, M.; Gu, X.; Zhang, W., et al. Identifying isomers of peroxy radicals in the gas phase: 1-C3H7O2vs. 2-C3H7O2. *Chem. Commun.* **2020,** *56* (99), 15525-15528.
(160) Battin-Leclerc, F.; Herbinet, O.; Glaude, P.-A.; Fournet, R.; Zhou, Z.; Deng, L.; Guo, H.; Xie, M.; Qi, F. Experimental Confirmation of the Low-Temperature Oxidation Scheme of Alkanes. *Angew. Chem.* **2010,** *122* (18), 3237-3240.
(161) Zhang, Y.; El-Merhubi, H.; Lefort, B.; Le Moyne, L.; Curran, H. J.; Kéromnès, A. Probing the low-temperature chemistry of ethanol via the addition of dimethyl ether. *Combust. Flame* **2018,** *190*, 74-86.
(162) Frenklach, M.; Wang, H. Detailed Mechanism and Modeling of Soot Particle Formation. In *Soot Formation in Combustion*, 1994; pp 165-192.

(163) Hansen, N.; Klippenstein, S. J.; Taatjes, C. A.; Miller, J. A.; Wang, J.; Cool, T. A.; Yang, B.; Yang, R.; Wei, L.; Huang, C., et al. Identification and chemistry of C4H3 and C4H5 isomers in fuel-rich flames. *J. Phys. Chem. A* **2006,** *110* (10), 3670-8.
(164) Bierkandt, T.; Kasper, T.; Akyildiz, E.; Lucassen, A.; Oßwald, P.; Köhler, M.; Hemberger, P. Flame structure of a low-pressure laminar premixed and lightly sooting acetylene flame and the effect of ethanol addition. *Proc. Combust. Inst.* **2015,** *35* (1), 803-811.
(165) Bierkandt, T.; Hemberger, P.; Oßwald, P.; Krüger, D.; Köhler, M.; Kasper, T. Flame structure of laminar premixed anisole flames investigated by photoionization mass spectrometry and photoelectron spectroscopy. *Proc. Combust. Inst.* **2019,** *37* (2), 1579-1587.
(166) Hemberger, P.; Custodis, V. B. F.; Bodi, A.; Gerber, T.; van Bokhoven, J. A. Understanding the mechanism of catalytic fast pyrolysis by unveiling reactive intermediates in heterogeneous catalysis. *Nature Communications* **2017,** *8*, 15946-15946.
(167) Felsmann, D.; Lucassen, A.; Krüger, J.; Hemken, C.; Tran, L.-S.; Pieper, J.; Garcia, G. A.; Brockhinke, A.; Nahon, L.; Kohse-Höinghaus, K. Progress in Fixed-Photon-Energy Time-Efficient Double Imaging Photoelectron/Photoion Coincidence Measurements in Quantitative Flame Analysis. *Z. Phys. Chem.* **2016,** *230* (8), 1067-1097.
(168) Pereira, J. P. C.; van der Wielen, L. A. M.; Straathof, A. J. J. Perspectives for the microbial production of methyl propionate integrated with product recovery. *Bioresour. Technol.* **2018,** *256*, 187-194.
(169) Glarborg, P.; Miller, J. A.; Ruscic, B.; Klippenstein, S. J. Modeling nitrogen chemistry in combustion. *Prog. Energy Combust. Sci.* **2018,** *67*, 31-68.
(170) de Persis, S.; Pillier, L.; Idir, M.; Molet, J.; Lamoureux, N.; Desgroux, P. NO formation in high pressure premixed flames: Experimental results and validation of a new revised reaction mechanism. *Fuel* **2020,** *260*.
(171) Shrestha, K. P.; Seidel, L.; Zeuch, T.; Moréac, G.; Dagaut, P.; Mauss, F. On the implications of nitromethane – NO chemistry interactions for combustion processes. *Fuel* **2021,** *289*.
(172) Kovács, M.; Papp, M.; Zsély, I. G.; Turányi, T. Determination of rate parameters of key N/H/O elementary reactions based on H2/O2/NOx combustion experiments. *Fuel* **2020,** *264*.
(173) Kovács, M.; Papp, M.; Zsély, I. G.; Turányi, T. Main sources of uncertainty in recent methanol/NOx combustion models. *Int. J. Chem. Kinet.* **2021**.
(174) Rasmussen, C. L.; Hansen, J.; Marshall, P.; Glarborg, P. Experimental measurements and kinetic modeling of CO/H2/O2/NOxconversion at high pressure. *Int. J. Chem. Kinet.* **2008,** *40* (8), 454-480.
(175) Kaczmarek, D.; Atakan, B.; Kasper, T. Investigation of the partial oxidation of methane/n-heptane-mixtures and the interaction of methane and n-heptane under ultra-rich conditions. *Combust. Flame* **2019,** *205*, 345-357.
(176) Kaczmarek, D.; Atakan, B.; Kasper, T. Plug-Flow Reactor Study of the Partial Oxidation of Methane and Natural Gas at Ultra-Rich Conditions. *Combust. Sci. Technol.* **2019,** *191* (9), 1571-1584.
(177) Chen, X.; Fuller, M. E.; Franklin Goldsmith, C. Decomposition kinetics for HONO and HNO2. *Reaction Chemistry & Engineering* **2019,** *4* (2), 323-333.
(178) Chai, J.; Goldsmith, C. F. Rate coefficients for fuel + NO2: Predictive kinetics for HONO and HNO2 formation. *Proc. Combust. Inst.* **2017,** *36* (1), 617-626.
(179) Fuller, M. E.; Goldsmith, C. F. On the relative importance of HONO versus HNO2 in low-temperature combustion. *Proc. Combust. Inst.* **2019,** *37* (1), 695-702.
(180) Marrodán, L.; Song, Y.; Herbinet, O.; Alzueta, M. U.; Fittschen, C.; Ju, Y.; Battin-Leclerc, F. First detection of a key intermediate in the oxidation of fuel + NO systems: HONO. *Chem. Phys. Lett.* **2019,** *719*, 22-26.
(181) Weng, J.-J.; Tian, Z.-Y.; Zhang, K.-W.; Ye, L.-L.; Liu, Y.-X.; Wu, L.-N.; Yu, D.; Yang, J.-Z.; Cao, C.-C.; Zou, J.-B. Experimental and kinetic investigation of pyrolysis and oxidation of nitromethane. *Combust. Flame* **2019,** *203*, 247-254.

(182) Taatjes, C. A.; Osborn, D. L.; Cool, T. A.; Nakajima, K. Synchrotron photoionization measurements of combustion intermediates: the photoionization efficiency of HONO. *Chem. Phys. Lett.* **2004,** *394* (1-3), 19-24.
(183) Hoener, M.; Bodi, A.; Hemberger, P.; Endres, T.; Kasper, T. Threshold photoionization shows no sign of nitryl hydride in methane oxidation with nitric oxide. *Phys. Chem. Chem. Phys.* **2021,** *23* (2), 1265-1272.
(184) Savee, J. D.; Papajak, E.; Rotavera, B.; Huang, H.; Eskola, A. J.; Welz, O.; Sheps, L.; Taatjes, C. A.; Zádor, J.; Osborn, D. L. Direct observation and kinetics of a hydroperoxyalkyl radical (QOOH). *Science* **2015,** *347* (6222), 643-646.
(185) Zádor, J.; Huang, H.; Welz, O.; Zetterberg, J.; Osborn, D. L.; Taatjes, C. A. Directly measuring reaction kinetics of ˙QOOH – a crucial but elusive intermediate in hydrocarbon autoignition. *Phys. Chem. Chem. Phys.* **2013,** *15* (26), 10753-10760.
(186) Taatjes, C. A.; Meloni, G.; Selby, T. M.; Trevitt, A. J.; Osborn, D. L.; Percival, C. J.; Shallcross, D. E. Direct Observation of the Gas-Phase Criegee Intermediate (CH2OO). *J. Am. Chem. Soc.* **2008,** *130* (36), 11883-11885.
(187) Sheps, L. Absolute Ultraviolet Absorption Spectrum of a Criegee Intermediate CH2OO. *J. Phys. Chem. Lett.* **2013,** *4* (24), 4201-4205.
(188) Huang, H.; Eskola, A. J.; Taatjes, C. A. Pressure-Dependent I-Atom Yield in the Reaction of CH2I with O2 Shows a Remarkable Apparent Third-Body Efficiency for O2. *J. Phys. Chem. Lett.* **2012,** *3* (22), 3399-3403.
(189) Eskola, A. J.; Wojcik-Pastuszka, D.; Ratajczak, E.; Timonen, R. S. Kinetics of the reactions of CH2Br and CH2I radicals with molecular oxygen at atmospheric temperatures. *Phys. Chem. Chem. Phys.* **2006,** *8* (12), 1416-1424.
(190) Lee, J.; Bozzelli, J. W. Thermochemical and kinetic analysis of the allyl radical with O2 reaction system. *Proc. Combust. Inst.* **2005,** *30* (1), 1015-1022.
(191) Schleier, D.; Reusch, E.; Gerlach, M.; Preitschopf, T.; Mukhopadhyay, D. P.; Faßheber, N.; Friedrichs, G.; Hemberger, P.; Fischer, I. Kinetics of 1- and 2-methylallyl + O2 reaction, investigated by photoionisation using synchrotron radiation. *Phys. Chem. Chem. Phys.* **2021,** *23* (2), 1539-1549.
(192) Bouwman, J.; Bodi, A.; Oomens, J.; Hemberger, P. On the formation of cyclopentadiene in the C3H5˙ + C2H2 reaction. *Phys. Chem. Chem. Phys.* **2015,** *17* (32), 20508-20514.
(193) Melius, C. F.; Colvin, M. E.; Marinov, N. M.; Pit, W. J.; Senkan, S. M. Reaction mechanisms in aromatic hydrocarbon formation involving the C5H5 cyclopentadienyl moiety. *Symposium (International) on Combustion* **1996,** *26* (1), 685-692.
(194) Kaiser, R. I.; Hansen, N. An Aromatic Universe-A Physical Chemistry Perspective. *J. Phys. Chem. A* **2021,** *125* (18), 3826-3840.
(195) Parker, D. S. N.; Kaiser, R. I.; Troy, T. P.; Ahmed, M. Hydrogen Abstraction/Acetylene Addition Revealed. *Angew. Chem. Int. Ed.* **2014,** *53* (30), 7740-7744.
(196) Zhao, L.; Kaiser, R. I.; Xu, B.; Ablikim, U.; Ahmed, M.; Zagidullin, M. V.; Azyazov, V. N.; Howlader, A. H.; Wnuk, S. F.; Mebel, A. M. VUV Photoionization Study of the Formation of the Simplest Polycyclic Aromatic Hydrocarbon: Naphthalene (C10H8). *J. Phys. Chem. Lett.* **2018,** *9* (10), 2620-2626.
(197) Zhao, L.; Prendergast, M. B.; Kaiser, R. I.; Xu, B.; Ablikim, U.; Ahmed, M.; Sun, B.-J.; Chen, Y.-L.; Chang, A. H. H.; Mohamed, R. K., et al. Synthesis of Polycyclic Aromatic Hydrocarbons by Phenyl Addition–Dehydrocyclization: The Third Way. *Angew. Chem. Int. Ed.* **2019,** *58* (48), 17442-17450.
(198) Doddipatla, S.; Galimova, G. R.; Wei, H.; Thomas, A. M.; He, C.; Yang, Z.; Morozov, A. N.; Shingledecker, C. N.; Mebel, A. M.; Kaiser, R. I. Low-temperature gas-phase formation of indene in the interstellar medium. *Science Advances* **2021,** *7* (1), eabd4044.
(199) Zhao, L.; Kaiser, R. I.; Lu, W.; Xu, B.; Ahmed, M.; Morozov, A. N.; Mebel, A. M.; Howlader, A. H.; Wnuk, S. F. Molecular mass growth through ring expansion in polycyclic aromatic hydrocarbons via radical–radical reactions. *Nature Communications* **2019,** *10* (1), 3689.

(200) Kaiser, D.; Reusch, E.; Hemberger, P.; Bodi, A.; Welz, E.; Engels, B.; Fischer, I. The ortho-benzyne cation is not planar. *Phys. Chem. Chem. Phys.* **2018,** *20* (6), 3988-3996.
(201) West, B.; Sit, A.; Bodi, A.; Hemberger, P.; Mayer, P. M. Dissociative Photoionization and Threshold Photoelectron Spectra of Polycyclic Aromatic Hydrocarbon Fragments: An Imaging Photoelectron Photoion Coincidence (iPEPICO) Study of Four Substituted Benzene Radical Cations. *J. Chem. Phys. A* **2014,** *118* (47), 11226-11234.
(202) Runge, W.; Kosbahn, W.; Kroner, J. The Molecular Structure of Allenes and Ketenes II [1] Photoelectron Spectra, Absorption Spectra, and CNDO/S-Calculations of Phenyl and Methyl Substituted Allenes. *Ber. Bunsenges. Phys. Chem.* **1975,** *79* (4), 371-381.
(203) Elbel, S.; Lienert, K.; Krebs, A.; Dieck, H. T. Photoelektronenspektren von Phenylethinen, I. Phenylethin - Mustersonde für Substituenteneffekte. *Liebigs Ann. Chem.* **1981,** *1981* (10), 1785-1797.
(204) Comandini, A.; Abid, S.; Chaumeix, N. Polycyclic Aromatic Hydrocarbon Growth by Diradical Cycloaddition/Fragmentation. *J. Chem. Phys. A* **2017,** *121* (31), 5921-5931.
(205) Bouwman, J.; Bodi, A.; Hemberger, P. Nitrogen matters: the difference between PANH and PAH formation. *Phys. Chem. Chem. Phys.* **2018,** *20* (47), 29910-29917.
(206) Twarowski, A. Photometric determination of the rate of H2O formation from H and OH in the presence of phosphine combustion products. *Combust. Flame* **1993,** *94* (4), 341-348.
(207) Twarowski, A. The influence of phosphorus oxides and acids on the rate of H + OH recombination. *Combust. Flame* **1993,** *94* (1), 91-107.
(208) Bolshova, T. A.; Shvartsberg, V. M.; Korobeinichev, O. P.; Shmakov, A. G. A skeletal mechanism for flame inhibition by trimethylphosphate. *Combust. Theory Model.* **2016,** *20* (2), 189-202.
(209) Korobeinichev, O. P.; Ilyin, S. B.; Mokrushin, V. V.; Shmakov, A. G. Destruction Chemistry of Dimethyl Methylphosphonate in H2/O2/Ar FlameStudied by Molecular Beam Mass Spectrometry. *Combust. Sci. Technol.* **1996,** *116-117* (1-6), 51-67.
(210) Liang, S.; Hemberger, P.; Levalois-Grützmacher, J.; Grützmacher, H.; Gaan, S. Probing Phosphorus Nitride (P≡N) and Other Elusive Species Formed upon Pyrolysis of Dimethyl Phosphoramidate. *Chemistry – A European Journal* **2017,** *23* (23), 5595-5601.
(211) Liang, S.; Hemberger, P.; Steglich, M.; Simonetti, P.; Levalois-Grützmacher, J.; Grützmacher, H.; Gaan, S. The Underlying Chemistry to the Formation of PO2 Radicals from Organophosphorus Compounds: A Missing Puzzle Piece in Flame Chemistry. *Chemistry – A European Journal* **2020,** *26* (47), 10795-10800.
(212) Osborn, D. L.; Hayden, C. C.; Hemberger, P.; Bodi, A.; Voronova, K.; Sztaray, B. Breaking through the false coincidence barrier in electron-ion coincidence experiments. *J. Chem. Phys.* **2016,** *145* (16), 164202.
(213) Kamphus, M.; Liu, N. N.; Atakan, B.; Qi, F.; McIlroy, A. REMPI temperature measurement in molecular beam sampled low-pressure flames. *Proc. Combust. Inst.* **2002,** *29* (2), 2627-2633.
(214) Mercier, X.; Faccinetto, A.; Batut, S.; Vanhove, G.; Božanić, D. K.; Hróðmarsson, H. R.; Garcia, G. A.; Nahon, L. Selective identification of cyclopentaring-fused PAHs and side-substituted PAHs in a low pressure premixed sooting flame by photoelectron photoion coincidence spectroscopy. *Phys. Chem. Chem. Phys.* **2020,** *22* (28), 15926-15944.
(215) Yang, J. Photonionization Cross Section Database Version 2.0. http://flame.nsrl.ustc.edu.cn/database/.
(216) Loison, J.-C. Absolute Photoionization Cross Section of the Methyl Radical. *J. Chem. Phys. A* **2010,** *114* (23), 6515-6520.
(217) Savee, J. D.; Soorkia, S.; Welz, O.; Selby, T. M.; Taatjes, C. A.; Osborn, D. L. Absolute photoionization cross-section of the propargyl radical. *J. Chem. Phys.* **2012,** *136* (13), 134307.
(218) Gozem, S.; Gunina, A. O.; Ichino, T.; Osborn, D. L.; Stanton, J. F.; Krylov, A. I. Photoelectron Wave Function in Photoionization: Plane Wave or Coulomb Wave? *J. Phys. Chem. Lett.* **2015,** *6* (22), 4532-4540.

(219) Bodi, A.; Hemberger, P.; Tuckett, R. P. Coincident velocity map image reconstruction illustrated by the single-photon valence photoionisation of CF₃SF₅. *Phys. Chem. Chem. Phys.* **2017,** *19* (44), 30173-30180.
(220) Durif, O.; Capron, M.; Messinger, J. P.; Benidar, A.; Biennier, L.; Bourgalais, J.; Canosa, A.; Courbe, J.; Garcia, G. A.; Gil, J. F., et al. A new instrument for kinetics and branching ratio studies of gas phase collisional processes at very low temperatures. *Rev. Sci. Instrum.* **2021,** *92* (1), 014102.
(221) Gans, B.; Garcia, G. A.; Holzmeier, F.; Krüger, J.; Röder, A.; Lopes, A.; Fittschen, C.; Loison, J.-C.; Alcaraz, C. Communication: On the first ionization threshold of the C2H radical. *J. Chem. Phys.* **2017,** *146* (1), 011101.
(222) Schleier, D.; Humeniuk, A.; Reusch, E.; Holzmeier, F.; Nunez-Reyes, D.; Alcaraz, C.; Garcia, G. A.; Loison, J.-C.; Fischer, I.; Mitric, R. Diborene: Generation and Photoelectron Spectroscopy of an Inorganic Biradical. *J. Phys. Chem. Lett.* **2018,** *9* (20), 5921-5925.
(223) Mukhopadhyay, D. P.; Schleier, D.; Fischer, I.; Loison, J. C.; Alcaraz, C.; Garcia, G. A. Photoelectron spectroscopy of boron-containing reactive intermediates using synchrotron radiation: BH2, BH, and BF. *Phys. Chem. Chem. Phys.* **2020,** *22* (3), 1027-1034.
(224) Komorek, R.; Xu, B.; Yao, J.; Kostko, O.; Ahmed, M.; Yu, X.-Y. Probing sulphur clusters in a microfluidic electrochemical cell with synchrotron-based photoionization mass spectrometry. *Phys. Chem. Chem. Phys.* **2020,** *22* (26), 14449-14453.
(225) Sui, X.; Xu, B.; Yao, J.; Kostko, O.; Ahmed, M.; Yu, X.-Y. New Insights into Secondary Organic Aerosol Formation at the Air–Liquid Interface. *J. Phys. Chem. Lett.* **2021,** *12* (1), 324-329.
(226) Yang, L.; Yu, X.-Y.; Zhu, Z.; Iedema, M. J.; Cowin, J. P. Probing liquid surfaces under vacuum using SEM and ToF-SIMS. *Lab on a Chip* **2011,** *11* (15), 2481-2484.
(227) Seemann, B.; Alon, T.; Tsizin, S.; Fialkov, A. B.; Amirav, A. Electron ionization LC-MS with supersonic molecular beams—the new concept, benefits and applications. *J. Mass Spectrom.* **2015,** *50* (11), 1252-1263.
(228) Granot, O.; Amirav, A. LC–MS with electron ionization of cold molecules in supersonic molecular beams. *Int. J. Mass spectrom.* **2005,** *244* (1), 15-28.
(229) Couch, D. E.; Buckingham, G. T.; Baraban, J. H.; Porterfield, J. P.; Wooldridge, L. A.; Ellison, G. B.; Kapteyn, H. C.; Murnane, M. M.; Peters, W. K. Tabletop Femtosecond VUV Photoionization and PEPICO Detection of Microreactor Pyrolysis Products. *J. Chem. Phys. A* **2017,** *121* (28), 5280-5289.
(230) Davies, J. A.; LeClaire, J. E.; Continetti, R. E.; Hayden, C. C. Femtosecond time-resolved photoelectron–photoion coincidence imaging studies of dissociation dynamics. *J. Chem. Phys.* **1999,** *111* (1), 1-4.
(231) Stolow, A.; Bragg, A. E.; Neumark, D. M. Femtosecond Time-Resolved Photoelectron Spectroscopy. *Chem. Rev.* **2004,** *104* (4), 1719-1758.
(232) Steglich, M.; Knopp, G.; Hemberger, P. How the methyl group position influences the ultrafast deactivation in aromatic radicals. *Phys. Chem. Chem. Phys.* **2019,** *21* (2), 581-588.